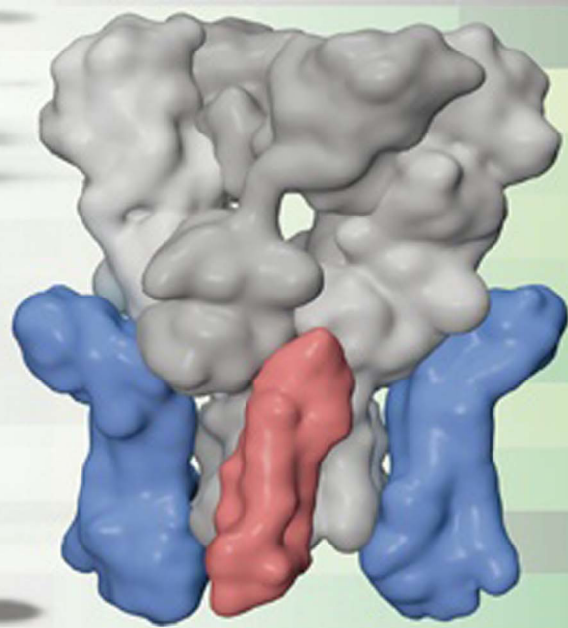
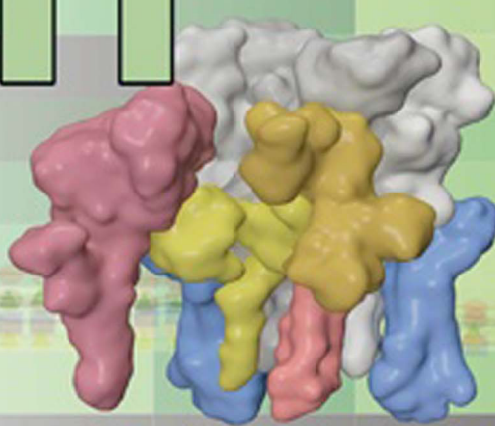


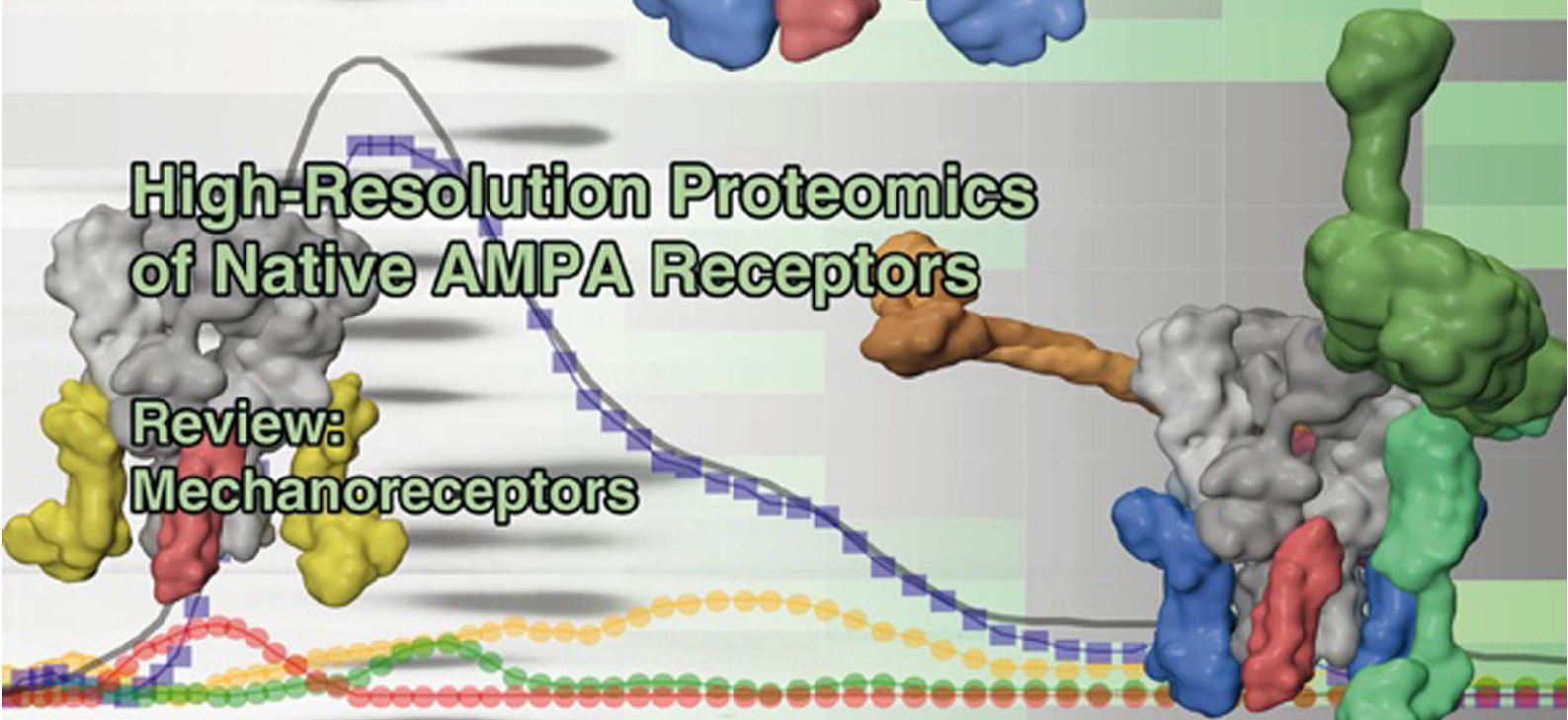
Neuron

Volume 74
Number 4
May 24, 2012
www.cellpress.com



High-Resolution Proteomics of Native AMPA Receptors

Review:
Mechanoreceptors



High-Resolution Proteomics Unravel Architecture and Molecular Diversity of Native AMPA Receptor Complexes

Jochen Schwenk,^{1,4,5} Nadine Harmel,^{3,5} Aline Brechet,¹ Gerd Zolles,¹ Henrike Berkefeld,¹ Catrin Swantje Müller,¹ Wolfgang Bildl,¹ David Baehrens,¹ Björn Hüber,¹ Akos Kulik,^{1,4} Nikolaj Klöcker,³ Uwe Schulte,^{1,2,4,*} and Bernd Fakler^{1,4,*}

¹Institute of Physiology, University of Freiburg, Hermann-Herder-Str. 7, 79104 Freiburg, Germany

²Logopharm GmbH, Hermann-Herder-Str. 7, 79104 Freiburg, Germany

³Institute of Neuro- and Sensory Physiology, University of Düsseldorf Medical Faculty, 40225 Düsseldorf, Germany

⁴Centre for Biological Signaling Studies (BIOS), Albertstr. 10, 79104 Freiburg, Germany

⁵These authors contributed equally to this work

*Correspondence: uwe.schulte@physiologie.uni-freiburg.de (U.S.), bernd.fakler@physiologie.uni-freiburg.de (B.F.)

DOI 10.1016/j.neuron.2012.03.034

SUMMARY

AMPA-type glutamate receptors (AMPARs) are responsible for a variety of processes in the mammalian brain including fast excitatory neurotransmission, postsynaptic plasticity, or synapse development. Here, with comprehensive and quantitative proteomic analyses, we demonstrate that native AMPARs are macromolecular complexes with a large molecular diversity. This diversity results from coassembly of the known AMPAR subunits, pore-forming GluA and three types of auxiliary proteins, with 21 additional constituents, mostly secreted proteins or transmembrane proteins of different classes. Their integration at distinct abundance and stability establishes the heteromultimeric architecture of native AMPAR complexes: a defined core with a variable periphery resulting in an apparent molecular mass between 0.6 and 1 MDa. The additional constituents change the gating properties of AMPARs and provide links to the protein dynamics fundamental for the complex role of AMPARs in formation and operation of glutamatergic synapses.

INTRODUCTION

Fast excitatory neurotransmission in the mammalian brain largely relies on AMPA receptors (AMPARs) that control fundamental aspects of development and signal transduction in glutamatergic synapses. During the early phase of synaptogenesis, AMPARs are recruited to dendritic sites of contact with axons where they promote both formation and maturation of synapses (McAllister, 2007; McKinney, 2010). In established synapses, AMPARs mediate the fast excitatory postsynaptic current (EPSC) that initiates propagation of the electrical signal and controls Ca^{2+} entry into the postsynaptic spine (Cull-Candy et al., 2006; Garaschuk et al., 1996; Jonas and Spruston, 1994; Raman and Trussell, 1992; Sah et al., 1990; Silver et al., 1992).

The time course and the amplitude of the AMPAR-mediated EPSCs are quite variable among neurons and strongly depend upon the gating properties of the receptor channels (Conti and Weinberg, 1999; Jonas, 2000). The number of AMPARs in the postsynaptic membrane is determined by trafficking and endo/exocytic processes (Bredt and Nicoll, 2003; Carroll et al., 2001; Choquet, 2010; Choquet and Triller, 2003; Shepherd and Huganir, 2007). All of these processes appear to be regulated via post-translational modifications and protein interactions and together are thought to endow excitatory synaptic transmission with the activity-dependent plasticity underlying learning, memory, and/or maintenance of synapses (Derkach et al., 2007; Malenka and Nicoll, 1999; Malinow and Malenka, 2002; Newpher and Ehlers, 2008).

On the molecular level, the complexity in the cell biology of AMPARs is met by a number of distinct protein constituents: native AMPARs are assembled from the pore-forming GluA1–4 proteins (Collingridge et al., 2009; Hollmann and Heinemann, 1994; Seuberg, 1993) and at least three types of auxiliary subunits, the transmembrane AMPAR regulatory proteins (TARPs γ -2, γ -3, γ -4, γ -5, γ -7, γ -8; Cho et al., 2007; Milstein et al., 2007; Soto et al., 2009; Tomita et al., 2003), the *cornichon* homologs (CNIH-2, CNIH-3; Schwenk et al., 2009), and the CKAMP44 protein (von Engelhardt et al., 2010). Alone or in combination, these auxiliary subunits control the gating and pharmacology of the AMPARs and profoundly impact their biogenesis and protein processing (Bats et al., 2007; Chen et al., 2000; Gill et al., 2011; Harmel et al., 2012; Kato et al., 2010; Schober et al., 2011; Schwenk et al., 2009; Soto et al., 2007; Tomita et al., 2005; Vandenberghe et al., 2005; von Engelhardt et al., 2010).

It is not clear, however, whether these auxiliary proteins represent the whole set of building blocks for native AMPARs or whether they contain additional yet unknown protein constituents. Likewise, quantitative data on the subunit composition of native AMPAR complexes are not yet available. This information may be obtained from comprehensive and quantitative proteomic analyses as have recently been presented for the Cav2 family of voltage-gated calcium channels (Müller et al., 2010).

Here we used two orthogonal biochemical strategies, multiepitope and target knockout-controlled affinity purifications (Bildl et al., 2012; Müller et al., 2010) and newly developed high-resolution quantitative analyses of protein complexes separated on native gels (BN-MS), for investigation of the subunit composition of AMPARs from total brain. These analyses unravel native AMPARs as macromolecular complexes of unanticipated complexity and identify 21 novel protein constituents, mostly transmembrane or secreted proteins of low molecular mass and with distinct functions. Subsequent studies using antibody shift assays, binding studies, and electrophysiological recordings reveal the architecture of native AMPARs and demonstrate that properties and function of the receptor complexes may be quite distinct strongly depending on the particular subunit composition.

RESULTS

Multiepitope Proteomic Analysis of AMPAR Complexes in the Brain

For comprehensive proteomic analysis of native AMPARs, we performed multiepitope affinity purifications (ME-APs) (Müller et al., 2010; Schwenk et al., 2010) with ten different antibodies (ABs) specific for the GluA1–4 proteins on membrane fractions prepared from total brains of adult rats, wild-type (WT) mice, and AB-target knockout mice (see *Experimental Procedures*). For ME-APs the membrane fractions were treated with detergent buffers of either mild (CL-47) or intermediate (CL-91) stringency (Müller et al., 2010; Schwenk et al., 2010) solubilizing ~40% and 100% of the total pool of AMPARs, respectively (Figures S1A and S1B). These buffers were selected as the two extremes in a test series probing the solubilization efficiency of various CL-buffers as well as of RIPA and Triton X-100, the buffers most widely used with AMPARs (Kim et al., 2010; Shi et al., 2009, 2010; Vandenberghe et al., 2005; solubilization efficiency of ~60%, Figure S1B). Both CL-47 and CL-91 preserved high-molecular-weight AMPAR complexes (Schwenk et al., 2009) as demonstrated by blue native polyacrylamide gel electrophoresis (BN-PAGE); the AMPAR complexes focused over an apparent molecular mass range of ~0.4 MDa under either condition, although they appeared slightly smaller in CL-91 than in CL-47 (Figure 1A). Total eluates of APs with the *anti-GluA* ABs or with pools of preimmunization immunoglobulins G (IgG) were analyzed by high-resolution nanoflow liquid chromatography tandem mass spectrometry (nano-LC MS/MS), which provided data on both the identity and the amount of proteins. Protein amounts were determined from the peak volumes (PVs) of their best-correlating tryptic peptides (TopCorr method [Bildl et al., 2012]; see also *Experimental Procedures*), a label-free quantification method offering a linear dynamic range of up to four orders of magnitude (Bildl et al., 2012; Müller et al., 2010; Schwenk et al., 2010).

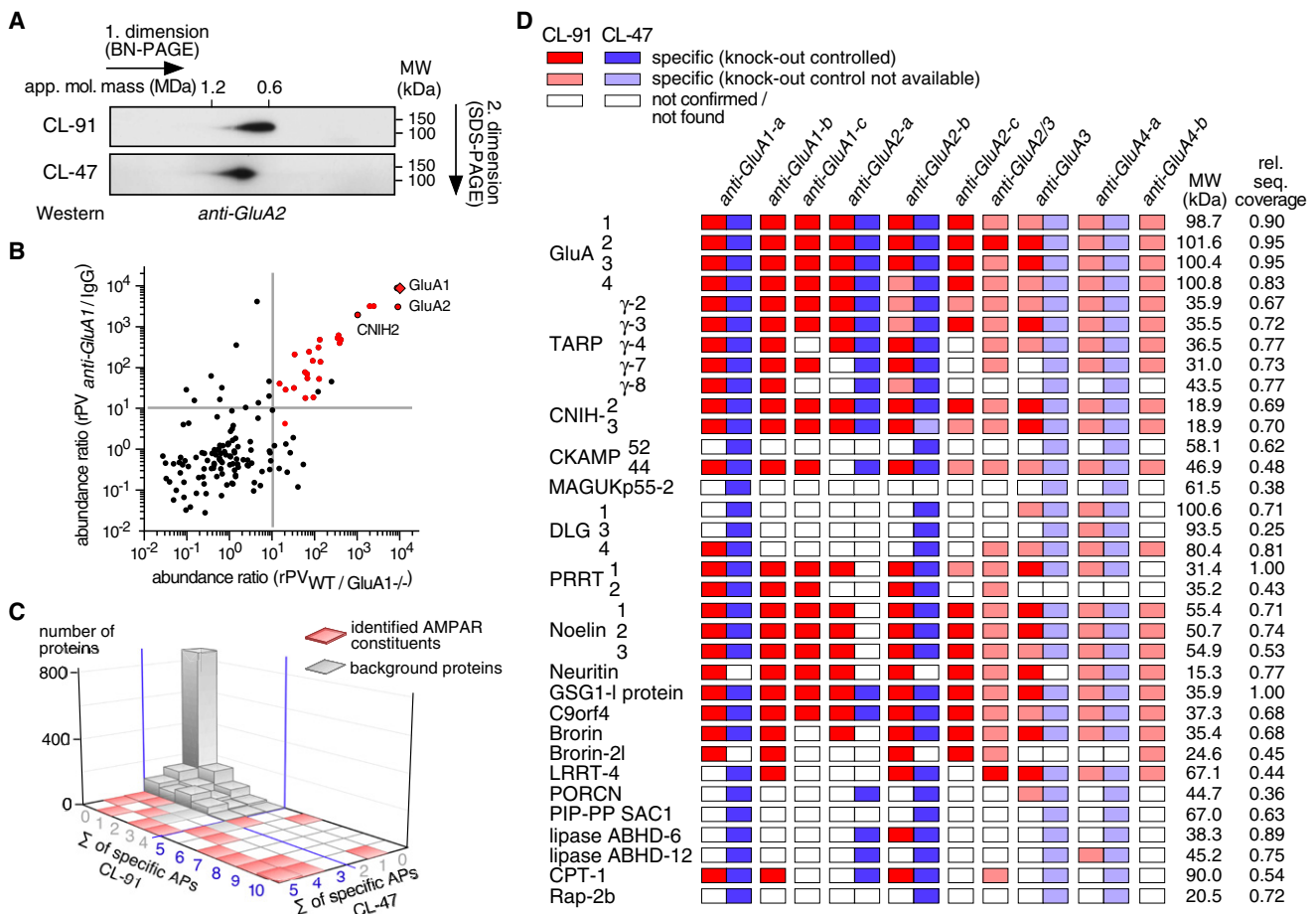
The results of these MS analyses showed that AMPARs were retained in all APs with high efficiency as reflected by the PV values and the extensive coverage provided for the primary sequence of the GluA1–4 proteins by the MS/MS-identified peptides (relative sequence coverage of 90%, 95%, 95%, 83% for GluA1 to GluA4, respectively; Tables S1–S3; detailed information on all aspects related to MS analyses were deposited at <http://www.channel-proteomes.com/projects>). The other

proteins identified by mass spectrometry in the *anti-GluA* APs (and surpassing the threshold PV, see *Experimental Procedures*) were evaluated for both their specificity and consistency of copurification with the GluA proteins based on the quantitative data of protein amounts. Specificity of copurification was determined from abundance ratio plots using both target knockouts and preimmunization IgGs as negative controls (upper-right quadrant in Figure 1B; Table S3; Bildl et al., 2012; Müller et al., 2010). Consistency was assessed by the number of specific copurifications of a given protein across the *anti-GluA* APs; a protein was considered consistent if it was specifically retained in at least five (out of ten) or three (out of five) *anti-GluA* APs using solubilization with CL-91 and CL-47, respectively.

Together, the criteria abundance threshold, specificity, consistency, and confirmation by at least one of the knockout controls defined a sharp-profiled proteome (Figure 1C), identifying 34 (out of 1,711 detected) proteins as high-confidence constituents of native AMPARs in the rodent brain (Table 1). As summarized in Figure 1D, these constituents comprise the aforementioned AMPAR subunits GluA1–4, five members of the TARP family (γ -5 was unambiguously detected in only three out of 15 APs, albeit in small amounts), CNIHs 2,3, and CKAMP44 as well as another 22 proteins of which only DLG4 (or PSD95) has been previously described as an AMPAR interactor (Chen et al., 2000). Similar to the known auxiliary subunits, the majority of the newly identified AMPAR constituents are low-molecular-weight proteins (between 15.3 and 55.4 kDa; Figure 1D) and most of them were copurified effectively under both solubilization conditions resulting in a marked relative coverage of their primary sequences (between 25% and 100%, Figure 1D). Interestingly, 12 of these new constituents (out of 21) are transmembrane (TM) proteins of different classes (1–8 TM domains), while five are secreted and four are cytoplasmic proteins (Table 1). Robust association of these proteins with native AMPARs was corroborated in reverse APs where ABs targeting a selected set of known and newly identified AMPAR constituents replaced the *anti-GluA* ABs. As shown in Figure S1C, all of the ABs effectively retained the GluA proteins together with many of the other AMPAR proteome constituents.

Quantification of Subunit Composition by BN-Mass Spectrometry

While ME-APs are suited to reliably identify constituents of protein assemblies, they may not entirely reflect their native abundances and stoichiometries, mainly due to the inherent properties of ABs (Müller et al., 2010; Schulte et al., 2011). We therefore used an AB-free BN-MS approach (Remmerie et al., 2011; Wessels et al., 2009) exploiting the sharp focusing of AMPAR complexes in the BN-PAGE (Figure 1A). Sections of native gel regions harboring the AMPARs (from total brain of adult rats) were sliced with a cryotome (thickness of slices 400 μ m) and collected, and each slice was analyzed individually for its protein composition by quantitative MS-analysis (Figure 2A; see *Experimental Procedures*). Together with calibration peptides specific for the identified AMPAR constituents (Figure 1D) and concatenated into fusion proteins at defined stoichiometry (QconCAT proteins; Pratt et al., 2006; Figure S2A, Table S4), this procedure allowed for quantitative assessment of the molecular composition of AMPAR

**Figure 1. ME-AP Proteomics Identify the Protein Constituents of Native AMPARs**

(A) Two-dimensional gel separation of AMPAR complexes from rat brain solubilized with CL-91 and CL-47; both gel separations were western-probed with the indicated antibody. Size (BN-PAGE) and molecular weight (SDS-PAGE) are as indicated.

(B) Two-dimensional logarithmic abundance-ratio plot illustrating the medians of PV ratios (rPV) obtained for any protein in APs from rat membranes with the anti-GluA1-a AB versus IgG (y axis) and in anti-GluA1-a APs from mouse membranes of WT versus GluA1 knockout animals (x axis). Gray bars (rPVs of 10) represent the specificity threshold for this AB on either rPV scale and place specifically purified proteins in the upper-right quadrant. Red dots denote finally annotated AMPAR constituents (D, Table 1); black dots symbolize all other proteins. Red dot in the lower-right and black dots in the upper-right quadrant represent peculiarities of the anti-GluA1-a AP.

(C) Three-dimensional plot illustrating the consistency of specifically copurified proteins detected in the anti-GluA APs performed with CL-91 (10 APs) and CL-47 (5 APs). Blue lines indicate the consistency thresholds given in the text, and numbers are the count of APs that specifically copurified a given protein. Red bars refer to the counts of finally annotated AMPAR constituents, and gray bars denote counts of background proteins; the four proteins surpassing the consistency threshold of CL-47 failed confirmation by knockout controls. Note the sharp discrimination between AMPAR constituents and background.

(D) Table summarizing the results for all of the finally annotated AMPAR constituents across the 15 APs performed with the indicated anti-GluA ABs. Color coding given in the upper left; MW and relative coverage of the primary sequence as indicated on the right.

complexes of a given apparent molecular mass (Figure 2A; see Experimental Procedures).

Figure 2B shows the resulting abundance profiles obtained from 81 consecutive gel slices for the most ample constituents of AMPARs solubilized with CL-47. Thus, the major portion of AMPAR complexes exhibited an apparent molecular mass of about 0.6–1.0 MDa, markedly exceeding the size of the GluA tetramers (mass of ~0.5 MDa, Figure S2C). For the pore-forming subunits, BN-MS revealed an abundance sequence of GluA2 > GluA1 > GluA3 > GluA4, with the molecular amount of GluA2 being equal to the sum of the other GluAs (Figure 2B, upper

panel). Among the known auxiliary subunits, TARP γ -8 and CNIH-2 were by far the most abundant (Figures 2B and 2E). Comparison of the abundance value determined for all TARP and CNIH proteins with that obtained for the entire pool of AMPARs (defined as GluA tetramers, GluA_{tetra}) yielded a ratio of about 4:1 (Figure 2C), strongly suggesting that, on average, AMPAR complexes contain up to four TARP or CNIH proteins in line with previous reports on heterologously expressed AMPARs (Kim et al., 2010; Shi et al., 2009).

Moreover, the BN-MS approach revealed cosegregation of the newly identified AMPAR constituents with the GluA proteins,

Table 1. Protein Constituents of Native AMPARs as Identified by ME-APs

Protein ID	Name	Alternative Name(s)	Acc. No. (SwissProt)
GluA1	AMPA-type glutamate receptor 1	GluR-A	P19490
GluA2	AMPA-type glutamate receptor 2	GluR-B	P19491
GluA3	AMPA-type glutamate receptor 3	GluR-C	P19492
GluA4	AMPA-type glutamate receptor 4	GluR-D	P19493
TARP γ-2	Transmembrane AMPA-regulatory protein γ-2	Stargazin	O88602
TARP γ-3	TARP γ-3		Q8VHX0
TARP γ-4	TARP γ-4		Q8VHW9
TARP γ-7	TARP γ-7		P62957
TARP γ-8	TARP γ-8		Q8VHW5
CNIH-2	protein <i>cornichon</i> homolog 2		Q5BJU5
CNIH-3	protein <i>cornichon</i> homolog 3		Q6ZWS4
CKAMP44	Cystine-knot AMPAR modulating protein of 44 kDa	Protein shisa-9	Q9CZN4
CKAMP52	Cystine-knot AMPAR modulating protein of 52 kDa	Protein shisa-6	Q3UH99
MAGUKp55-2	MAGUK p55 subfamily member 2	Protein MPP2	Q9WV34
DLG1	Disk large homolog 1	SAP-97	Q62696
DLG3	Disk large homolog 3	SAP-102	Q62936
DLG4	Disk large homolog 4	PSD-95, SAP-90	Q62108
PRRT1	Proline-rich transmembrane protein 1	NG-5, SynDIG4	Q6MG82
PRRT2	Proline-rich transmembrane protein 2		Q7Z6L0
Noelin1	Noelin-1	Olfactomedin-1, Pancortin	Q62609
Noelin2	Noelin-2	Olfactomedin-2	Q8BM13
Noelin3	Noelin-3	Olfactomedin-3	P63057
Neuritin	Neuritin	CPG-15	O08957
GSG1-I protein	Germ cell-specific gene 1-like protein		Q6UXU4
C9orf4	Uncharacterized protein C9orf4	brain protein CG-6	Q9PK9
Brorin	Brorin, von Willebrand factor C domain-containing protein 2	brain-specific chordin-like protein	Q8C8N3
Brorin-2l	von Willebrand factor C domain-containing protein 2-like		Q505H4
LRRT4	Leucine-rich repeat transmembrane neuronal protein 4		Q80XG9
PORCN	Probable protein-cysteine N-palmitoyltransferase porcupine	Porc, Ppn	Q9JJJ7
PIP-PP SAC1	Phosphatidylinositide phosphatase SAC1		Q9EP69
lipase ABHD-6	Monoacylglycerol lipase ABHD6		Q8R2Y0
lipase ABHD-12	Monoacylglycerol lipase ABHD12		Q99LR1
CPT-1	Carnitine O-palmitoyltransferase 1 (brain isoform)	CPT-1C	Q8BGD5
Rap-2b	Ras-related protein Rap-2b		P61227

transmembrane secreted cytoplasmic

Accession numbers refer to the UniProt/SwissProt database; protein classification is given by the color-coding at the bottom.

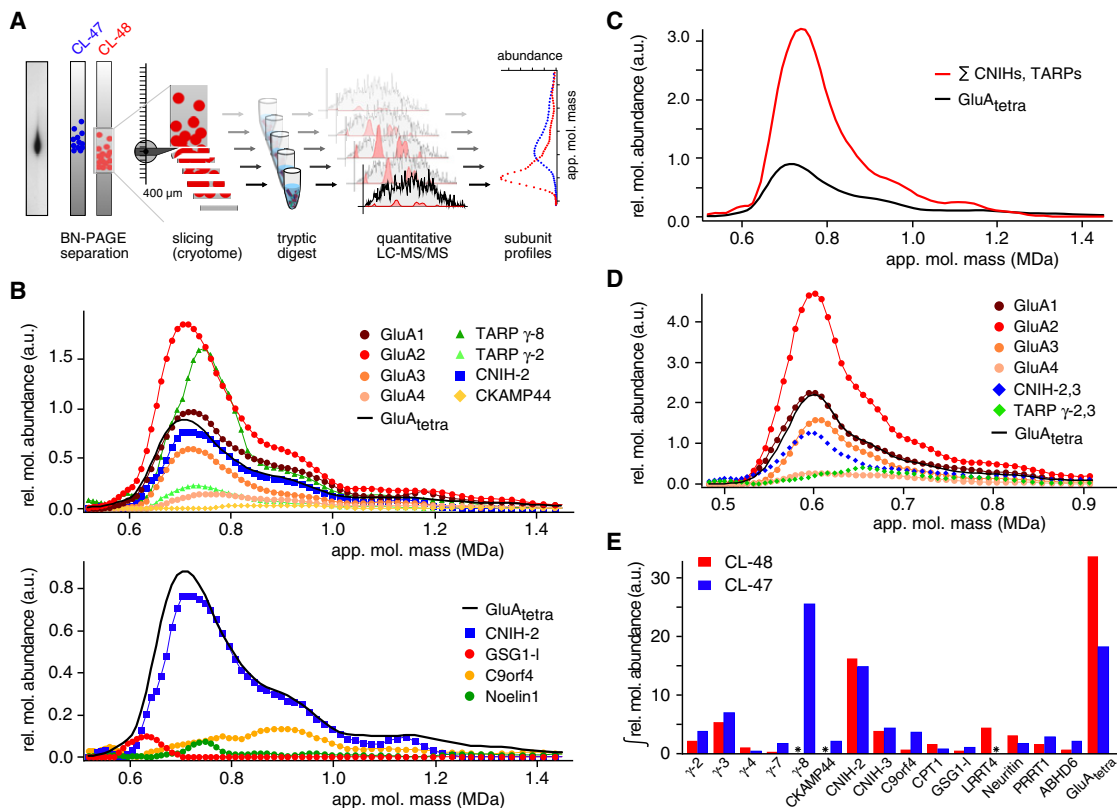


Figure 2. BN-MS Quantifies Subunit Composition of Native AMPAR Complexes of Given Molecular Mass

(A) Scheme illustrating the BN-MS approach used for high-resolution analysis of the subunit composition of native AMPARs (details in the text and Experimental Procedures).

(B and C) Abundance-mass profiles determined for AMPAR complexes solubilized with CL-48. Each data point represents the amount determined for the respective protein in one gel slice (total of 81 gel slices); symbols are as indicated. GluA_{tetra} (black line) refers to the summed amounts of GluA1–4 divided by 4, and the red line in (C) is the sum of protein amounts determined for CNIHs 2,3 and TARPs γ-2,3,4,7,8. Note the distinct profiles obtained for GSG1-I, C9orf4 and Noelin-1.

(D) Abundance-mass profiles as in (C) but determined for AMPAR complexes solubilized with CL-47 (total of 69 gel slices).

(E) Bar graph illustrating total relative molecular abundance (integral over the investigated mass range) of the indicated AMPAR constituents determined in buffers CL-48 (red) and CL-47 (blue); asterisks denote missing data.

thus providing independent evidence for their robust association with native AMPAR complexes (Figure 2B, lower panel). As indicated by the abundance-mass profiles, these proteins either assemble into distinct AMPAR complexes of defined molecular mass (such as GSG1-I or Noelin1, Figure 2B, lower panel) or may be integrated into multiple types of complexes extending over a broader mass range (such as C9orf4 or CKAMP44, Figure 2B, upper and lower panel). The abundance values of all newly identified proteins were below those of TARP γ-8 and CNIH-2, but well in the range of the other TARPs, CNIH-3, or CKAMP44 (Figures 2B and 2E).

Subsequent BN-MS analysis of AMPAR complexes solubilized with buffers of intermediate stringency (CL-48, CL-91) revealed three further important features. First, the difference in the observed molecular size of AMPARs (Figure 1A), corresponding to ~0.1 MDa, is predominantly due to the almost complete dissociation of TARP γ-8 from the AMPARs under these conditions (Figures 2D and 2E); this quantitative dissociation was confirmed in density gradient centrifugations (Fig-

ure S2B) but was only seen with TARP γ-8, while the other TARPs remained largely unaffected (Figures 2D and 2E; Figure S2B). Second, some of the newly identified constituents including LRRT4 and Neuritin were more abundantly detected with the intermediate stringency buffers (Figure 2E). Third, the abundance profiles of CNIHs 2,3 and TARPs γ-2,3 indicate that they are predominantly assembled into distinct AMPAR complexes at an approximate ratio of 3:1 (Figure 2D), in line with our previous work (Schwenk et al., 2009).

Together, the results from ME-APs and BN-MS indicated that native AMPARs are in fact formed by a multitude of protein complexes assembled from up to 34 proteins at distinct abundance.

Multiple Populations of AMPAR Complexes with Distinct Stability

The assembly of native AMPARs was further investigated in AB-shift assays separating complexes in BN-PAGE by the additional mass of target-specific ABs and in APs probing the stability of

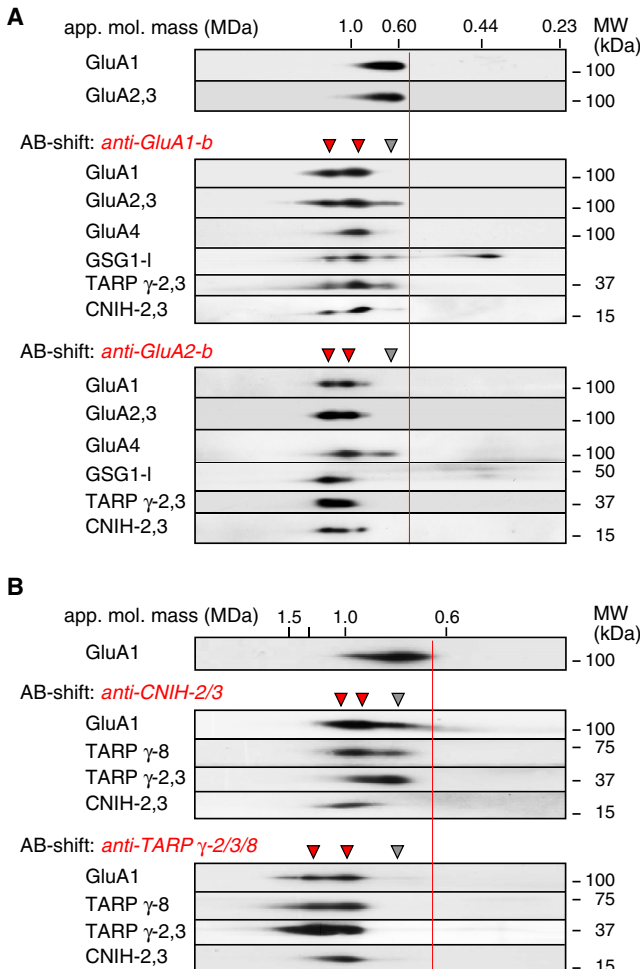


Figure 3. AMPAR Constituents Cosegregate into Multiple Populations of AMPAR Complexes

(A) Two-dimensional gel separation of AMPARs as in Figure 1 without (upper panel) and with ABs specific for either GluA1 (*anti-GluA1-b*) or GluA2 (*anti-GluA2-b*; lower two panels, AB-shift assay) added to the membrane fractions solubilized with CL-91; all gel separations were western-probed with ABs against the indicated proteins. Arrowheads denote unshifted (gray) or populations of AMPARs shifted by addition of one or two ABs (red).

(B) AB-shift assay as in (A) but with ABs targeting either CNIHs 2,3 or TARP γ -2,3,8 and membrane fractions solubilized with CL-47.

complexes by an array of solubilization buffers with different stringency.

ABs specific for GluA1 and GluA2 shifted the majority of all GluAs to higher molecular weights (Figure 3A), with the discrete increments most likely reflecting assembly of at least one or two of these subunits into the respective AMPARs (also Figure S3); additionally, both assays revealed a small fraction of AMPARs devoid of either GluA1 or GluA1-3. The known auxiliary subunits TARP γ -2,3 and CNIH-2,3 were coshifted with both *anti-GluAs*, very similar to the GSG1-I protein, as expected for tightly associated complex constituents (Figure 3A). Interestingly, *anti-GluA2*, different from *anti-GluA1*, shifted the complete pool of GSG1-I, strongly suggesting preferred association of this newly identified

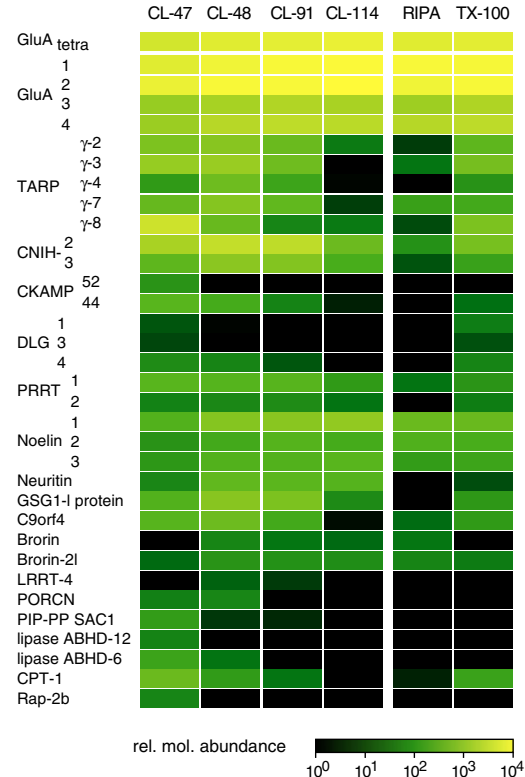
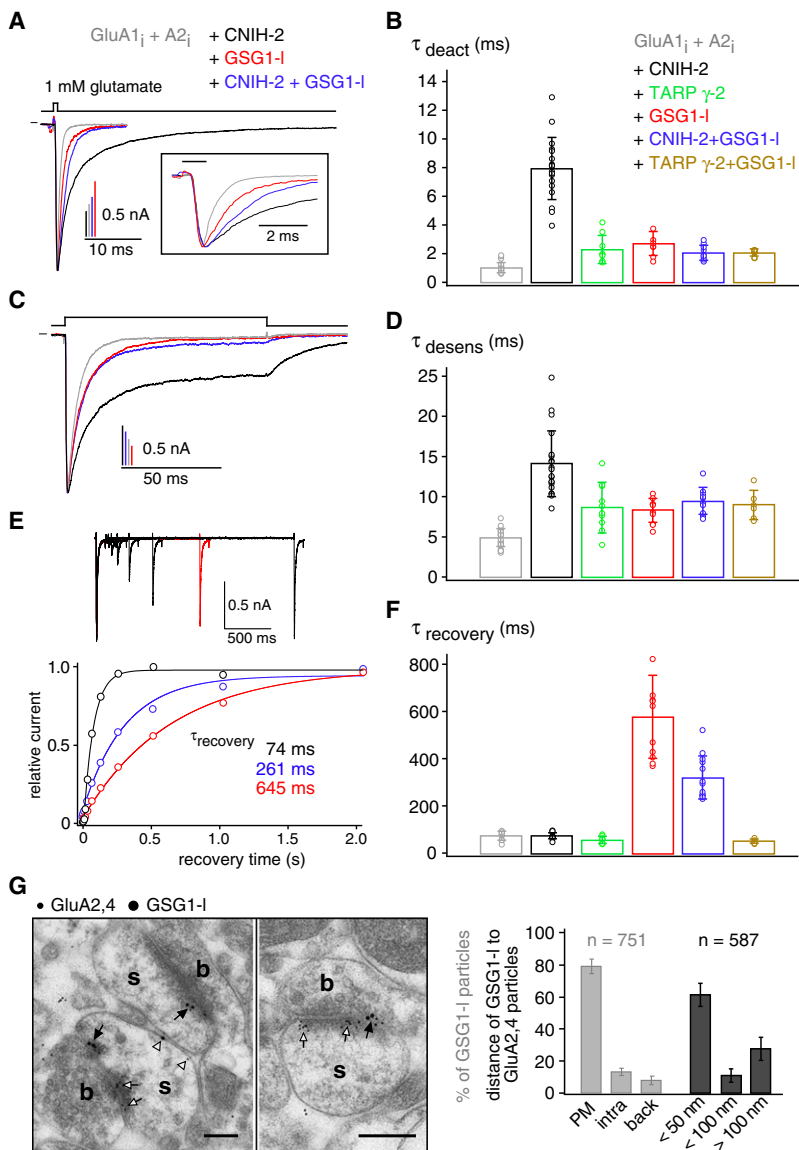


Figure 4. AMPAR Constituents Coassemble into AMPAR Complexes with Distinct Stability

Heat map indicating the molecular abundance of all AMPAR constituents determined in *anti-GluA1-a* APs from membrane fractions solubilized with the indicated buffers. Stringency of solubilization buffers increased from CL-47 to CL-114 (Müller et al., 2010); results obtained with two widely used buffers, Triton X-100 and RIPA, were added for comparison.

subunit with GluA2-containing AMPARs (Figure 3A). Shift assays with *anti-CNIH-2/3* showed that the majority of AMPARs solubilized at CL-47 (Figure S3B) are associated with the CNIHs (also Figure 2D), as well as with TARP γ -8, while most of the TARP γ -2,3 proteins are assembled into distinct subpopulations of AMPARs (Figure 3B, upper panel). Moreover, an AB targeting TARPs γ -2,3,8 indicated that virtually all AMPARs solubilized under these conditions contained at least one of the three TARP isoforms; AB-shift assays with both *anti-TARP γ -2/3/8* and *anti-CNIH-2/3* showed that these auxiliary subunits assemble into all native AMPARs and that the obtained mass shift (Figure S3C) is in line with the 4:1 ratio determined for GluA tetramers and TARPs plus CNIHs (Figure 2C). Notably, the two shift assays in Figure 3B (separated on the same gel) point toward distinct stoichiometries of these auxiliary subunits in native AMPARs, up to two CNIHs and two or more TARPs γ -2,3,8 per complex.

The stability of the AMPAR assemblies was assessed by determining the molecular abundance (using the QconCAT proteins as in Figure 2) of its constituents retained in *anti-GluA1-a* APs under solubilization conditions of increasing stringency (Müller et al., 2010) (see Experimental Procedures). Analysis of the resulting heat map (Figure 4) suggested that the



underlying protein interactions may be classified into three main categories: interactions (1) that are largely unaffected by both intermediate (CL-48, CL-91) and high-stringency conditions (CL-114; as for CNIHs, Noelins, Neuritin, or PRRTs), (2) that are markedly reduced under conditions of high stringency (as for TARPs γ -2,3,4,7, GSG1-I, C9orf4, CKAMP44, DLG4, or PORCN), and (3) interactions mainly preserved at low-stringency conditions (CL-47; as for TARP γ -8, SAC1, DLG1,3, or CKAMP52). It is noteworthy that the stability of individual interactions was independent of their topology and in most cases not dependent upon the presence of the abundant auxiliary subunits. Thus, CNIH-2,3 and other tightly associated constituents were extensively retained in APs using conditions that did not preserve assembly of TARP γ -8 (Figure 4), or where the TARP γ -8 protein was absent after gene knockout (Figure S4). In addition, the heat map demonstrated that solubilization with

Figure 5. The GSG1-I Protein Assembles into Synaptic AMPARs and Modifies the Gating Kinetics of Receptor Channels in a Subunit-Dependent Manner

(A) Representative current responses of AMPARs recorded upon 1 ms (A) and 100 ms (C) applications of 1 mM glutamate (indicated above the current trace) in giant outside-out patches excised from *Xenopus* oocytes expressing GluA1_i and GluA2_i, either alone (gray trace) or in combination with either CNIH-2 (black trace), GSG1-I (red trace) or both (blue trace). cRNAs of GluA1_i and GluA2_i, CNIH-2, and GSG1-I were injected at equal amounts. Inset: current responses at expanded time scale; agonist application indicated by the horizontal bar.

(B and D) Bar graphs summarizing the time constants for deactivation and desensitization (mean \pm SD of 6–19 experiments, represented by dots).

(E) Recovery of the same AMPARs as in (A) and (C) from steady-state desensitization recorded with a double-pulse protocol (pair of a 100 ms and a 50 ms glutamate pulse separated by increasing time intervals). Data points are peak currents recorded during the second pulse and normalized to the maximal current (recorded during the first glutamate application). Lines are monoexponential fits to the data points with the indicated $\tau_{recovery}$. Inset: Original current recordings from GluA1_i+A2_i+GSG1-I receptors; red trace is response with a recovery interval of 1024 ms.

(F) Bar graph summarizing the recovery time constants (mean \pm SD of 6–15 experiments, represented by dots).

(G) Immunoelectron micrographs for GluA2,4 and GSG1-I in the CA3 region of the adult mouse hippocampus detected by postembedding immuno-EM (left panel) and respective statistics (right panel). Immunoparticles for GluA2 and GluA4 (10 nm, open arrows) and GSG1-I (15 nm, filled arrows) were mostly found over asymmetrical synapses between boutons (b) and dendritic spines (s) of pyramidal cells and were sparsely detected at extrasynaptic sites (arrowheads). Note that most immunoparticles for GSG1-I were detected in close spatial relationship (<100 nm) with those for GluA2 and GluA4. Scale bars are 0.2 nm; bars on the right are mean \pm SD of three independent experiments. PM, intra, and back denote localization of immunoparticles to the plasma membrane, intracellular sites, and background, respectively.

RIPA and Triton X-100 buffers failed to preserve integrity of all AMPAR complexes, resulting in the loss of a number of constituents (including LRRT4, Neuritin, Brorin, Brorin-2I, CKAMP52, and PORCN) readily detected in mild and/or intermediate stringency CL-buffers (Figure 4).

Functional Diversity by Heteromultimerization of Complex Constituents

The robust integration into defined AMPAR complexes together with CNIHs and TARPs (Figures 2B, 3, and 4), prompted us to investigate the functional significance of the GSG1-I protein for which no primary function has yet been described. Figures 5A and 5C show representative current responses recorded in giant outside-out patches from *Xenopus* oocytes upon 1 ms and 100 ms applications of 1 mM glutamate to AMPARs assembled either from the flip variants of GluA1 and GluA2 alone or in

combination with the additional constituents GSG1-I or CNIH-2 or both. Channel activation was similar in all four types of receptors (20%–80% rise times of ~0.3 ms), but the time courses of deactivation (Figure 5A) and desensitization (Figure 5C) were markedly different, strongly depending upon the subunit composition of the AMPARs. While GSG1-I alone caused a moderate slowing of both kinds of channel closure very similar to TARP γ -2 ($p < 0.001$, Wilcoxon rank test for \pm GSG1-I; Figures 5B and 5D), it largely reversed the pronounced effects of CNIH-2 on the time constants of deactivation and desensitization when coassembled into the same AMPARs ($p < 0.001$, Wilcoxon rank test for CNIH-2 versus CNIH-2+GSG1-I; Figures 5B and 5D). Moreover, receptor channels assembled from GluA1, GluA2, CNIH-2, and GSG1-I no longer exhibited the marked non-desensitizing steady-state current (I_{ss}) observed with receptors composed of the GluA1, GluA2, and CNIH subunits alone (I_{ss} of $25\% \pm 10\%$ [mean \pm SD, $n = 20$] and $6\% \pm 3\%$ [$n = 12$] for GluA1+A2+CNIH-2 and GluA1+A2+CNIH-2+GSG1-I channels, respectively). In contrast to the moderate slowing of desensitization, GSG1-I decelerated the reverse process, recovery from desensitization, by almost 10-fold, and a pronounced slowing was still present upon addition of CNIH-2, albeit to a lesser extent ($p < 0.001$, Wilcoxon rank test for \pm GSG1-I and \pm GSG1-I+CNIH-2; Figures 5E and 5F). Interestingly, the dominant effects of GSG1-I over CNIH-2 in AMPAR gating were not recapitulated in receptors where CNIH-2 was replaced by TARP γ -2 ($p > 0.7$, Wilcoxon rank test for TARP γ -2 versus TARP γ -2+GSG1-I; Figures 5B, 5D, and 5F). Conversely, the CNIH-2 effects on gating were only moderately affected by coassembly of the TARP γ -8 subunit(s) ($p > 0.7$ and $p < 0.001$ Wilcoxon rank test for τ_{desens} and $\tau_{recovery}$, respectively; Figure S5A).

Together, these results demonstrated that coassembly of various auxiliary subunits generates AMPARs with quite distinct functional properties. The particular effects of GSG1-I may modulate the gating of AMPARs in various regions of the brain including the hippocampal CA3 region, where postembedding immunogold electron microscopy colocalized this protein with GluA2- and/or GluA4-containing AMPARs in dendritic spines of pyramidal cells (Figures 5G and S5B).

Subunit Composition and Architecture of Native AMPARs

Next, we used comparison of protein amounts obtained in anti-GluA APs from WT and GluA1 or GluA2 knockout mice and quantitative data from BN-PAGE separations (as in Figures 2 and 3, see Experimental Procedures) to probe whether the identified AMPAR constituents are preferentially associated with one of the two most abundant GluA subunits. Figure 6A summarizes the respective results together with the topology of the complex constituents suggested by public databases. Accordingly, very few of the AMPAR constituents are preferentially associated with either GluA1 (PRRT1,2) or GluA2 (GSG1-I, LRRT4, Brorin, and Brorin-2I). Twelve proteins (out of 30) appeared to exclusively associate with AMPARs (over other complexes in membrane fractions from adult brain) including the TARPs, CKAMP44, C9orf4, LRRT4, GSG1-I, and the two CNIH proteins whose complete pool was copurified with anti-GluAs (Figure S6A).

Finally, we combined the proteomic, biochemical and functional data (Figures 1–5) with Pearson correlation analyses across all data sets (Figure S6B) and binding assays on heterologously coexpressed complex constituents (Figure S6C) to derive a general (working) model for the assembly of native AMPARs in the brain. Accordingly, the model projected onto the recently resolved crystal structure of the GluA tetramer (Sobolevsky et al., 2009) reflects binding sites, their potential occupancies, and/or direct interactions of complex constituents, while exact stoichiometries of individual AMPARs or structural details are not implicated. As illustrated in Figure 6B, AMPARs share a common “inner core” that is assembled from four GluAs and four major auxiliary subunits (Figure 2C) arranged in a two-fold symmetry determined by the structure of the GluA tetramer just above the membrane plane (gray line in Figure 6A; Sobolevsky et al., 2009). Of the two pairs of distinct binding sites (solid circles in red and gray, Figure 6B), one is occupied either by CNIHs 2,3 (70%–80%, Figures 2 and 3) or TARPs γ -2,3 (20%–30%, Figures 2 and 3), the other harbors TARPs γ -8,4,2,3 or GSG1-I (Figures 2, 3, and 5). This inner core of the AMPARs is complemented by “outer core” constituents binding directly to the GluA proteins (Figure S6C) at sites distinct from the interaction sites of the inner core constituents (dashed circles in orange, Figure 6B): the one TM-domain proteins PRRTs 1,2, CKAMP44, or C9orf4, as well as the membrane-anchored Neuritin. As an entity, the proteins of the inner and outer core serve as a platform for other, more peripherally associated AMPAR constituents including the Noelin, Brorin-2I, and CPT-1 (Figure 6B); the latter were found tightly correlated with Neuritin and C9orf4, respectively (Figure S6B).

Together, the arrangement of a common inner core and variable extensions toward the periphery promotes formation of AMPARs with the range in size and variability in molecular composition unraveled by our proteomic analyses (Figures 1–4).

DISCUSSION

We showed that native AMPARs in the adult mammalian brain are multiprotein assemblies with unanticipated complexity. Coassembly of the known subunits with the 21 newly identified constituents into core and periphery of the receptor channels generates AMPARs with diverse properties and reflects the complex cell physiology of this main excitatory neurotransmitter receptor.

The Subunit Assembly of Native AMPARs

For thorough analysis of the building blocks of native AMPARs we used two complementary approaches, the ME-AP procedure (Figure 1) for identification of the protein constituents and an advanced BN-MS technique (Figure 2) for determination of their relative molecular abundance and quantitative analysis of the subunit assembly. Comprehensiveness and specificity of the identified AMPAR proteome were ensured by several key features of the ME-AP approach: (1) the use of multiple ABs compensating for the pitfalls intrinsic to individual ABs (Müller et al., 2010; Schulte et al., 2011), (2) sensitivity and dynamic range of our nano-LC MS/MS analysis extending over three to four orders of magnitude (Bildl et al., 2012; Müller et al., 2010),

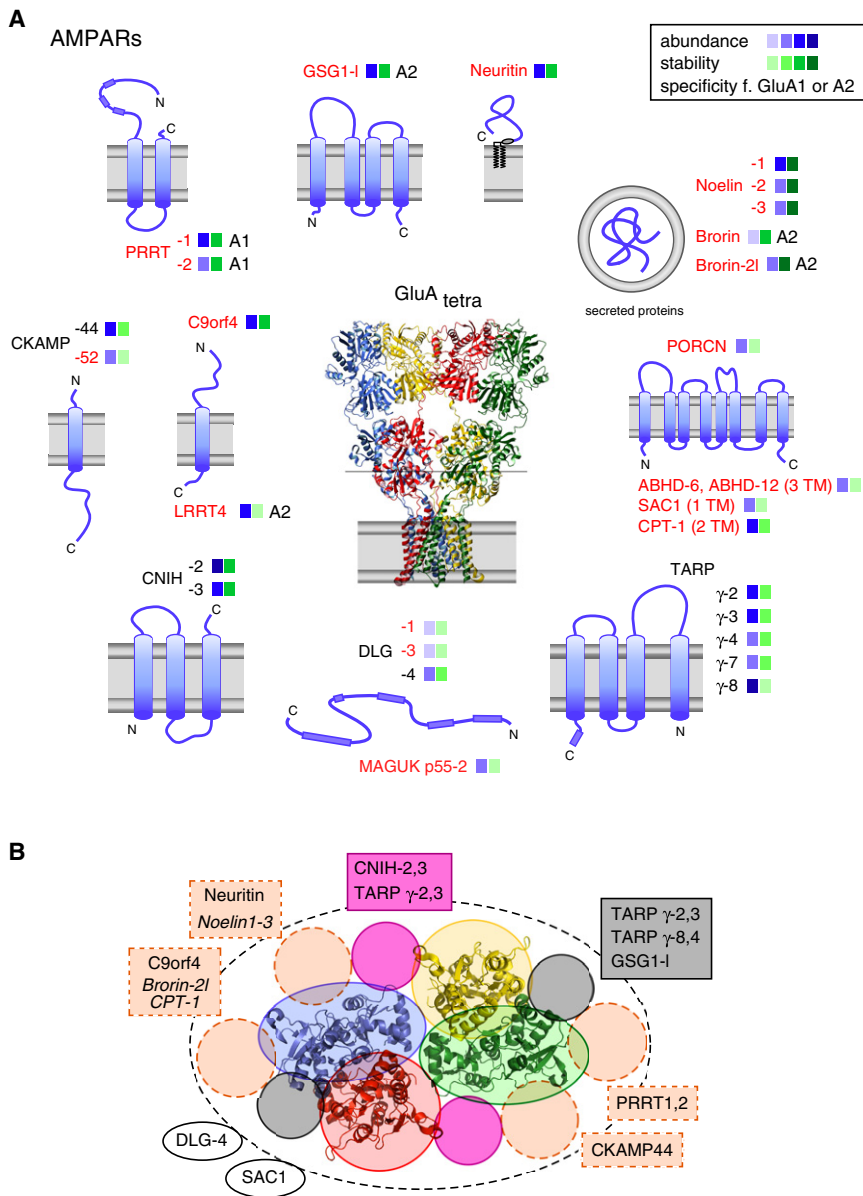


Figure 6. Assembly of Native AMPARs as Determined by Topology and Binding Properties of Their Constituents

(A) Topology of all AMPAR constituents (newly identified proteins in red) and characteristics of their integration into AMPAR complexes. Color coding for their abundance and association stability (from left (minimal) to right (maximal) derived from the data in Figures 2 and 4) in the upper-right corner. Specificity denoted for interaction with GluA1 or GluA2 is indicated.

(B) Model for the assembly of native AMPARs as derived from the proteomic (abundance, stoichiometry of CNIHs and TARPs, populations of AMPARs, Figure 2), biochemical (formation of distinct complexes, direct interaction with GluAs, distinct binding characteristics/stabilities of TARPs γ -8 and γ -2,3, Figures 2–4, Figure S6C), and functional analyses (formation of heteromers from CNIH-2 and GSG1-I, Figures 2 and 5) described in the text and the present knowledge from literature/databases. The view of the GluA-tetramer is from a cross-section of the crystal structure (Sobolevsky et al., 2009) above the membrane plane (gray line in A); solid circles in red and gray depict the suggested asymmetric pairs of binding sites for the indicated inner core constituents; dashed circles in orange are suggested binding sites for the indicated outer core components PRRTs, CKAMP44, C9orf4, and Neuritin that interact directly with the GluA proteins (Figure S6C). The Noelins, Brin-2I, and CPT-1 are boxed with Neuritin and C9orf4 with which they were found tightly correlated (Pearson correlation analyses, Figure S6B). Dashed line in black delineates periphery/entity of the AMPAR complex; open circles indicate constituents without yet defined interaction with the core proteins. AMPAR constituents for which no further information on binding or coassembly is in hand were left out.

and, importantly, (3) the use of control tissue from AB-target knockout animals. In addition, the consistency criterion guaranteed reliability of the identified AMPAR constituents. The resulting well-defined proteome of the AMPARs from rodent brain covered the previously known pore-forming and auxiliary subunits, and in addition identified 21 proteins as novel constituents of AMPAR complexes (Figure 1). Most of them are secreted or TM proteins of low molecular weight, constraints imposing intrinsic difficulties on their detection and quantification by mass spectrometry.

Subsequent BN-MS analysis provided data on the relative molecular abundance of individual AMPAR constituents based on protein quantification by calibration peptides (label-free QconCAT technique, Figures 2 and 4) and directly visualized

multiple populations of AMPARs with different size and molecular composition (Figure 2). In addition, BN-MS was instrumental to monitor the changes in AMPAR composition induced by the distinct stringencies of solubilization buffers (Figures 2 and 4). It is noteworthy that the entire pool of AMPARs was soluble with buffers of mild/intermediate stringency, in line with the significant mobility of AMPARs in the synaptic membrane (Heine et al., 2008), but in marked contrast to NMDA-type glutamate receptors (Figure S2B) or Cav2 channels (Müller et al., 2010) that are both embedded into larger protein networks. Thus, AMPARs are multiprotein complexes of defined size with an architecture characterized by a common core and variable periphery (Figure 6B). This core offers two pairs of asymmetric binding sites that, in the vast majority of AMPARs, are occupied by different types of auxiliary subunits, TARP γ -8 and CNIH-2 being presumably the most abundant combination therein (Figure 2; also Kato et al., 2010). In fact, at one pair of these sites the CNIHs compete with TARPs γ -2,3, in line with a recent

suggestion (Gill et al., 2011), while the other pair may be occupied by TARP γ -2,3,4,8 or the structurally related GSG1-I (Figures 6A and 6B). The stability of association observed for the individual components of core and periphery of the AMPAR complexes may be quite distinct (Figure 4). Consequently, comprehensive analysis of the native AMPARs required solubilization with a set of conditions, rather than use of a single buffer system (Nakagawa et al., 2005; Schulte et al., 2011). In addition, it should be noted that the presented AMPAR proteome relies on the sensitivity and dynamic range of our MS analyses. Thus, proteins interacting with the AMPAR complexes at high dynamics or proteins with very low or highly select expression (resulting in protein amounts < 0.1 femtomole) may have escaped detection (Bildl et al., 2012; Müller et al., 2010).

Implications for AMPAR Physiology in Excitatory Synaptic Transmission

About half of the newly identified AMPAR constituents lack any annotation of primary function(s) in public databases and scientific literature, while others have not yet been investigated for their role in AMPAR function. Thus, the results obtained with the not yet annotated GSG1-I protein are significant in two aspects: first, they assign GSG1-I the role of an inner core constituent modifying the gating of AMPARs similar to the other known auxiliary subunits (Figures 2–5). Second, they demonstrate the distinct functional consequences generated by coassembly of different types of auxiliary subunits into the same AMPAR (Figure 5). This observation emphasizes the general importance of heteromultimeric assemblies, as observed with most AMPARs in the brain (Figures 2 and 3), and indicates that AMPAR functions beyond ligand-driven channel gating may be largely determined by their non-GluA constituents.

For a few of the AMPAR constituents identified here, databases and literature offer some striking links toward AMPAR function and physiology. Thus, the membrane-anchored Neuritin, originally identified as *cpg15* in a screen for plasticity-related genes in the hippocampus (Nedivi et al., 1993), was shown to promote maturation of synapses supposedly by recruiting AMPARs to the postsynapse (Cantallopis et al., 2000). Similar roles may be expected for LRRT4, a member of the LRRTM family of proteins recently shown to promote formation of excitatory synapses (Ko et al., 2009; Linhoff et al., 2009), or for PRRTs 1,2 that are structurally related to SynDIG1, a protein involved in the development of excitatory synapses (Kalashnikova et al., 2010). Finally, CPT-1 and PORCN are TM proteins with enzymatic activities involved in palmitoylation of cysteine residues, a posttranslational modification that was shown to occur on all GluAs and to modulate receptor trafficking (Hayashi et al., 2005); similarly, modulation of AMPAR trafficking related to synaptic plasticity has been reported for the small GTP-binding protein Rap-2b (Hussain et al., 2010; Zhu et al., 2002).

In conclusion, the AMPAR proteome as presented here defines the molecular framework for the complex cell physiology of AMPARs in excitatory synaptic transmission and provides a roadmap for further in-depth structural and functional investigations.

EXPERIMENTAL PROCEDURES

Molecular Biology

Preparation and injection of cRNAs into *Xenopus* oocytes were done as described (Fakler et al., 1995). All cDNAs were verified by sequencing; GenBank accession numbers of the clones used are as follows: M38060.1 (GluA1 α , flip variant of GluA1), NM_017261.2 (GluA2 β), NM_053351 (TARP γ -2), NM_001025132 (CNIH-2), NM_080696.2 (TARP γ -8), XM_574558.2 (GSG1-I), NM_014334.2 (C9orf4), NM_053346.1 (Neuritin), NM_001174086.1 (CKAMP44), and NM_001032285.1 (PRRT1). Characterization of AB-specific immunoreactivity (Figure S5) was done as described in (Schwenk et al., 2009).

Biochemistry

Membrane Protein Solubilization

Plasma membrane-enriched protein fractions were prepared from brains (Berkefeld et al., 2006) of adult rat and mice (pooled from more than 20 WT and one to four knockout animals, respectively). Membrane proteins were solubilized for 30 min at 4°C with one of the following buffers (at 1 mg protein / ml): CL-47, CL-48, CL-91, CL-114 (Logopharm GmbH), Triton-buffer (50 mM Tris/HCl pH 8.0 / 150 mM NaCl / 1% Triton X-100), or RIPA-buffer (50 mM Tris/HCl pH 7.4 / 150 mM NaCl / 1% NP40 / 0.5% Deoxycholate / 0.1% SDS); each buffer was supplemented with freshly added protease inhibitors. Nonsolubilized material was subsequently removed by ultracentrifugation (10 min at 150,000 × g). The efficiency of solubilization was controlled by western blot analysis of SDS-PAGE resolved aliquots of the soluble fraction (supernatant) and the pellets.

Analytical BN-PAGE

Two-dimensional BN-PAGE/SDS-PAGE separations were essentially done as described (Schwenk et al., 2009). Protein complexes were solubilized in CL-47, CL-48, or CL-91 and centrifuged on a sucrose gradient (400,000 × g, 60 min) to replace salt by 0.5 M betaine. For AB-shift experiments the solubilisates were preincubated with the respective ABs for 30 min on ice. After addition of 0.05% Coomassie G250 the samples were separated on linear 3%–8% or 3%–15% polyacrylamide gradient gels in 15 mM BisTris / 50 mM Tricine / 0.01% Coomassie G250 running buffer and 15 mM BisTris (pH 7.0) as anode buffer. A mixture of native proteins (GE Healthcare, USA) and rat mitochondrial membrane protein complexes (Wittig et al., 2010) were run as a standard for complex size in the first dimension. Excised BN-PAGE lanes were incubated for 15 min in Laemmli buffer and placed on top of 10% or 15% SDS-PAGE gels. After electroblotting on PVDF membranes the blot was cut horizontally into different molecular weight ranges and stained with the indicated ABs.

Preparative BN-PAGE

For BN-MS analysis, protein complexes were solubilized from 3 mg (CL-47) or 1 mg (CL-48) rat brain membranes and prepared as detailed above. Samples were resolved on linear 1%–11% polyacrylamide gels (2.5 cm lanes) using the described BN-PAGE buffer system, and the respective gel lanes were collected and frozen at –20°C. The section of interest (~3 × 2 cm) was trimmed, frozen, and sliced in 0.4 mm sections on a cryomicrotome (Leica CM 1950). Slices were thoroughly washed with fixative (30% ethanol / 15% acetic acid) and subjected to in-gel tryptic digestion (81 slices for CL-47 and 69 slices for CL-48 separations).

Affinity Purifications

Solubilisates (1.5 ml) were directly incubated with 10 µg immobilized ABs at 4°C for 2 hr. The following ABs were used for affinity purifications: anti-GluA1-a (Millipore, #AB1504), anti-GluA1-b (Synaptic System, #182-003), anti-GluA1-c (Synaptic System, #182-011), anti-GluA2-a (Millipore, #AB1768), anti-GluA2-b (NeuroMab, #75-002), anti-GluA2-c (Santa Cruz, #sc-7610), anti-GluA2/3 (Millipore, #07-598), anti-GluA3 (Synaptic System, #182-203), anti-GluA4-a (Millipore, #AB1508), anti-GluA4-b (Santa Cruz, #sc-7614), anti-CNIH-2/3 (Hoshino et al., 2007), anti-TARP γ -8 (Frontier Institute, RB Af1000-1), anti-TARP γ -2 (Upstate, #07-577), anti-CKAMP44 (kind gift of Dr. R. Sprengel, von Engelhardt et al., 2010), anti-GSG1-like (raised in rabbit against aa 257–278 of Swiss-Prot accession Q6UXU4, affinity purified), anti-PRRT1 (raised in rabbit against aa 36–54 of Swiss-Prot accession Q6MG82, affinity purified), anti-Noelin1 (R&D Systems, #AF4636), and anti-FLAG (Sigma, #F3165). After brief washing with the respective detergent buffer bound

proteins were eluted with Laemmli buffer (DTT added after elution). Isolated proteins were shortly run into SDS-PAGE gels, silver stained, cut in two pieces of MW > 50 and MW < 50 kDa, and in-gel digested with trypsin (Pandey and Mann, 2000).

Western analyses were performed with anti-GluA1-a, anti-GluA2 (Millipore, MAB397), anti-GluA2/3, anti-GluA3, anti-GluA4-a, anti-TARP γ -2, anti-TARP γ -8, anti-CKAMP44, anti-GSG1-like (Sigma, #HPA014479), and anti-CNIH-2/3 ABs. The AB-stained bands were visualized by anti-mouse, -rabbit, -goat IgG-HRP (all Santa Cruz), and ECL+ (GE Healthcare).

QconCAT Calibration Standard

Two to six consistent peptides specific for each of the identified AMPAR constituents (Table S4) as well as three control proteins were selected and randomly fused in silico to form three N- and C-terminally tagged standard (QconCAT) proteins (84, 60, and 82 peptides resulting in QconCAT proteins of 907 aa, 743 aa, and 942 aa, respectively). The corresponding gene sequences were synthesized (GenScript) and subcloned in a modified pET16 vector; calibration proteins were expressed in *Escherichia coli* BL21(DE3). After verification of full-length expression by dual western blots using anti-tag ABs, two-fold dilutions of the QconCAT proteins (seven to nine steps) were separated by SDS-PAGE. The corresponding protein bands were visualized by Coomassie staining, excised, and separately digested by trypsin for subsequent triplicate mass spectrometric analysis.

Mass Spectrometry

LC-MS/MS Analysis

Extracted postdigest peptide mixtures dissolved in 0.5% (v/v) trifluoroacetic acid were analyzed by nano-LC-MS/MS with a LTQ FT Ultra mass spectrometer as described (Müller et al., 2010). Precursor signals were acquired with a target value of 1,000,000 and a nominal resolution of 100,000 (FWHM) at m/z 400 (scan range 370 to 1700 m/z). Up to five data-dependent CID fragment spectra per scan cycle were acquired in the ion trap with a target value of 10,000 (maximum injection time 400 ms) with dynamic exclusion enabled. Total MS acquisition times were 105 min (75 min rising acetonitrile concentration, 30 s dynamic MS/MS exclusion) for AP eluate fractions and 170 min (140 min rising acetonitrile concentration, 60 s dynamic MS/MS exclusion) for BN-PAGE fractions, respectively.

Database Search

LC-MS/MS data was extracted using the extract_msn utility and searched against the UniProt Knowledgebase release 2010_11 using the Mascot search engine (version 2.3.01; Matrix Science) with tolerance for peptide mass and fragment mass set to 15 ppm and 0.8 ppm, respectively. One missed trypsin cleavage and common variable modifications were accepted for peptide identification. After linear shift mass recalibration the peptide mass window was narrowed to \pm 5 ppm for final searches. The final search database contained all UniProtKB/Swiss-Prot entries for *Mus musculus*, *Rattus norvegicus*, and *Homo sapiens* including P00761, P00766, P02769, P11886, and P41921 as well as 22 UniProtKB/TrEMBL homologs to previously (in the course of this study) identified AMPAR complex constituents of these species. Proteins identified by only one specific MS/MS spectrum were not further considered. The average effective peptide FDR for all evaluated proteins (calculated as the number of corresponding peptides identified with a Mascot ion score \geq 20 for the real database versus respective hits in a decoy database) was 0.029 (SD 0.021).

Relative Amino Acid Sequence Coverage

Relative amino acid sequence coverage of proteins (Figures 1D and Table S2) was calculated as SC = Ni / (Ni + Nan), where Ni is the number of amino acid residues covered by identified peptides (Mascot e-value $<$ 0.05, retrieval in $>$ 2 independent APs) and Nan is the number of MS-accessible (peptides within 740 $<$ MW $<$ 3,000 with trypsin cleavage C-terminal to the basic amino acids, but not N-terminal to proline; missed cleavages were not considered) but not identified amino acids in the respective database sequence.

Protein Quantification Procedures

For peak volume-based quantification, m/z features along LC-MS scans were detected and quantified (as intensity \times retention time \times m/z width) using msInspect (Computational Proteomics Laboratory, Fred Hutchinson Cancer Research Center, Seattle, WA, USA). After correction of m/z shifts (based on MS-sequenced peptides using an in-house written script), features were

aligned between different LC-MS/MS runs and assigned to the peptides identified by Mascot (retention time tolerance: 3% or 1 min, m/z difference threshold: \pm 5 ppm). The resulting peptide peak volumes (PVs) were used for two different quantification procedures.

Protein Abundance Ratios (rPV). In AP versus control (Figure 1), these were determined using the TopCorr method detailed in (Bildl et al., 2012; Supplemental Experimental Procedures). Protein rPV values were plotted for each AB (AP versus controls, e.g., Figure 1B) to derive specificity thresholds from the resulting ratio distributions. Proteins were considered specifically copurified when rPV(versus IgG) $>$ threshold(IgG) in both rat and mouse, and no cross-reactivity was indicated by rPV(versus KO) $<$ threshold(versus KO) (Figure 1).

Relative Molar Abundances of Proteins. In a sample (Figures 2 and 4), these were determined as follows: dilution series of the QconCAT proteins (total of 171 peptides, see above) were measured by LC-MS/MS three times and the extracted peptide PVs checked for reproducibility and linearity over at least two orders of magnitude. For each peptide slope factors were determined by linear regression fits to the measured PVs versus dilution factor of the load reflecting each peptide's specific MS signal intensity (Figure S2; loads of the three concatenated standards were normalized to each other by their abundance_{norm} values; Zolles et al., 2009). These slope factors were then used to normalize the respective peptide PVs in APs or BN-PAGE slices to an equimolar basis. The relative molar abundance of each protein was then calculated as intensity-weighted mean (AP data sets) or median (BN-PAGE samples) of the respective normalized peptide PVs. To establish *protein profiles* across BN-PAGE samples (Figure 2), the respective PV tables were preprocessed: (1) each individual slice measurement (i.e., LC-MS data set) was scaled by dividing its average PV to a sliding average PV of the neighboring two slices (window of 5) to account for variations in slice thickness, peptide recovery and LC-MS sensitivity and (2) a filter was applied to eliminate false-positive PV assignments (identified as solitary values without backup from the neighboring two slices or $>$ 10-fold outliers with respect to the average of corresponding PVs in the neighboring two slices) and to bridge gaps resulting from false-negative assignments (individual missing values were replaced by the corresponding PV average of the neighboring slices, if available). The resulting relative molar protein abundances were finally smoothed by averaging (window of 3).

Electron Microscopy

Hippocampal sections of adult Wistar rats (CA3 area, 80 nm thick) were processed for the postembedding immunogold labeling as described earlier (Kulik et al., 2002; Schwenk et al., 2009) and stained with affinity-purified mouse anti-GluA2/4 (Millipore, #MAB396) and two different rabbit anti-GSG1-I ABs (raised against aa 83–102 and aa 257–278; Figure S5B). Secondary ABs (1:20; British Biocell International, Cardiff, UK) were coupled to either 10 nm gold particles (for GluR2/4) or 15 nm gold particles (for GSG1-I).

Electrophysiological Recordings and Data Analysis

Electrophysiological recordings from giant outside-out patches excised from oocytes were performed at room temperature (22°C–24°C) as described previously (Berkefeld et al., 2006). Currents were recorded with an EPC9 amplifier, low-pass filtered at 3 kHz and sampled at 5–10 kHz. Pipettes made from thick-walled borosilicate glass had resistances of 0.4–0.8 M Ω when filled with intracellular solution (K_{int} , in mM) 120 KCl, 5 HEPES, 10 EGTA, pH adjusted to 7.2. Extracellular solution (K_{ext}) applied to outside-out patches was composed as follows (mM): 120 KCl, 5 HEPES, 1.3 CaCl₂ (pH 7.2). Rapid application/removal of glutamate (1 mM, dissolved in K_{ex}) was performed using a Piezo-controlled fast application system with a double-barrel application pipette that enables solution exchanges within less than 100 μ s (20%–80%, measured from the open tip response during a switch between normal and 10 \times -diluted K_{ext}).

Deactivation, desensitization, and recovery from desensitization of AMPARs were characterized by time constants derived from monoexponential fits to the decay phase or recovery of the glutamate-activated currents; the quality of the fit result was judged from the sum of squared differences value. Curve fitting and further data analysis were done with Igor Pro 4.05A Carbon. Data in text and figures are given as mean \pm SD, unless specified differently.

SUPPLEMENTAL INFORMATION

Supplemental Information includes six figures, Supplemental Experimental Procedures, and four tables and can be found with this article online at doi:10.1016/j.neuron.2012.03.034.

ACKNOWLEDGMENTS

We thank J.P. Adelman for insightful comments and critical reading of the manuscript and A. Haupt for help with bioinformatics; moreover, we are indebted to R. Sprengel for GluA knockout animals. This work was supported by grants of the Deutsche Forschungsgemeinschaft to B.F. (SFB 746/TP16, SFB780/A3) and to A.K. (SFB780/A2).

Accepted: March 13, 2012

Published: May 23, 2012

REFERENCES

- Bats, C., Groc, L., and Choquet, D. (2007). The interaction between Stargazin and PSD-95 regulates AMPA receptor surface trafficking. *Neuron* 53, 719–734.
- Berkefeld, H., Sailer, C.A., Bildl, W., Rohde, V., Thumfart, J.O., Eble, S., Klugbauer, N., Reisinger, E., Bischofberger, J., Oliver, D., et al. (2006). BKCa-Cav channel complexes mediate rapid and localized Ca^{2+} -activated K^+ signaling. *Science* 314, 615–620.
- Bildl, W., Haupt, A., Muller, C.S., Binossek, M., Thumfart, J.O., Hüber, B., Fakler, B., and Schulte, U. (2012). Extending the dynamic range of label-free mass spectrometric quantification of affinity purifications. *Mol. Cell. Proteomics*. 11, M111.007955.
- Bredt, D.S., and Nicoll, R.A. (2003). AMPA receptor trafficking at excitatory synapses. *Neuron* 40, 361–379.
- Cantallops, I., Haas, K., and Cline, H.T. (2000). Postsynaptic CPG15 promotes synaptic maturation and presynaptic axon arbor elaboration *in vivo*. *Nat. Neurosci.* 3, 1004–1011.
- Carroll, R.C., Beattie, E.C., von Zastrow, M., and Malenka, R.C. (2001). Role of AMPA receptor endocytosis in synaptic plasticity. *Nat. Rev. Neurosci.* 2, 315–324.
- Chen, L., Chetkovich, D.M., Petralia, R.S., Sweeney, N.T., Kawasaki, Y., Wenthold, R.J., Bredt, D.S., and Nicoll, R.A. (2000). Stargazin regulates synaptic targeting of AMPA receptors by two distinct mechanisms. *Nature* 408, 936–943.
- Cho, C.H., St-Gelais, F., Zhang, W., Tomita, S., and Howe, J.R. (2007). Two families of TARP isoforms that have distinct effects on the kinetic properties of AMPA receptors and synaptic currents. *Neuron* 55, 890–904.
- Choquet, D. (2010). Fast AMPAR trafficking for a high-frequency synaptic transmission. *Eur. J. Neurosci.* 32, 250–260.
- Choquet, D., and Triller, A. (2003). The role of receptor diffusion in the organization of the postsynaptic membrane. *Nat. Rev. Neurosci.* 4, 251–265.
- Collingridge, G.L., Olsen, R.W., Peters, J., and Spedding, M. (2009). A nomenclature for ligand-gated ion channels. *Neuropharmacology* 56, 2–5.
- Conti, F., and Weinberg, R.J. (1999). Shaping excitation at glutamatergic synapses. *Trends Neurosci.* 22, 451–458.
- Cull-Candy, S., Kelly, L., and Farrant, M. (2006). Regulation of Ca^{2+} -permeable AMPA receptors: synaptic plasticity and beyond. *Curr. Opin. Neurobiol.* 16, 288–297.
- Derkach, V.A., Oh, M.C., Guire, E.S., and Soderling, T.R. (2007). Regulatory mechanisms of AMPA receptors in synaptic plasticity. *Nat. Rev. Neurosci.* 8, 101–113.
- Fakler, B., Brändle, U., Glowatzki, E., Weidemann, S., Zenner, H.P., and Ruppertsberg, J.P. (1995). Strong voltage-dependent inward rectification of inward rectifier K^+ channels is caused by intracellular spermine. *Cell* 80, 149–154.
- Garaschuk, O., Schneggenburger, R., Schirra, C., Tempia, F., and Konnerth, A. (1996). Fractional Ca^{2+} currents through somatic and dendritic glutamate receptor channels of rat hippocampal CA1 pyramidal neurones. *J. Physiol.* 491, 757–772.
- Gill, M.B., Kato, A.S., Roberts, M.F., Yu, H., Wang, H., Tomita, S., and Bredt, D.S. (2011). Cornichon-2 modulates AMPA receptor-transmembrane AMPA receptor regulatory protein assembly to dictate gating and pharmacology. *J. Neurosci.* 31, 6928–6938.
- Harmel, N., Cokic, B., Zolles, G., Berkefeld, H., Mauric, V., Fakler, B., Stein, V., and Klöcker, N. (2012). AMPA receptors commandeer an ancient cargo exporter for use as an auxiliary subunit for signaling. *PLoS ONE* 7, e30681.
- Hayashi, T., Rumbaugh, G., and Huganir, R.L. (2005). Differential regulation of AMPA receptor subunit trafficking by palmitoylation of two distinct sites. *Neuron* 47, 709–723.
- Heine, M., Groc, L., Frischknecht, R., Béïque, J.C., Lounis, B., Rumbaugh, G., Huganir, R.L., Cognet, L., and Choquet, D. (2008). Surface mobility of postsynaptic AMPARs tunes synaptic transmission. *Science* 320, 201–205.
- Hollmann, M., and Heinemann, S. (1994). Cloned glutamate receptors. *Annu. Rev. Neurosci.* 17, 31–108.
- Hoshino, H., Uchida, T., Otsuki, T., Kawamoto, S., Okubo, K., Takeichi, M., and Chisaka, O. (2007). Cornichon-like protein facilitates secretion of HB-EGF and regulates proper development of cranial nerves. *Mol. Biol. Cell* 18, 1143–1152.
- Hussain, N.K., Hsin, H., Huganir, R.L., and Sheng, M. (2010). MINK and TNIK differentially act on Rap2-mediated signal transduction to regulate neuronal structure and AMPA receptor function. *J. Neurosci.* 30, 14786–14794.
- Jonas, P. (2000). The Time Course of Signaling at Central Glutamatergic Synapses. *News Physiol. Sci.* 15, 83–89.
- Jonas, P., and Spruston, N. (1994). Mechanisms shaping glutamate-mediated excitatory postsynaptic currents in the CNS. *Curr. Opin. Neurobiol.* 4, 366–372.
- Kalashnikova, E., Lorca, R.A., Kaur, I., Barisone, G.A., Li, B., Ishimaru, T., Trimmer, J.S., Mohapatra, D.P., and Diaz, E. (2010). SynDIG1: an activity-regulated, AMPA-receptor-interacting transmembrane protein that regulates excitatory synapse development. *Neuron* 65, 80–93.
- Kato, A.S., Gill, M.B., Ho, M.T., Yu, H., Tu, Y., Siuda, E.R., Wang, H., Qian, Y.W., Nisenbaum, E.S., Tomita, S., and Bredt, D.S. (2010). Hippocampal AMPA receptor gating controlled by both TARP and cornichon proteins. *Neuron* 68, 1082–1096.
- Kim, K.S., Yan, D., and Tomita, S. (2010). Assembly and stoichiometry of the AMPA receptor and transmembrane AMPA receptor regulatory protein complex. *J. Neurosci.* 30, 1064–1072.
- Ko, J., Fuccillo, M.V., Malenka, R.C., and Südhof, T.C. (2009). LRRTM2 functions as a neurexin ligand in promoting excitatory synapse formation. *Neuron* 64, 791–798.
- Kulik, A., Nakadate, K., Nyiri, G., Notomi, T., Malitschek, B., Bettler, B., and Shigemoto, R. (2002). Distinct localization of GABA(B) receptors relative to synaptic sites in the rat cerebellum and ventrobasal thalamus. *Eur. J. Neurosci.* 15, 291–307.
- Linhoff, M.W., Laurén, J., Cassidy, R.M., Dobie, F.A., Takahashi, H., Nygaard, H.B., Airaksinen, M.S., Strittmatter, S.M., and Craig, A.M. (2009). An unbiased expression screen for synaptogenic proteins identifies the LRRTM protein family as synaptic organizers. *Neuron* 61, 734–749.
- Malenka, R.C., and Nicoll, R.A. (1999). Long-term potentiation—a decade of progress? *Science* 285, 1870–1874.
- Malinow, R., and Malenka, R.C. (2002). AMPA receptor trafficking and synaptic plasticity. *Annu. Rev. Neurosci.* 25, 103–126.
- McAllister, A.K. (2007). Dynamic aspects of CNS synapse formation. *Annu. Rev. Neurosci.* 30, 425–450.
- McKinney, R.A. (2010). Excitatory amino acid involvement in dendritic spine formation, maintenance and remodelling. *J. Physiol.* 588, 107–116.
- Milstein, A.D., Zhou, W., Karimzadegan, S., Bredt, D.S., and Nicoll, R.A. (2007). TARP subtypes differentially and dose-dependently control synaptic AMPA receptor gating. *Neuron* 55, 905–918.

- Müller, C.S., Haupt, A., Bildl, W., Schindler, J., Knaus, H.G., Meissner, M., Rammner, B., Striessnig, J., Flockerzi, V., Fakler, B., and Schulte, U. (2010). Quantitative proteomics of the Cav2 channel nano-environments in the mammalian brain. *Proc. Natl. Acad. Sci. USA* 107, 14950–14957.
- Nakagawa, T., Cheng, Y., Ramm, E., Sheng, M., and Walz, T. (2005). Structure and different conformational states of native AMPA receptor complexes. *Nature* 433, 545–549.
- Nedivi, E., Hevroni, D., Naot, D., Israeli, D., and Citri, Y. (1993). Numerous candidate plasticity-related genes revealed by differential cDNA cloning. *Nature* 363, 718–722.
- Newpher, T.M., and Ehlers, M.D. (2008). Glutamate receptor dynamics in dendritic microdomains. *Neuron* 58, 472–497.
- Pandey, A., and Mann, M. (2000). Proteomics to study genes and genomes. *Nature* 405, 837–846.
- Pratt, J.M., Simpson, D.M., Doherty, M.K., Rivers, J., Gaskell, S.J., and Beynon, R.J. (2006). Multiplexed absolute quantification for proteomics using concatenated signature peptides encoded by QconCAT genes. *Nat. Protoc.* 1, 1029–1043.
- Raman, I.M., and Trussell, L.O. (1992). The kinetics of the response to glutamate and kainate in neurons of the avian cochlear nucleus. *Neuron* 9, 173–186.
- Remmerie, N., De Vijlder, T., Valkenborg, D., Laukens, K., Smets, K., Vreeken, J., Mertens, I., Carpenter, S.C., Panis, B., De Jaeger, G., et al. (2011). Unraveling tobacco BY-2 protein complexes with BN PAGE/LC-MS/MS and clustering methods. *J. Proteomics* 74, 1201–1217.
- Sah, P., Hestrin, S., and Nicoll, R.A. (1990). Properties of excitatory postsynaptic currents recorded in vitro from rat hippocampal interneurons. *J. Physiol.* 430, 605–616.
- Schober, D.A., Gill, M.B., Yu, H., Gernert, D.L., Jeffries, M.W., Ornstein, P.L., Kato, A.S., Felder, C.C., and Bredt, D.S. (2011). Transmembrane AMPA receptor regulatory proteins and cornichon-2 allosterically regulate AMPA receptor antagonists and potentiators. *J. Biol. Chem.* 286, 13134–13142.
- Schulte, U., Müller, C.S., and Fakler, B. (2011). Ion channels and their molecular environments—glimpses and insights from functional proteomics. *Semin. Cell Dev. Biol.* 22, 132–144.
- Schwenk, J., Harmel, N., Zolles, G., Bildl, W., Kulik, A., Heimrich, B., Chisaka, O., Jonas, P., Schulte, U., Fakler, B., and Klöcker, N. (2009). Functional proteomics identify cornichon proteins as auxiliary subunits of AMPA receptors. *Science* 323, 1313–1319.
- Schwenk, J., Metz, M., Zolles, G., Turecek, R., Fritzius, T., Bildl, W., Tarusawa, E., Kulik, A., Unger, A., Ivankova, K., et al. (2010). Native GABA(B) receptors are heteromultimers with a family of auxiliary subunits. *Nature* 465, 231–235.
- Seeburg, P.H. (1993). The TINS/TiPS Lecture. The molecular biology of mammalian glutamate receptor channels. *Trends Neurosci.* 16, 359–365.
- Shepherd, J.D., and Huganir, R.L. (2007). The cell biology of synaptic plasticity: AMPA receptor trafficking. *Annu. Rev. Cell Dev. Biol.* 23, 613–643.
- Shi, Y., Lu, W., Milstein, A.D., and Nicoll, R.A. (2009). The stoichiometry of AMPA receptors and TARPs varies by neuronal cell type. *Neuron* 62, 633–640.
- Shi, Y., Suh, Y.H., Milstein, A.D., Isozaki, K., Schmid, S.M., Roche, K.W., and Nicoll, R.A. (2010). Functional comparison of the effects of TARPs and cornichons on AMPA receptor trafficking and gating. *Proc. Natl. Acad. Sci. USA* 107, 16315–16319.
- Silver, R.A., Traynelis, S.F., and Cull-Candy, S.G. (1992). Rapid-time-course miniature and evoked excitatory currents at cerebellar synapses in situ. *Nature* 355, 163–166.
- Sobolevsky, A.I., Rosconi, M.P., and Gouaux, E. (2009). X-ray structure, symmetry and mechanism of an AMPA-subtype glutamate receptor. *Nature* 462, 745–756.
- Soto, D., Coombs, I.D., Kelly, L., Farrant, M., and Cull-Candy, S.G. (2007). Stargazin attenuates intracellular polyamine block of calcium-permeable AMPA receptors. *Nat. Neurosci.* 10, 1260–1267.
- Soto, D., Coombs, I.D., Renzi, M., Zonouzi, M., Farrant, M., and Cull-Candy, S.G. (2009). Selective regulation of long-form calcium-permeable AMPA receptors by an atypical TARP, gamma-5. *Nat. Neurosci.* 12, 277–285.
- Tomita, S., Chen, L., Kawasaki, Y., Petralia, R.S., Wenthold, R.J., Nicoll, R.A., and Bredt, D.S. (2003). Functional studies and distribution define a family of transmembrane AMPA receptor regulatory proteins. *J. Cell Biol.* 161, 805–816.
- Tomita, S., Adesnik, H., Sekiguchi, M., Zhang, W., Wada, K., Howe, J.R., Nicoll, R.A., and Bredt, D.S. (2005). Stargazin modulates AMPA receptor gating and trafficking by distinct domains. *Nature* 435, 1052–1058.
- Vandenbergh, W., Nicoll, R.A., and Bredt, D.S. (2005). Stargazin is an AMPA receptor auxiliary subunit. *Proc. Natl. Acad. Sci. USA* 102, 485–490.
- von Engelhardt, J., Mack, V., Sprengel, R., Kaverstock, N., Li, K.W., Stern-Bach, Y., Smit, A.B., Seeburg, P.H., and Monyer, H. (2010). CKAMP44: a brain-specific protein attenuating short-term synaptic plasticity in the dentate gyrus. *Science* 327, 1518–1522.
- Wessels, H.J., Vogel, R.O., van den Heuvel, L., Smeitink, J.A., Rodenburg, R.J., Nijtmans, L.G., and Farhoud, M.H. (2009). LC-MS/MS as an alternative for SDS-PAGE in blue native analysis of protein complexes. *Proteomics* 9, 4221–4228.
- Wittig, I., Beckhaus, T., Wumaier, Z., Karas, M., and Schägger, H. (2010). Mass estimation of native proteins by blue native electrophoresis: principles and practical hints. *Mol. Cell. Proteomics* 9, 2149–2161.
- Zhu, J.J., Qin, Y., Zhao, M., Van Aelst, L., and Malinow, R. (2002). Ras and Rap control AMPA receptor trafficking during synaptic plasticity. *Cell* 110, 443–455.
- Zolles, G., Wenzel, D., Bildl, W., Schulte, U., Hofmann, A., Müller, C.S., Thumfart, J.O., Vlachos, A., Deller, T., Pfeifer, A., et al. (2009). Association with the auxiliary subunit PEX5R/Trip8b controls responsiveness of HCN channels to cAMP and adrenergic stimulation. *Neuron* 62, 814–825.

High-Resolution Proteomics Unravel Architecture and Molecular Diversity of Native AMPA Receptor Complexes

Jochen Schwenk, Nadine Harmel, Aline Brechet, Gerd Zolles, Henrike Berkefeld, Catrin Swantje Müller, Wolfgang Bildl, David Baehrens, Björn Hüber, Akos Kulik, Nikolaj Klöcker, Uwe Schulte, and Bernd Fakler

Figure S1 (information related to Figure 1)

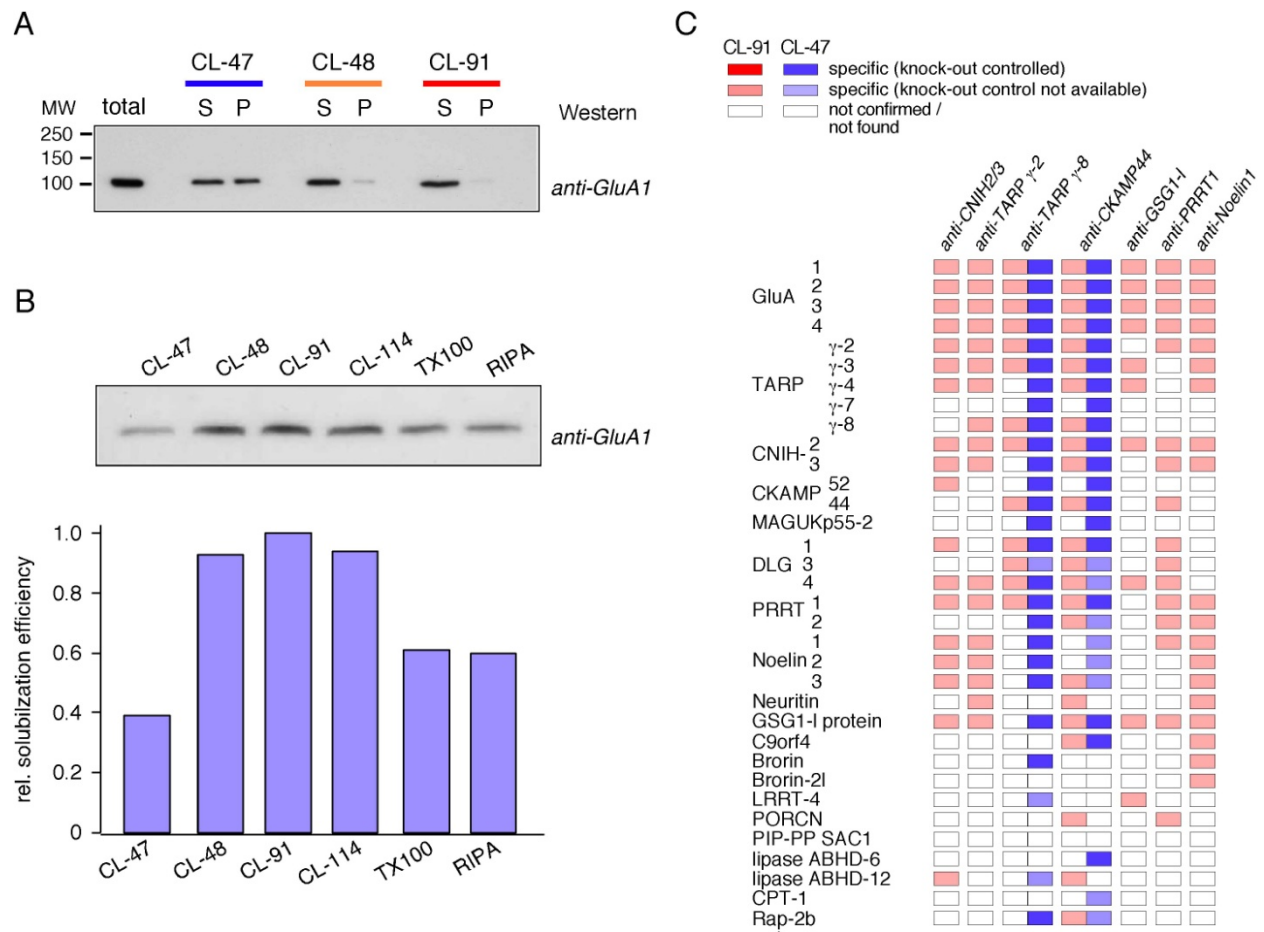
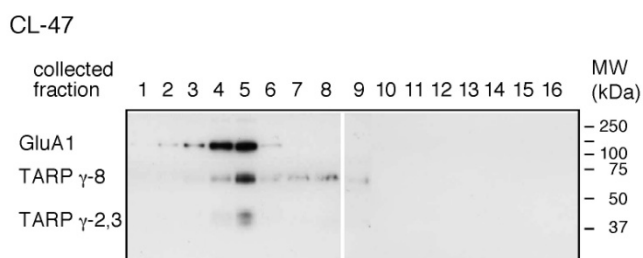
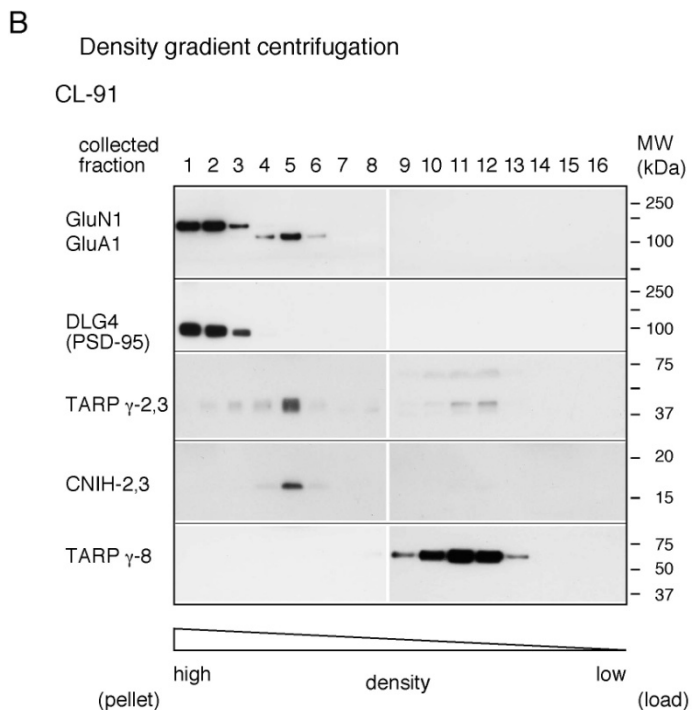
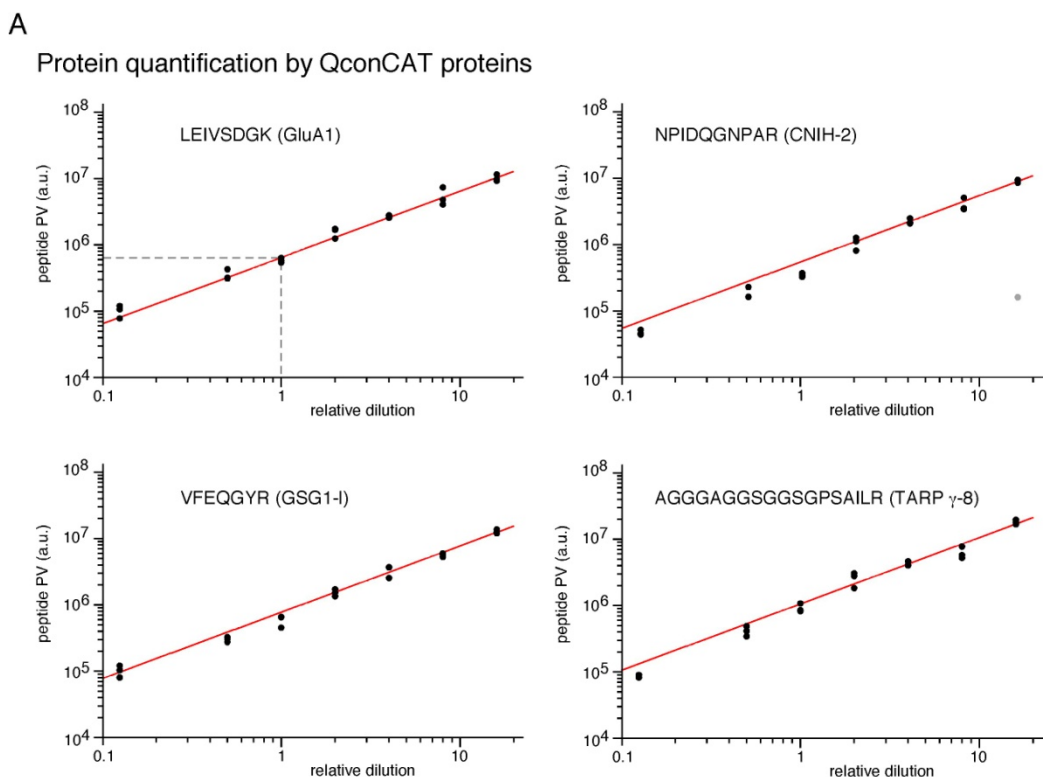


Figure S1

Solubilization efficiency of AMPARs in rat brain membrane fractions and APs of AMPARs using ABs targeting identified complex constituents. (A) SDS-PAGE separation of solubilized (S) and non-solubilized (P) protein fractions obtained with buffers CL-47, CL-48, CL-91 from rat brain membranes. Protein separations were Western-blotted and probed with an *anti-GluA1* AB; MW as indicated. (B) Bar graph illustrating relative solubilization efficiency of GluA1 determined from densitometric analysis of the Western probed protein separations shown in the upper panel. Densitometric signals were normalized to that obtained with CL-91. (C) Table (as in Figure 1D) indicating specific co-purification determined for the finally annotated AMPAR constituents across the APs performed under solubilization with buffers CL-91 (in red) or CL-47 (in blue) with ABs targeting the indicated AMPAR constituents. Colour coding is given in the upper left.

Figure S2 (information related to Figure 2)



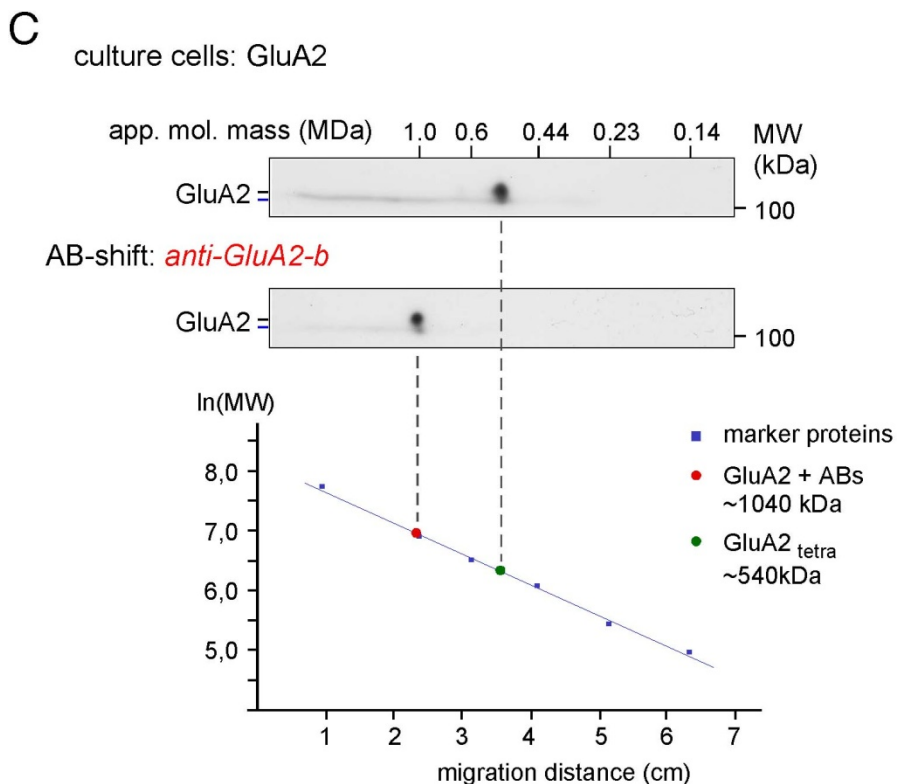


Figure S2

Protein quantification by the QconCAT method and stability of AMPAR complexes under solubilization conditions CL-91 and CL-47. (A) Plot of PVs determined for the indicated protein-specific peptides as a function of the amount of QconCAT protein (given as relative dilution). Data points were obtained from triplicate measurements and used for a line-fit (red line); the slope factor yielded by this fit (further details at www.channelproteomes.com/projects) was used for quantification of the respective AMPAR constituent. Double-logarithmic axes were used for illustrating linearity of the PV-amount relation and for estimating the quality of the fit. Dashed line (at dilution 1) indicates the slope factor (through the respective value at the y-axis). (B) TARP g-8, but not TARPs g-2,3, dissociates from AMPAR complexes in buffers of intermediate stringency. SDS-PAGE separation of protein fractions obtained from density gradient centrifugations of rat brain membranes solubilized (without prior ultracentrifugation) with CL-91 (upper panel) or CL-47 (lower panel), Western-probed with ABs specific for the indicated proteins. Note the distinct behaviour of TARPs g-8 and g-2,3, and the small overlap of GluA1 with GluN1 (NR1 subunit of the NMDA-type glutamate receptors).

(C) AB-shift assay (see also Figure 3) with the *anti-GluA2-b* AB performed on membrane fractions from tsA201-cells transfected with GluA2-specific cDNA (upper panel). Calibration of the BN-PAGE separation by marker proteins of distinct molecular mass (lower panel) allowed for determination of the apparent molecular mass of the GluA2 assemblies in the absence and presence of the AB. Thus, the molecular mass of GluA2 tetramers is about 0.5 MDa, the additional weight introduced by the *anti-GluA2* ABs is about 0.6 MDa, equivalent to 4 IgGs per GluA2 tetramer. Note the sharp focusing of the GluA2 homo-tetramers (in the absence and presence of the *anti-GluA2* ABs) in the BN-PAGE.

Figure S3 (information related to Figure 3)

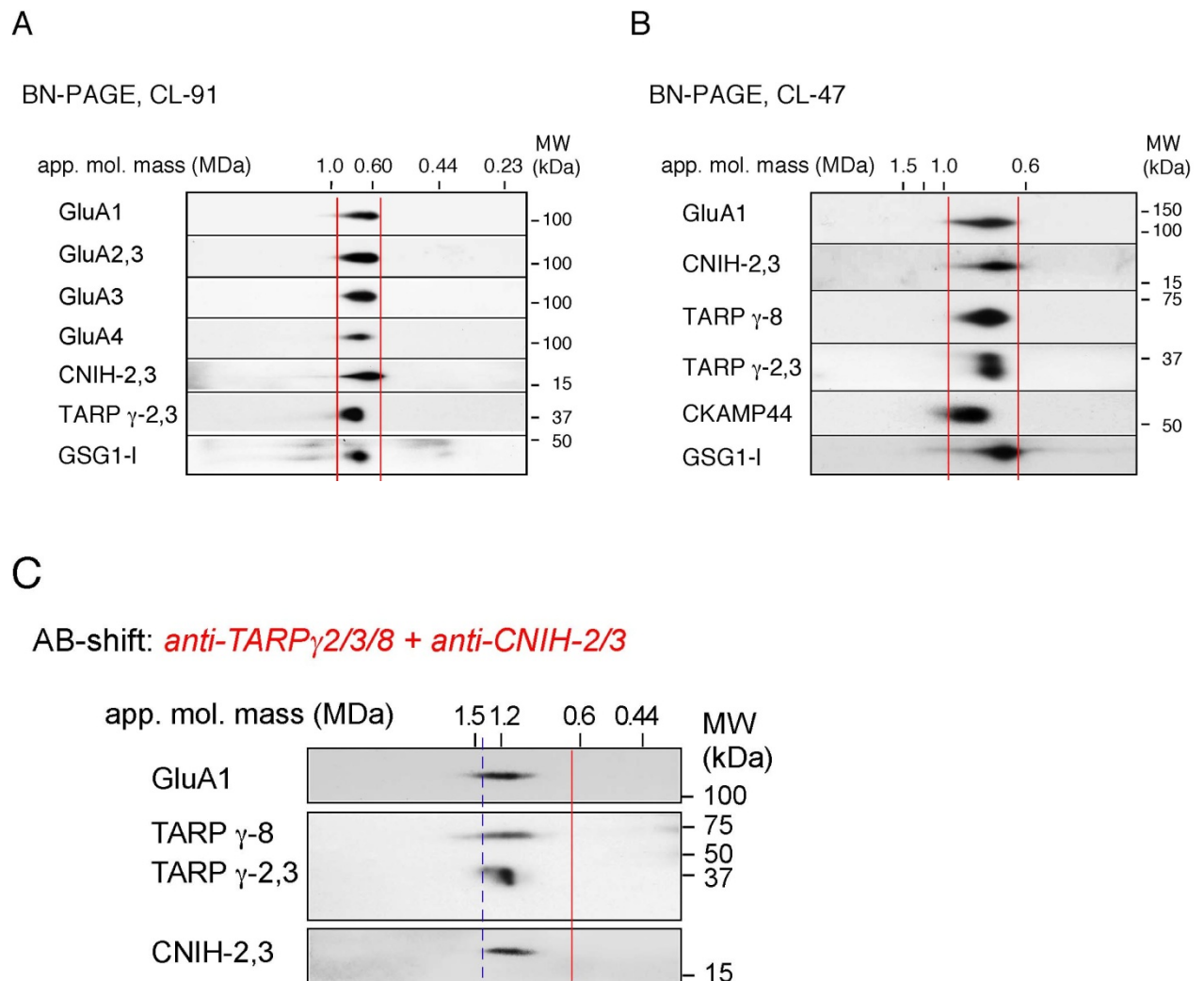


Figure S3

(A, B) Two-dimensional BN-PAGE/SDS-PAGE separation of native AMPARs in membrane fractions solubilized with CL-91 (A) or CL-47 (B), Western-probed with the ABs against the indicated AMPAR constituents. (C) AB-shift assay as in Figure 3 performed with the indicated ABs added to membrane fractions from rat brain solubilized with CL-47. Dotted line denotes apparent mass of 1.4 MDa (equivalent to the inner core of AMPARs (~0.7 MDa) plus 4 ABs (about 0.6-0.7 MDa)).

Figure S4 (information related to Figure 4)

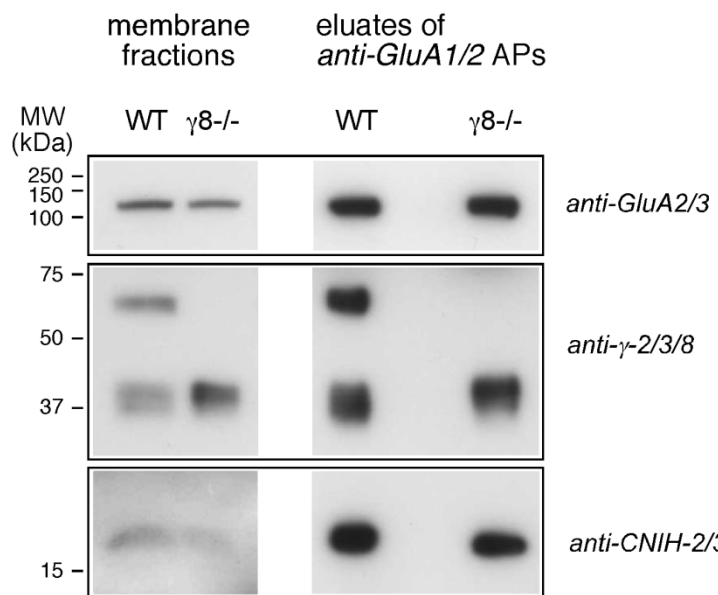


Figure S4

Assembly of AMPAR complexes is independent of the TARP g-8 protein.

Source material and eluates of APs with ABs targeting GluA1 and GluA2 from membrane fractions prepared either from WT or TARP g-8 knock-out mice. Both, input and eluates were separated by SDS-PAGE and Western-probed with the indicated ABs.

Figure S5 (information related to Figure 5)

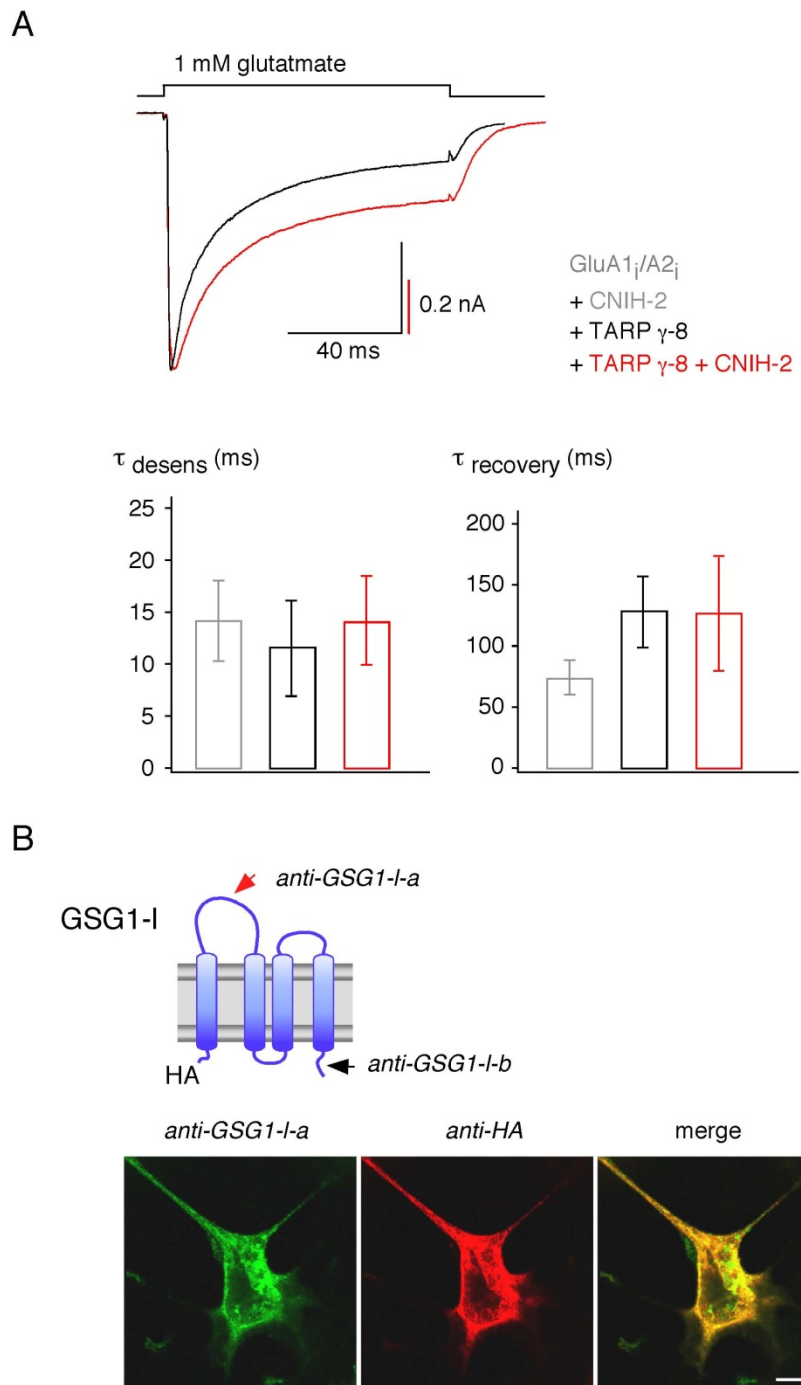


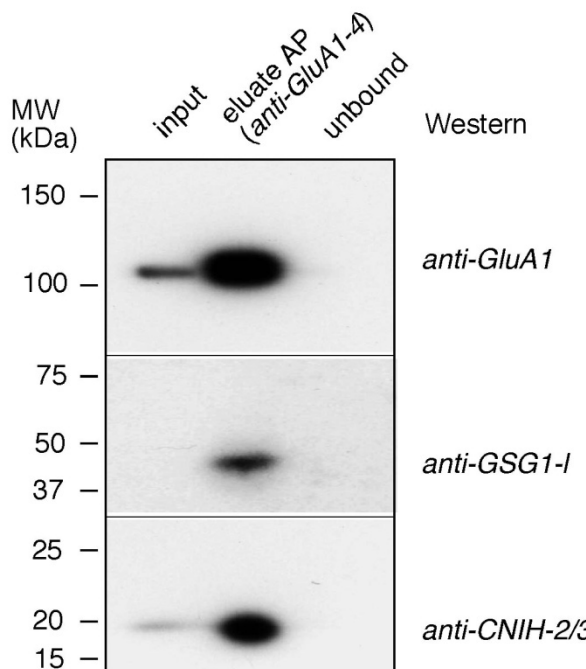
Figure S5

(A) Modulation of gating by assembly and co-assembly of TARP g-8 and CNIH-2. Upper panel: Representative current traces recorded upon 100-ms applications of 1 mM glutamate in giant outside-out patches with AMPARs assembled from the indicated proteins in *Xenopus* oocytes. Lower panel: Bar graph summarizing the results on receptor gating determined as in Figure 5; data are mean \pm SD of 8-19 experiments.

(B) Characterization of the immunoreactivity of anti-GSG1-I ABs. (A) Upper panel: Epitope localization of the indicated ABs on the GSG1-I protein. Lower panel: Staining of permeabilized tsA cells expressing N-terminally HA-tagged GSG1-I protein with anti-GSG1-I-a (left) or anti-HA (middle); right image is merge of left and middle panels; scale bar is 10 μ m.

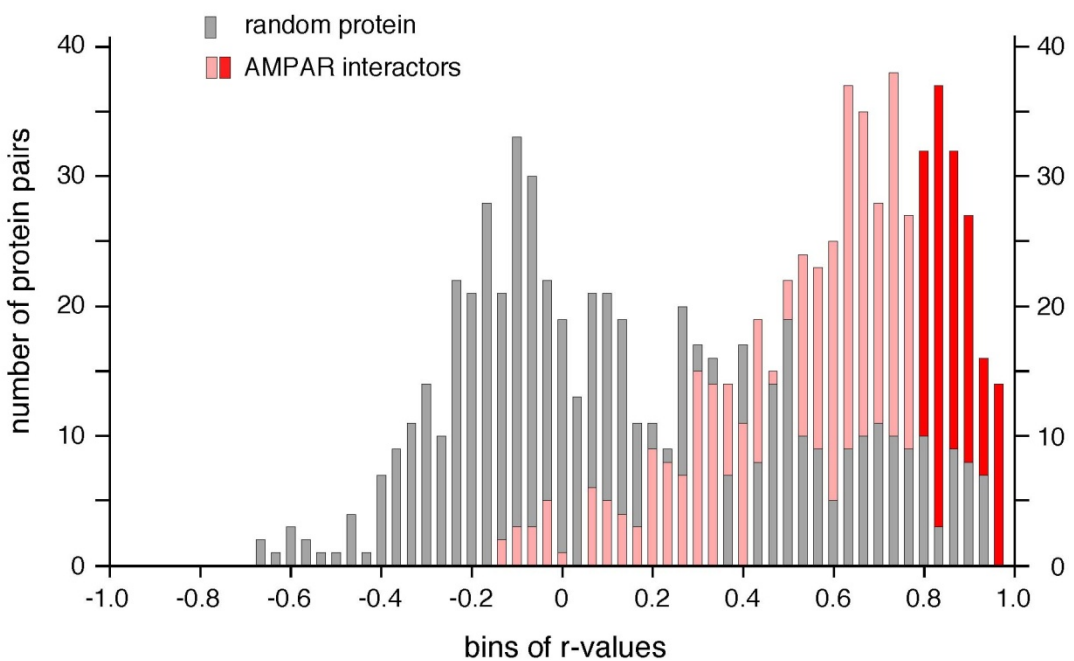
Figure S6 (information related to Figure 6)

A



B

pairwise Pearson correlation of abundance profiles



C

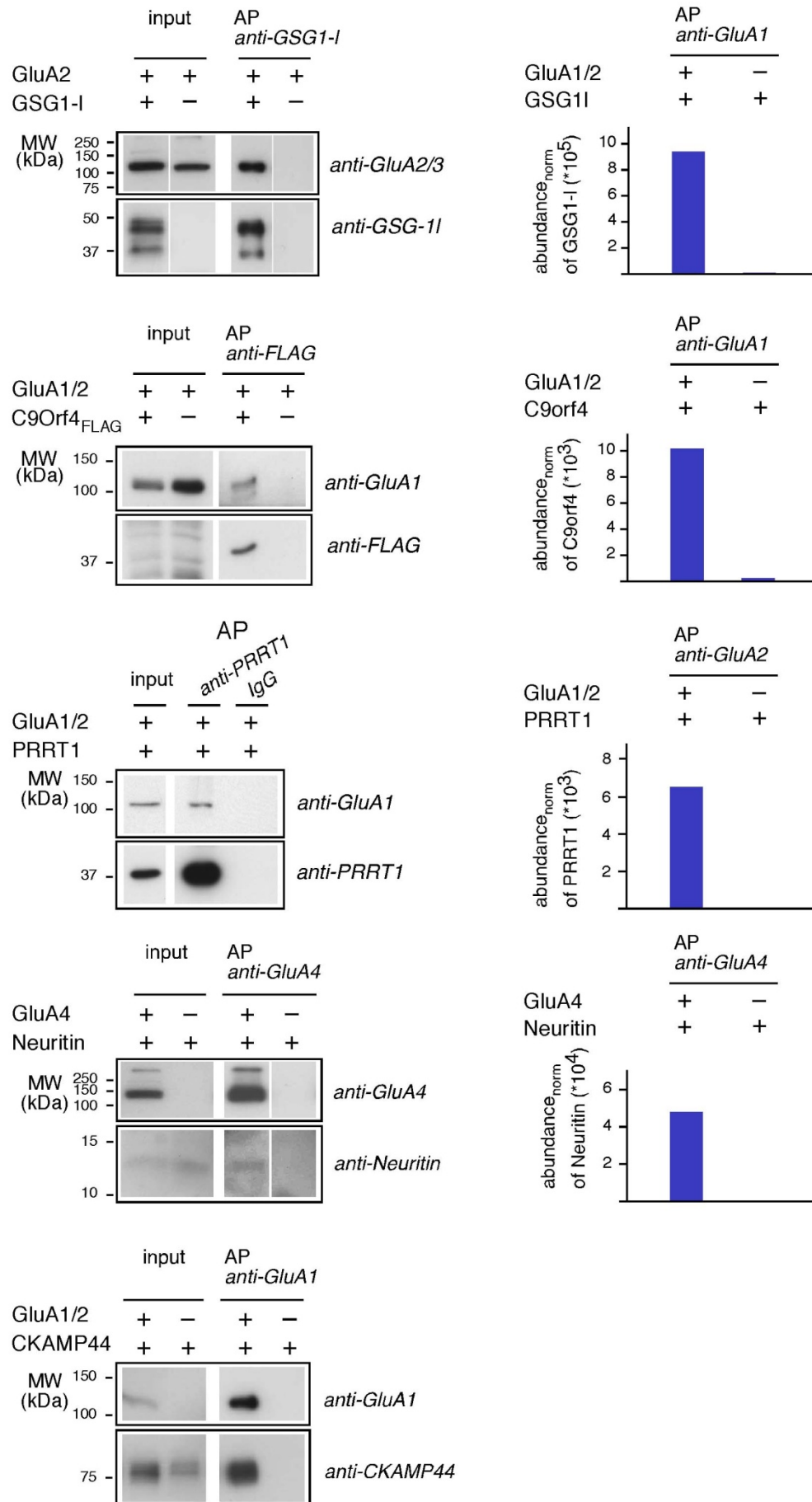


Figure S6

Additional biochemical and proteomic data used for establishment of the assembly model for native AMPARs.

(A) Co-depletion of CNIH-2,3 and GSG1-I protein in an AP purifying the entire pool of GluA protein. Western blot resolving solubilized total membranes from cultured hippocampal neurons ("input", 0.5 mg, CL-91), eluate from an AP using a mixture of *anti-GluA* ABs, and the solubilisate after AP ("unbound"). The three MW ranges of the blot were stained with the indicated ABs.

(B) Distribution of pairwise Pearson correlation coefficients determined for the AMPAR constituents (bars in red) and 30 other randomly selected proteins identified in GluA APs (bars in grey, CL-47). Note the strong accumulation of AMPAR constituent r-values to the right (compared to those of random proteins) confirming their high coherence (i.e. stable, exclusive and multisubunit assembly). Protein pairs with r-values > 0.8 (dark red) were considered for detailed inspection for establishing the model on the architecture of AMPAR complexes (Figure 6B).

(C) Binding assays probing association of various GluAs with GSG1-I, C9orf4, PRRT1, Neuritin and CKAMP44 upon co-expression in culture cells or *Xenopus* oocytes. APs with *anti-GluA* ABs were analysed by nano-LC MS/MS and quantitatively evaluated using abundance_{norm} values (right panel), APs with ABs targeting the indicated non-GluA constituents were Western-probed after separation on SDS-PAGE (left panel).

Supplemental Experimental Procedures

Density gradient ultracentrifugation. 3 mg of rat brain membrane proteins were suspended in CL-47 or CL-91 and incubated for 30 minutes on ice. The suspension was layered on top of a 32 ml linear gradient (5%(w/v) / 5%(v/v)-20%(w/v) / 30%(v/v) Sucrose / OptiPrep™ in 20 mM Tris/HCl pH 7.4, 150 mM NaCl, 1 mM EDTA, 0.05% respective detergent). After 6 hours ultracentrifugation at 400,000 x g, 16 fractions were collected from the bottom (including the pellet) to quantitatively recover all solubilized and insoluble proteins. Aliquots of all fractions were separated on SDS-PAGE, electroblotted on PVDF membrane and Western analyzed.

Binding studies with proteins heterologously expressed in *Xenopus* oocytes or cultured tsA cells were prepared as described (Schwenk et al., 2009). Briefly, crude membrane fractions (from 20 oocytes or 3 wells of a 6-well plate with cultured tsA cells) were solubilized in CL-47 or CL-48 and, after clearing by ultracentrifugation, incubated with 2 µg immobilized AB (APs as described above). The SDS-PAGE-separated AP eluates were analyzed by Western Blot or further processed for mass spectrometric investigation.

Peak-volume based quantification. Protein (isoform) specific peptide peak volumes (PVs) were ranked across the evaluated dataset (PV table) by their relative consistency using pair-wise linear correlation analysis (Pearson correlation). From the 20% highest-ranked peptides, a maximum of six (or less, if not available) peptide PVs were then selected from the best correlating PVs for calculation of the abundance ratio as medians of the respective PV ratios (rPV score). If less than two appropriate peptide intensities were found among the top 20%, lower ranked peptides were successively considered until two PV ratios could be formed. To ensure validity, sequenced peptides with missed PV assignment were omitted and at least two peptide ratios with total assigned PVs of 100,000 volume units were required; if no PV could be assigned to a peptide in the AP controls, the detection limit of

the spectrometer (3,000 volume units with the settings used here) was inserted as a minimum estimate for up to three peptides. Proteins representing exogenous contaminations like keratins, trypsin or immunoglobulins were not evaluated. Protein (isoform) specific peptide peak volumes (PVs) were ranked across the evaluated dataset (PV table) by their consistency using pair-wise linear correlation analysis (Pearson correlation).

Tables S1-S4 summarize details related to the MS analyses performed

Table S1

Peptides retrieved by nano-LC MS/MS and assigned by Mascot database searches for the identified AMPAR constituents in APs with the indicated *anti-GluA* ABs upon solubilization with CL-91 (A) and CL-47 (B); source material was rat brain (rb), or mouse brain from wildtype (mb-wt) or knock-out animals (mb-ko). U and N denote subtype-specific (unique, U) peptides or peptides shared by at least one other member of a given family of proteins (non-unique, N); MaxPepScore indicates the maximal Mascot peptide score, NumMatches refers to the total number of MS/MS spectra assigned to the respective peptide sequence.

Table S2

Coverage of the primary sequence of all AMPAR constituents derived from MS-retrieved peptides. Peptides identified by mass spectrometry are in red; those accessible to but not identified in MS/MS analyses are in black, and peptides not accessible to our MS/MS analyses used are given in grey.

Table S3

Table summarizing PV ratios (rPVs) obtained for the identified AMPAR constituents in APs with the indicated *anti-GluA* ABs upon solubilization with CL-91 (A) and CL-47 (B); source material was rat brain (rb), or mouse brain from wildtype (mb-wt) or knock-out animals (mb-ko). rPV threshold indicates the minimal PV ratio for considering a given protein specifically co-purified in the respective AP.

Table S4

Protein-specific peptides used for quantification with the label-free QconCAT method. Slope factors for the indicated peptides were determined from fits of the PV-amount relations as in Figure S2A. Peptides in red are the examples illustrated in Figure S2A.

Table S1A, Schwenk et al.

Mark Sequence	anti-GluA1-a				anti-GluA2-a				anti-GluA2-b				anti-GluA3				anti-GluA4-a				IgG						
	rb-wt	mb-wt	mb-Gria1ko		rb-wt	mb-wt	mb-Gria2ko		rb-wt	mb-wt	mb-Gria2ko		rb-wt	mb-wt	mb-Gria3ko		rb-wt	mb-wt	mb-Gria4ko		rb-wt	mb-wt	mb-Gria4ko				
	MaxRepScore	NumMatches	MaxRepScore	NumMatches	MaxRepScore	NumMatches	MaxRepScore	NumMatches	MaxRepScore	NumMatches	MaxRepScore	NumMatches	MaxRepScore	NumMatches	MaxRepScore	NumMatches	MaxRepScore	NumMatches	MaxRepScore	NumMatches	MaxRepScore	NumMatches	MaxRepScore	NumMatches			
P GluA1 (GRIA1)																											
U ADAVAAPLITLTVR	107	14	80	9	0	0	72	3	80	3	0	0	104	7	83	5	86	3	66	2	76	2	74	4	81	3	
U ALQQVRFEGLTGNVQFNEK	24	1	45	1	0	0	0	0	0	0	0	0	40	1	34	1	0	0	0	0	0	0	0	0	0	0	
U APLVQVYVYVYGR	85	15	75	10	0	0	73	3	84	4	0	0	81	8	62	7	72	3	62	2	78	1	77	4	96	3	
N EEVLDLFSKPFMSLGLSLMLK	51	3	0	0	0	0	41	3	0	0	0	0	74	14	0	0	0	0	0	0	0	0	0	0	0	0	
N EEVLDLFSKPFMSLGLSLMLKKPK	37	1	0	0	0	0	0	0	0	0	0	0	44	1	0	0	0	0	0	0	0	0	0	0	0	0	
U ERLVVDCESER	45	2	35	1	0	0	0	0	0	0	0	0	50	1	25	1	0	0	0	0	0	0	0	0	0	0	
U FALSOTEPKK	97	21	85	10	0	0	66	3	85	2	0	0	103	10	83	4	92	4	69	2	37	1	85	4	78	5	
U FCQSOFSK	36	1	34	4	0	0	0	0	28	1	0	0	32	1	25	2	26	1	0	0	0	0	21	1	25	1	
U FEGLTGNVIFONEK	72	12	73	5	0	0	63	1	67	1	0	0	76	7	74	2	74	1	67	1	85	1	62	2	91	2	
U FSPYEWHSEEEFEGR	64	5	35	2	0	0	0	0	0	0	0	0	64	3	22	1	26	1	0	0	0	0	0	0	0	0	
U GFCLLPQPSLNEALR	97	14	70	3	0	0	94	2	91	2	0	0	103	10	67	3	71	4	32	1	41	1	69	3	41	2	
N GKAYAILESTMEYLQR	34	2	0	0	0	0	0	0	0	0	0	0	44	2	42	1	0	0	23	1	40	1	0	0	0	0	
U GLSVLQR	48	11	45	6	0	0	0	0	43	2	0	0	46	2	52	3	41	3	0	0	36	1	40	1	46	1	
U GNAGDCCLANPAWPWGQQLDLQR	60	7	61	2	0	0	59	2	53	2	0	0	59	2	0	0	58	1	44	1	0	0	49	2	67	1	
U GPVNLAVK	81	6	63	4	0	0	60	1	71	1	0	0	71	2	77	3	62	1	80	1	53	1	66	3	67	1	
U GSPNLLPSSLEGGVLDK	0	0	26	1	0	0	0	0	0	0	0	0	40	0	0	0	0	0	0	0	0	0	0	0	0	0	
U GSALRNPNVPLAVLK	35	2	47	1	0	0	0	0	0	0	0	0	40	0	0	0	0	0	0	0	0	0	0	0	0	0	
U GVYALFGFYER	75	19	58	3	0	0	68	4	53	2	0	0	69	10	55	2	59	2	59	2	47	2	65	6	64	7	
N GYGLATPK	44	2	27	1	0	0	0	0	0	0	0	0	26	1	0	0	0	0	0	0	0	0	0	0	0	0	
U HVGYSYR	49	15	34	5	0	0	47	2	52	2	0	0	49	4	35	1	44	1	47	2	46	1	46	1	42	1	
U KLGYNWEDDK	28	1	31	1	0	0	0	0	0	0	0	0	0	26	1	0	0	0	0	0	0	0	0	0	0	0	
N KPCDTMK	48	1	0	0	0	0	0	0	0	0	0	0	44	2	50	1	0	0	0	0	0	0	0	0	0	0	
N KPCDTMKVGQNLDSK	27	1	0	0	0	0	0	0	0	0	0	0	21	1	26	1	0	0	0	0	0	0	0	0	0	0	
N LDLSR	25	1	0	0	0	0	0	0	0	0	0	0	0	0	0	0	0	0	0	0	0	0	0	0	0	0	
U LEKNGLYHYLLANGLFMDDLNK	68	3	25	2	0	0	0	0	0	0	0	0	81	3	0	0	0	0	0	0	0	0	0	0	0	0	
U LEVSDGDN	60	7	48	4	0	0	50	3	54	3	0	0	60	4	47	2	57	1	37	2	0	0	47	2	49	2	
U LGRDLSR	42	1	37	1	0	0	34	1	34	1	0	0	35	1	41	1	0	0	0	0	0	0	0	0	0	0	
U LMQWHR	35	8	24	0	0	0	80	2	0	0	0	0	35	4	34	5	23	1	21	0	0	0	33	2	22	0	
U UNALLGCVL	70	9	57	8	0	0	48	2	56	1	0	0	65	5	62	5	69	2	46	1	70	1	44	2	78	2	
N UNALLGCVLKEK	64	4	76	2	0	0	0	0	0	0	0	0	71	4	34	1	0	0	0	0	0	0	0	0	0	0	
N UNEQGLDK	49	10	49	7	0	0	46	2	38	2	0	0	53	5	51	7	46	1	32	2	37	2	31	1	30	1	
N UNEQGLDKL	62	11	49	9	0	0	44	4	34	2	0	0	65	14	68	8	45	3	51	2	46	3	45	2	42	3	
U LSEQQGVLDK	65	9	51	7	0	0	48	3	46	2	0	0	51	5	59	4	50	1	46	2	40	1	60	1	45	2	
U LSEQQGVLDKL	50	10	51	5	0	0	49	4	54	3	0	0	52	10	44	4	42	2	43	4	47	3	31	2	31	2	
U LVVVDCESER	66	18	68	13	0	0	48	2	44	3	0	0	64	5	63	5	47	2	55	2	57	1	37	2	53	2	
U LVVVDCESERNALLGQLVK	62	4	46	1	0	0	64	1	0	0	0	0	61	3	51	1	0	0	0	0	0	0	0	0	0	0	
U MKGFCLLPQPSLNEALR	59	3	42	2	0	0	0	0	0	0	0	0	37	3	33	1	0	0	0	0	0	0	0	0	0	0	
U MLFQDLEK	48	14	40	5	0	0	30	3	32	3	0	0	45	4	36	5	30	3	0	0	28	1	44	5	39	4	
U MLOQDEKK	27	1	0	0	0	0	0	0	0	0	0	0	26	1	0	0	0	0	0	0	0	0	0	0	0	0	
N MVSPLESAELDAK	90	12	40	4	0	0	92	3	71	4	0	0	90	10	56	7	90	4	96	5	84	4	84	4	107	4	
U NWIVWIK	22	4	0	0	0	0	0	0	0	0	0	0	20	2	0	0	0	0	0	0	0	0	0	0	0	0	
U NANOFEGNDK	39	2	45	1	0	0	0	0	0	0	0	0	20	2	0	0	0	0	0	0	0	0	0	0	0	0	
U NANOFEGNDRYEGCVLEAELAK	89	12	0	0	0	0	66	1	62	1	0	0	107	8	0	0	0	0	0	0	0	0	0	0	0	0	
U NGLGYHYLLANGLFMDDLNK	103	25	76	6	0	0	82	3	0	0	0	0	81	15	80	2	0	0	0	59	1	0	0	72	2	77	2
U NGLGYHYLLANGLFMDDLNFK	102	9	0	0	0	0	91	2	0	0	0	0	89	4	0	0	0	0	0	0	0	0	0	0	0	0	
N NKWWDY	0	0	26	1	0	0	0	0	0	0	0	0	24	1	26	1	0	0	0	0	0	0	0	0	0	0	
U NPVNLAVK	74	12	61	6	0	0	52	3	64	1	0	0	66	7	70	3	70	1	50	1	57	1	53	2	48	1	
U NSGAGASGGGGSGENGRVVSQDFPK	65	8	0	0	0	0	43	1	0	0	0	0	63	4	0	0	0	0	0	0	0	0	0	0	0	0	
U NWQVATNLLTTEGYR	120	13	141	6	0	0	112	3	120	2	0	0	113	5	120	3	109	2	127	2	112	2	120	3	126	3	
U QRLDLSR	33	3	32	1	0	0	32	1	25	1	0	0	28	2	39	1	25	1	0	0	0	0	0	0	0	0	
U QTETLTLGAEASTKEFFR	137	18	111	10	0	0	106	3	103	2	0	0	132	11	117	5	108	3	111	1	107	1	103	1	105	1	
U RCGADCLANPAWPWGQQLDLQR	41	1	0	0	0	0	0	0	0	0	0	0	0	0	0	0	0	0	0	0	0	0	0	0	0	0	
U RPKYTSLTYLGDVK	70	12	65	2	0	0	48	1	0	0	0	0	72	6	66	5	55	6	56	1	45	1	40	1	35	1	
N SAEPSPVFR	71	15	55	5	0	0	59	4	78	3	0	0	73	25	31	2	42	4	31	51	1	36	2	55	2	0	0
U SKWWDY	28	1	29	1	0	0	0	0	0	0	0	0	0	30	1	0	0	0	0	0	0	0	0	0	0	0	
U SMQSLPCMHSQGMLPATGL	81	11	0	0	0	0	53	1	0	0	0	0	85	4	0	0	0	0	0	0	0	0	0	0	0	0	
U TSTLPRNSAGASGGGGSGENGR	71	8	0	0	0	0	0	0	0	0	0	0	62	6	0	0	0	0	0	0	0	0	48	1	0	0	
U TSTLPRNSAGASGGGGSGENGR	0	0	75	2	0	0	0	0	0	0	0	0	0	61	2	0	0	0	0	0	0	0	0	69	1	0	0
U TTEEGMLRV	43	1	24	1	0	0	0	0	0	0	0	0	33	2	0	0	0	0	0	0	0	0	0	0	0	0	
U TYLVTLLEDPVYMLK	83	7	90	4	0	0	93	2	74	1	0	0	89	4	89	3	82	2	79	1	83	1	76	2	77	1	
U VGGDLSK	62	8</																									

U	LAQLLSACALLSK	96	1	74	1	0	0	57	1	55	1	0	0	0	73	1	78	1	0	0	0	76	1	41	1	0	65	1	57	1	0	0	0	0					
U	LGLPSYLK	26	2	21	1	0	0	25	2	50	0	0	0	0	46	1	37	1	0	0	0	21	1	0	0	23	1	20	1	0	0	0	0						
P SAC1																																							
U	ATDFDVLSYKK	0	0	37	1	0	0	0	0	0	0	0	0	0	0	0	54	1	0	0	0	0	0	0	0	0	0	0	0	0	0	0	0	0					
U	ATDFDVLSYKRR	0	0	0	0	0	0	0	0	0	0	0	0	0	0	31	1	0	0	0	0	0	0	0	0	0	0	0	0	0	0	0	0	0					
U	ELSAOPELR	44	2	33	2	0	0	0	0	0	0	0	0	0	0	37	1	0	0	0	0	0	0	0	0	0	0	0	0	0	0	0	0	0					
U	FVLSLFLSLR	22	1	21	1	0	0	0	0	0	0	0	0	0	0	0	0	0	0	0	0	0	0	0	0	0	0	0	0	0	0	0	0	0					
U	ULDSEGHAAVNVETEQLVHYSGNR	0	0	45	1	0	0	0	0	0	0	0	0	0	0	38	1	37	1	0	0	0	0	0	0	0	0	0	0	0	0	0	0	0					
U	GSEKPKEOTFAK	54	2	0	0	0	0	0	0	0	0	0	0	0	0	44	1	0	0	0	0	0	0	0	0	0	0	0	0	0	0	0	0	0					
U	GSLPVFWSPRLNK	20	1	0	0	0	0	0	0	0	0	0	0	0	0	47	2	0	0	0	0	0	0	0	0	0	0	0	0	0	0	0	0	0					
U	HFDSSVLLYLGK	42	1	51	1	0	0	0	0	0	0	0	0	0	0	37	1	35	1	0	0	0	0	0	0	0	0	0	0	0	0	0	0	0					
U	LEEQDEFEK	40	1	57	1	0	0	0	0	0	0	0	0	0	0	45	1	46	1	0	0	0	0	0	0	0	0	0	0	0	0	0	0	0					
U	LGVLHVQK	33	1	0	0	0	0	0	0	0	0	0	0	0	0	0	0	31	1	0	0	0	0	0	0	0	0	0	0	0	0	0	0	0	0				
U	LSLLDQVAEMQDELSYFLVDSAGK	0	0	0	0	0	0	0	0	0	0	0	0	0	0	105	2	0	0	0	0	0	0	0	0	0	0	0	0	0	0	0	0	0	0				
U	LSNTSPFOEMLSLR	75	1	0	0	0	0	0	66	1	0	0	0	0	0	83	1	0	0	0	0	0	0	0	0	0	0	0	0	0	0	0	0	0	0				
U	MVSSLGSGMLR	55	1	0	0	0	0	0	38	1	0	0	0	0	0	58	1	0	0	0	0	0	0	0	0	0	0	0	0	0	0	0	0	0	0				
U	NAWDANANACK	69	1	0	0	0	0	0	0	0	0	0	0	0	0	71	1	60	1	0	0	0	0	0	0	0	0	0	0	0	0	0	0	0	0				
U	NNFSDFGR	45	1	26	1	0	0	0	0	0	0	0	0	0	0	0	39	1	0	0	0	0	0	0	0	0	0	0	0	0	0	0	0	0	0				
U	QKFLVNEK	21	1	0	0	0	0	0	0	0	0	0	0	0	0	32	2	0	0	0	0	0	0	0	0	0	0	0	0	0	0	0	0	0	0				
U	SLOAQLR	0	0	28	1	0	0	0	0	36	1	0	0	0	0	41	2	28	1	0	0	29	1	33	1	0	0	27	1	0	0	0	0	0					
U	SMQHDLQDCLR	0	0	0	0	0	0	0	0	0	0	0	0	0	0	39	1	0	0	0	0	0	0	0	0	0	0	0	0	0	0	0	0	0	0				
U	SMHLHTDLODNK	0	0	0	0	0	0	0	0	0	0	0	0	0	0	0	36	1	0	0	0	0	0	0	0	0	0	0	0	0	0	0	0	0	0				
U	TNLQSLALAR	50	1	36	1	0	0	0	32	1	0	0	0	0	0	0	0	0	0	0	32	1	41	1	31	1	0	0	0	0	0	0	0	0					
U	TQLGLLMDGFNSLRL	0	0	0	0	0	0	0	0	0	0	0	0	0	0	0	0	0	0	0	80	1	0	0	0	0	0	0	0	0	0	0	0	0					
U	TQLGLVMDGFNSLRL	113	1	0	0	0	0	0	0	0	0	0	0	0	0	102	1	0	0	0	0	0	0	0	0	0	0	0	0	0	0	0	0	0	0				
U	VANHMDGQFR	40	1	0	0	0	0	0	0	0	0	0	0	0	0	37	1	39	1	0	0	0	0	0	0	0	0	0	0	0	0	0	0	0	0				
U	VGECCFHAWWR	0	0	34	2	0	0	0	0	0	0	0	0	0	0	0	26	1	0	0	0	0	0	0	0	0	0	0	0	0	0	0	0	0	0				
U	VGEFFNHVLWK	32	1	0	0	0	0	0	0	0	0	0	0	0	0	37	1	0	0	0	0	0	0	0	0	0	0	0	0	0	0	0	0	0	0				
U	VSTEVTLAVK	0	0	59	1	0	0	0	0	0	0	0	0	0	0	38	1	41	1	0	0	0	0	0	0	0	0	0	0	0	0	0	0	0	0				
U	VSTEVTLAVK	0	0	0	0	0	0	0	0	0	0	0	0	0	0	35	1	0	0	0	0	0	0	0	0	0	0	0	0	0	0	0	0	0	0				
U	VVTNDGQFR	0	0	0	0	0	0	0	35	1	0	0	0	0	0	0	36	1	0	0	0	0	0	0	0	0	0	0	0	0	0	0	0	0	0	0			
U	VVTNEQGQFR	39	1	0	0	0	0	0	0	0	0	0	0	0	0	57	1	0	0	0	0	0	0	0	0	0	0	0	0	0	0	0	0	0	0	0			
U	YFDWLSSR	55	1	53	1	0	0	41	1	0	0	0	0	0	0	57	1	0	0	0	0	0	0	0	0	0	0	0	0	0	0	0	0	0	0	0			
P ABHD-6																																							
U	DMWLSVVK	48	2	41	2	0	0	43	2	40	1	0	0	0	0	39	2	42	2	0	0	0	0	32	1	39	1	43	1	0	0	0	0	0	0	0	0	0	0
U	ELEESAAOLK	0	0	39	1	0	0	0	0	45	1	0	0	0	0	0	0	48	2	42	1	48	3	43	2	52	2	70	2	0	0	0	0	0	0	0	0	0	0
U	FKVPOQOLLOGLVDVR	74	5	41	2	0	0	56	3	56	4	0	0	0	0	72	5	45	2	41	1	48	3	43	2	52	2	72	2	0	0	0	0	0	0	0	0	0	0
U	KLFLELVIEK	0	0	47	2	0	0	0	0	59	2	0	0	0	0	0	59	2	29	1	0	0	0	0	51	2	0	0	0	0	0	0	0	0	0	0			
U	KLFLELVIEK	49	3	0	0	0	0	57	2	0	0	0	0	0	0	60	3	0	0	0	0	0	0	0	35	1	0	0	0	0	0	0	0	0	0	0			
U	LFLELVIEK	0	0	53	2	0	0	0	0	57	1	0	0	0	0	0	56	3	0	0	0	0	0	0	0	45	1	0	0	0	0	0	0	0	0	0	0		
U	LUVQFVECLK	48	2	0	0	0	0	45	2	0	0	0	0	0	0	47	2	0	0	0	0	0	0	0	68	1	0	0	49	1	0	0	0	0	0	0			
U	LUVQFVECLK	23	1	32	2	0	0	32	1	26	1	0	0	0	0	32	2	33	2	0	0	0	0	0	32	1	0	0	0	0	0	0	0	0	0	0			
U	LUVQFVECLK	76	5	0	0	0	0	68	5	0	0	0	0	0	0	74	6	0	0	0	0	0	0	0	70	2	0	0	66	2	0	0	0	0	0	0			
U	LUVQFVECLK	51	2	42	2	0	0	48	2	57	2	0	0	0	0	66	1	0	0	0	0	0	0	0	77	5	0	0	0	0	0	0	0	0	0	0			
U	LUVQFVECLK	72	1	0	0	0	0	72	1	0	0	0	0	0	0	66	1	0	0	0	0	0	0	0	0	0	0	0	0	0	0	0	0	0	0	0			
U	LUVQFVECLK	79	2	64	3	0	0	88	2	74	1	0	0	0	0	69	3	68	4	72	1	67	1	84	1	112	1	73	1	0	0	0</td							

Table S1B, Schwenk et al.

Table S2

Sequence coverage of the identified constituents of the AMPAR proteome
(alphabetic order)

GluA1, GRIA1_RAT (P19490)

Coverage is **62.4%** absolute, **88.9%** relative

0001	MPYIFAFFCT	GFLGAVVGAN	FPNNIQIGGL	FPNQQSQEHA	AFR FALSQ LT
0051	EPPKLLPQID	IVNISDSFEM	TYR FCSQFSK	GVYAIFGFYE	RRTVNMLTSF
0101	CGALHVCFIT	PSFPVDTSNQ	FVLQLRPELQ	EALISIIDHY	KWQT FVYIYD
0151	ADRGLSVLQR	VLDTAAEKNW	QVTAVNILT	TEEGYRMLFQ	DLEKK KE RLV
0201	VVDCESERLN	AILGQIVKLE	KNGIGYHYIL	ANLGFMIDIL	NKF KES GANV
0251	TGFQLVNYTD	TIPARIMQQW	RTSDSRDHTR	VDWKRPKYTS	ALTYDGVKVM
0301	AEAFQSLRRQ	RIDI SRRGNA	GDCLANPAVP	WGQGIDIQRA	LQQVRFEGLT
0351	GNVQFNEKGR	P <small>T</small> NYTLHVIE	MKHDGIRKIG	YNEDDKFVP	AATDAQAGGD
0401	NSSVQNR <small>T</small> YI	VTTILEDPYV	MLKKNNQFE	GND RYEGYCV	ELAAEI A KHV
0451	GYSYRLEIVS	DGKYGARDPD	TKAWNGMVGE	LVYGRADVAV	APLTITLVRE
0501	EVIDFSKPFM	SLGISIMIKK	PQKSKPGVFS	FLDPLAYEIW	MCIVFAYIGV
0551	SVVLFLVSF	SPYEWHSEEF	EEGRDQTTSD	QSNEFGIFNS	LWFSLGAFMQ
0601	QGCDISPRSL	SGRIVGGVWW	FFTLIIISSY	TANLAAFLTV	ER MV SPIESA
0651	EDLA KOTEIA	YGTLEAGSTK	EFFR <small>R</small> SKIAV	FEKMWTYMK	AEP SVF VRTT
0701	EEGMIRVRKS	KGKYAYILLES	TMNEYIEQRK	PCDTMKVGGN	LDSKGYGIAT
0751	PKGSALRNPV	NLAVLKLNEQ	GLLDKLKNKW	WYDKGECGSG	GGDSK D KTSA
0801	LSLSNVAGVF	YILIGGLGIA	MLVALIEFCY	KSRSESKRMK	GFCLIPQQSI
0851	NEAIRTSTLP	RNSGAGASGG	GGSGENGRVV	SQDFPKSMQS	IPCM SH SSGM
0901	PLGATGL				

GluA2, GRIA2_RAT (P19491)

Coverage is **69.2%** absolute, **95.2%** relative

0001	MQKIMHISVL	LSPVLWGLIF	GVSSNSIQIG	GLFPRGADQE	YSAFRVGMVQ
0051	FSTSEFRLTP	HIDNLEVANS	FAVTNAFCSQ	FSRGVVAIFG	FYDKKSVNTI
0101	TSFCGTLHVS	FITPSFPTDG	THPFVIQMRP	DLK GALLSLI	EYYQWDKFAY
0151	LYDSDRGLST	LQAVLDSAEE	KKWQVTAINV	GNINNDKKDE	TYRSLFQDLE
0201	LKKERRVILD	CERDKVNDIV	DQVITIGKHV	KGYHYIIANL	GFTDGDLLKI
0251	QFGGANVSGF	QIVDYDDSLV	SKFIERWSTL	EEKEYPGAHT	ATIKYTSALT
0301	YDAVQVMTEA	FRNLRKQRIE	ISRRGNAGDC	LANPAPWGQ	GVEIERALKQ
0351	VQVEGLSGNI	KFDQNGKRIN	YTINIMELKF	NGPRKIGYWS	EVDK MV VTLT
0401	ELPSGNDTSG	LENKTVVTT	ILESPTYVMMK	KNHEMLEGNE	RYEGYCVDLA
0451	AEIAKHCGFK	YKLTIVGDGK	YGARDADTKI	WNGMVGE LY	GKADIAIAPL
0501	TITLVREEVI	DFSKPFMSLG	ISIMIKKPQK	SKPGVFSFLD	PLAYEIWMCI
0551	VFAYIGVSVV	LFLVSRFSPY	EWHTEEFEDG	RETQSSESTN	EGIFNSLWF
0601	SLGAFMQQGC	DISPRSLSGR	IVGGVWWFFT	LIIISSYTAN	LAAFLTVER M
0651	VSPIESAEDI	SKQTEIAYGT	LDSGSTKEFF	RRSKIAVFDK	MWTYMRSAEP
0701	SVFVRTTAEG	VARVRKSKGK	YAYLLESTMN	EYIEQRKPCD	TMKVGGNLDS
0751	KGYGIATPKG	SSLGNAVNLA	VLKLNEQGLL	DKLKKNWWYD	KGECGSGGGD
0801	SK EKT SALSL	SNVAGVFYIL	VGGLGLAMLV	ALIEFCYKSR	AEAKRM K VAK
0851	NPQNINPSSS	QNSQNFATYK	EGYNVYGIES	VKI	

GluA3, GRIA3_RAT (P19492)

Coverage is **58.7%** absolute, **94.6%** relative

0001 MGQSVLRAVF FLVLGLLGHs HGGFPNTISI GGLFMRNTVQ EHSAFRFAVQ
0051 LYNTNQNTTE KPFHLNYHVD HLDSSNSFSV TNAFCSQFSR GVYAIFGFYD
0101 QMSMNTLTSF CGALHTSFVT PSFPTDADVQ FVIQMRPALK GAILSLLSYY
0151 KWEKFVYLYD TERGFSVLQA IMEAAVQNNW QVTARSGVNI KDVQEFRRII
0201 EEMDRRQEKR YLIDCEVERI NTILEQVVIL GKHSRGYHYM LANLGFTDIL
0251 LERVMHGGAN ITGFQIVNNE NPMVQOFIQR WVRLDEREFP EAKNAPLKYT
0301 SALTHDAILV IAEAFRYLRR QRVDVSRRGS AGDCLANPAV PWSQGIDIER
0351 ALKMVQVQGM TGNIQFDTYG RRTNYTIDVY EMKVSGSRKA GYWNEYERFV
0401 PFSDQQISND SSSSENRTIV VTTILESPYV MYKKNHEQLE GNERYEYGV
0451 DLAYEIHKHV RIKYKLSIVG DGKYGARDPE TKIWNGMVGE LVYGRADIAV
0501 APLTITLVRE EVIDFSKPFM SLGISIMIKK PQKSKPGVFS FLDPLAYEIW
0551 MCIVFAYIGV SVVLFVLVSF SPYEWHLEDN NEEPRDPQSP PDPPNEFGIF
0601 NSLWFSLGAF MQQGCDISPR SLSGRIVGGV WWFFTLIIIS SYTANLAAFL
0651 TVERMVSPIE SAEDLAKQTE IAYGTLDSGS TKEFFRRSKI AVYEKMWSYM
0701 KSAEPSVFTK TTADGVARVR KSKGKFAFLL ESTMNEYIEQ RKPCDTMKVG
0751 GNLDLDSGYGV ATPKGSLGN AVNLAVLKLN EQGLLDKLKN KWWYDKGEKG
0801 SGGGDSKDKT SALSLNVAG VFYILVGGLG LAMMVALIEF CYKSRAESKR
0851 MKLTKNTQNF KPAPATNTQN YATYREGYNV YGTESVKI

GluA4, GRIA4_RAT (P19493)

Coverage is **53.8%** absolute, **82.8%** relative

0001 MRIICRQIVL LFSGFWGLAM GAFPSSVQIG GLFIRNTDQE YTAFRLAIFL
0051 HNTSPNASEA PFNLVPHVDN IETANSFAVT NAFCSQYSRG VFAIFGLYDK
0101 RSVHTLTSFC SALHISLITP SFPTEGESQF VLQLRPSLRG ALLSLLDHYE
0151 WNCFVFLYDT DRGYSILQAI MEKAGQNGWH VSAICVENFN DVSYRQLLEE
0201 LDRRQEKKFV IDCEIERLQN ILEQIVSVGK HVKGYHYIIA NLGFKDISLE
0251 RFIHGGANVT GFQLVDFNTP MVTKLMDRWK KLDQREYPGS ETTPPKYTSAL
0301 TYDGVLVMAE TFRSLRRQKI DISRRGNAGD CLANPAAPWG QGIDMERTLK
0351 QVRIQGLTGN VQFDHYGRV NYTMDVFELK STGPRKVGYW NDMDKLVLIQ
0401 DMPTLGNDTA AIENRTVVVT TIMESPYVMY KKNHEMFEGN DKYEGYCVDL
0451 ASEIAKHIGI KYKIAIVPDG KYGARDADTK IWNGMVGELV YGKAEIAIAP
0501 LTITLVREEV IDFSKPFMSL GISIMIKKPQ KSKPGVFSFL DPLAYEIWMC
0551 IVFAYIGVSV VLFLVSRFSP YEWHTEEPED GKEGPBSDQPP NEFGIFNSLW
0601 FSLGAFMQQG CDISPRSLSG RIVGGVWWFF TLIIIISSYTA NLAAFLTVER
0651 MVSPIESAED LAKQTEIAYG TLDGSTKEF FRRSKIAVYE KMWTYMRSAE
0701 PSVFTRTTAE GVARVRKSKG KFAFILLESTM NEYTEQRKPC DTMKVGGNLD
0751 SKGYGVATPK GSSLGNNAVNL AVLKLNEQGL LDKLKKNWWY DKGECCSGGG
0801 DSKDKTSALS LSNVAGVFYI LVGGGLGLAML VALIEFCYKS RAEAKRMKLT
0851 FSEATRNRKAR LSITGSVGEN GRVILTPDCPK AVHTGTAIRQ SSGLAVIASD
0901 LP

TARP γ -2, CCG2_HUMAN (Q9Y698)

Coverage is 34.4% absolute, 67.3% relative

0001 MGLFDRGVQM LLTTVGAFAA FSLMTIAVGT DYWLYSRGVC KTK**SVSENET**
0051 SK**KNEEVMT**H SGLWRTCCLE GNFKGLCK**QI** DHFPEDADYE **ADTAEYFLRA**
0101 VR**ASSIFPIL** SVILLFMGGI CIAASEFYKT RHNIILSAGI FFVSAGLSNI
0151 IGIIVYISAN AGDPSKSDSK KNSYSYGWSF YFGALSIIA EMVGVLAVHM
0201 FIDRHQLRA TAR**ATDYLQA** SAITRIPSYR YRYQRRSRSS SR**STEPHSR**
0251 DASPVGIKG**F** NTLPSTEISM YTLSRDPLKA ATTPTATYNS DRDNSFLQVH
0301 NCI**QKENKDS** LHSNTANRRT TPV

TARP γ -3, CCG3_RAT (Q8VHX0)

Coverage is 34.9% absolute, 71.9% relative

0001 MRMCDRGIQM LITTVGAFAA FSLMTIAVGT DYWLYSRGVC RTK**STSDNET**
0051 SR**KNEEVMT**H SGLWRTCCLE GAFRGVCK**KI** DHFPEDADYE **QDTAEYLLRA**
0101 VF**ASSVFPI**L SVTLLFFGGL CVAASEFHR**S** RHSVILSAGI FFVSAGLSNI
0151 IGIIVYISAN AGDPGQRDSK KSYSYGWSFY FGAFSIIAE IVGVVAVHIY
0201 IEKHQQLRAR **SHSELLK**KST FARLPPYRYR FRRRSSSRST EPR**SRDLSP**I
0251 SKGFHTIPST DISMFTLSRD PSKLTMG**T**LL NSDRDHAFLQ FHNSTPKEFK
0301 ESLHNNPANR RTTPV

TARP γ -4, CCG4_RAT (Q8VHW9)

Coverage is 33.9% absolute, 77.1% relative

0001 MVRCDRGLQM LLTTAGAFAA FSLMAIAIGT DYWLYSSAHI CNGTNLTMD**D**
0051 GPPPR**ARGD** LTHSGLWRVC CIEGIYK**GHC** FR**INHFEDN** DYDHDSSEYL
0101 LR**IVRASSVF** PILSTI~~LLL~~ GGLCIGAGRI YSRKNNIVLS AGILFVAAGL
0151 SNIIGIIVYI SSNTGDP~~SDK~~ RDEDKKNHYN YGWSFYFGAL SFIVAETVG**V**
0201 LAVNIYIEKN KELRFKTKRE FLK**ASSSSPY** SRMPSYRYRR RRSRSSS**ST**
0251 EASPSRDASP VGLKITGAIP MGELS~~MYTLS~~ REPLKVTTAA SYSPDQDAGF
0301 LQMHDFFQQD LKEGFHVSM~~L~~ NRRTTPV

TARP γ -5, CCG5_RAT (Q8VHW8)

Coverage is 13.5% absolute, 30.6% relative

0001 MSTCGRKALT LLSSVFAVCG LG~~LLGIAVST~~ DYWLYLEEGI ILPQNQSTEV
0051 KMSLHSGLWR **VCFILEGER** RCFTIEYVMP MNSQMTSEST VNVLK**MIRSA**
0101 TPFPLVSLFF MFIGFILSNI GH~~IRPHRTIL~~ AFVSGIFFIL SG~~LSLVVGLV~~
0151 LYISSINDEM LNRTK**DAETY** FNYKYGWSFA FAAISFLLTE SAGVMSVYLF
0201 MKRYTAEDMY RPHPGFYRPR LSNCSDYSGQ FLHPDAWIRG RSPSDISSDA
0251 SLQMNSNYP*A* LLKCPDYDQM SSSPC

TARP γ -7, CCG7_RAT (P62957)

Coverage is 38.2% absolute, 72.9% relative

0001 MSHCSSRALT LLSSVFGACG LLLVGIAVST DYWLWYMEEGT VLPQNQTTEV
0051 KMALHAGLWR VCFFAGREKG RCVASEYFLE PEINLVENT ENILKTVRTA
0101 TPPFMVSLFL VFTAFVISNI GHIRPQRTIL AFVSGIFFIL SGLSLVVGLV
0151 LYISSINDEV MNRPSSSEQY FHYRYGWSFA FAASSFLLKE GAGVMSVYLF
0201 TKRYAEEEMY RPHPAFYRPR LSDCSDYSGQ FLQPEAWRG RSPSDISSLV
0251 SIQMTQNYPP AIKYPDHLHI STSPC

TARP γ -8, CCG8_RAT (Q8VHW5)

Coverage is 46.6% absolute, 76.9% relative

0001 MESLKRWNEE RGLWCEKGVQ VLLTTIGAFA AFGLMTIAIS TDYWLWYTPAL
0051 ICNTTNLTAG DDGPPHRGGGS GSSEKKDPGG LTHSGLWRIC CLEGLKRGVC
0101 VKINHFPEDT DYDHDSAELY LRVVRASSIF PILSAILLLL GGVCVAASRV
0151 YKSKRNIIILG AGILFVAAGL SNIIGVIVYI SANAGEPGPK RDEEKKNHYS
0201 YGWSFYFGGL SFILAEVIGV LAVNIYIERS REAHCQSRSD LLKAGGGAGG
0251 SGGSGPSAIL RLPSYRFRYR RRSRSSRGGS SEASPSRDAS PGGPGPGFA
0301 STDISMYTLS RDPSKGSVAA GLASAGGGGG GAGVGAYGGA AGAAGGGGTG
0351 SERDRGSSAG FLTLHNAFPK EAASGVTVTV TGPPAAPAPA PPAPAAPAPG
0401 TLSKEAAASN TNTLNKTP V

CNIH2, CNIH2_RAT (Q5BJU5)

Coverage is 31.2% absolute, 69.4% relative

0001 MAFTFAAFCY MLTLVLCAIS IFFVIWHIIA FDELRTDFKN PIDQGNPARA
0051 RERLNIERI CCLLRKLVVP EYSIHGLFCI MFLCAAEWVT LGlnipLLFY
0101 HLWRYFHRPA DGSEVMYDAV SIMNADILNY CQKEAWCKLA FYLLSFFYYL
0151 YSMVYTLVSF

CNIH3, CNIH3_MOUSE (Q6ZWS4)

Coverage is 32.5% absolute, 70.3% relative

0001 MAFTFAAFCY MLSLVLCAAL IFFAIWHIIA FDELRTDFKS PIDQCNPVHA
0051 RERLRNIERI CFLLRKLVLP EYSIHSLFCI MFLCAQEWT LGlnVPLLFB
0101 HFWRYFHCPA DSSELAYDPP VVMNADTLSY CQKEAWCKLA FYLLSFFYYL
0151 YCMIYTLVSS

CKAMP44, SHSA9_MOUSE (Q9CZN4)

Coverage is 42.2% absolute, 61.9% relative

0001 MRRVLRLLLGFCLTELCARM CRAQERSGHG QLAQLGGVLL LTGGNRSGAA
0051 SGEAGEGVGG SDAPPTRAPT PDSCRGYFDV MGQWDPPFNC SSGDFIFCCG
0101 TCGFRFCCTF KKRLNQSTC TNYDTPLWLN TGKPPARKDD PLHDPTKDGT
0151 NLIVYIICGV VAVMVLVGIF TKLGLEKAHR PQREHMSRAL ADVMRPQGHC
0201 NTDHMERDLN IVVHVQHYEN MDSRTPINNL HTTQMNNAVP TSPLLQQMGH
0251 PHSYPNLGQI SNPYEQQPPG KELNKYASLK AVGNSDGDWA VATLKSPKAD
0301 KVNDDFYAKR RHLAELAVKG NLPLHPVRVE DEPRAFSPEH GPAQQNGQKS
0351 RTNKMPPHPL AYNSTANFKT WDP PSDQSLRR QAYGNKGFLG IAESGSCDPL
0401 GTRTQHFPPQPYFITNSKT EVTV

CKAMP52, SHSA6_MOUSE (B1ATQ6)

Coverage is 34.6% absolute, 47.7% relative

0001 GRNELNSTARA SGVPEAGSRR GQSAAAAAAA AAAASATVTY ETCWGYYDVS
0051 GQYDKEFECHN NSESGYLYCC GTCYYRFCCK KRHEKLDQFQ CTNYQSPVWV
0101 QTPSTKVVSP GPENKYDPEK DKTNFTVYIT CGVIAFVIVA GVFAKVSYDK
0151 AHRRPPREMNI HRALADILRQ QGPIPIAHCE RETISAIDTS PKENTPVRST
0201 SKNYHTPVRT AKQTPGHYHK DAYFSGGPDL HNFISSGFVT LGRGHTKGDR
0251 QYNHPILSSA TQTPTHEKPR MNNILTSATE PYDLSFSRSY QNLAHLPPSY
0301 ESAVEKTNPSK YSSLKRLTDK EADEYYMRRR HLPDLAARGT LPLNVIQMSQ
0351 QKPLPRERPR RPIRAMSQDR VLSPRRGLPD EFGMPYDRIL SDEQLLSTER
0401 LHSQDPLLSP ERTAFPEQSI SRAISHTDVF VSTPVLDYR MTKMHSHPSA
0451 SNNSYATLGQ SQTAAKRHAF ASRFHNTVEQ LHYIPGHHTC YTASKEVTV

MAGUK p55 subfamily member 2, MPP2_MOUSE (Q9WV34)

Coverage is 26.1% absolute, 37.9% relative

0001 MPVAATNSE AMQQVLDNLG SLPNATGAAE LDLIFLRGIM ESPIVRSI
0051 AHERLEETKL EAVPDNNLEL VQEILRDLAE LAEQSSTAAE LARIILQEPHF
0101 QSLLETHDSV ASKTYETPPP SPGLDPTFSN QPVPPDAVRM VGIRKTAGEH
0151 LGVTFRVEGG ELVIARILHG GMVAQQGLLH VGDIIKEVNG QPGVGS
0201 QELLRSASGS VILKILPSYQ EPHLPRQVFV KCHFDYDPAR DSLS
0251 LRFNAGDILQ IVNQDDANWW QACHVEGGS GLIPSQLLEE KRKA
0301 ELPTPTSGTLC GSLSGKKKKR MMYLTTKNAE FDRHELLIYE EVAR
0351 KTLVLIQAGQ VGRRSLKNFL ILWDPDRYGT TVPYTSRRPK DSER
0401 FVSRGEMEAD IRAGRYLEHG EYEGNLYGTR IDSIRGVVAS GK
0451 QAVKVLRTAE FVPYVVFIEA PDYETLRAMN RALESGVST KQLTEADLRR
0501 TVEESSRIQR GYGHYFDLSL VNSNLERTFR ELQTAMEKLR TE
0551 VY

DLG1, DLG1_RAT (Q62696)

Coverage is 34.7% absolute, 70.7% relative

0001 MPVRKQDTQR **ALHLLEEYRS** KLSQTEDRQL RSSIERVISI FQSNLFQALI
0051 DIQE FYEVTL LDNP KCDVHS KQCE PVQPGN PWES GSLSSA AVTSE SLPGG
0101 LSPPVEKYRY QDEEVLP SER ISPQ VPNEVL GPELVH VSEK SLSEIEN VH
0151 FVSH SHISPI KPTE AVPPSS PIVP VT PALP VPAESP VVLP STPQAN PPPV
0201 LVNTD SLET P TYVNG TDAD Y EYEITL ERG NSGLGFSIAG GTDNPHIGDD
0251 SSIFITKII T GGAAA QDGR L RVND CILR VN EADVR DVTHS KAVE ALKEAG
0301 SIVRLYVKRR KAFRK NHEIK LIKGPK GLGF SIAGGVGNQH IPGDNSIYVT
0351 KII EGGA AHK DGKLQIGDK L LAVNSVCLEE VTHEEAVTAL KNTSDFVYLK
0401 AAKPTSMYIN DGYAPPD ITN SSSQSVDNHV SPSSY LGQTP ASPARYSPIS
0451 KAVLG DDEIT REPRK VVLHR GSTGLGF NIV GGEGE GIFI SFILAGGPAD
0501 LSGELRKGD R IISVNSVDLR AASHEQ AAAA LK NAGQAVTI VAQYRPEEYS
0551 RFEAKIHDLR ETMMN SSVSS GSGSLR TSQK RSLYVR ALFD YDKTKD SGLP
0601 SQGLNF KFGD ILHVINASDD EWWQARQVTP DGE SDEV GVI PSKR RVEKKE
0651 RARLKT VFKFN SKTRGDK GEI PDDMGS KGLK HVTSN ASDSE SSYHEYGC SK
0701 GGQEEYVLSY EPVNQ QEVNY TRPVII LGPM KDR VNDDLIS EFPDK FGSCV
0751 PHTTRPKRDY EVDGRDYHFV TSRE QMEKDI QEHK FIEAGQ YNNHLYGTSV
0801 QSVRAVAEKG KHCILD VSGN AIKRLQIAQL YPISIFIKPK SMENIMEMNK
0851 RLTDEQARKT FERAVRLEQ FTEHFT AIVQ GDTLEDIYNQ VK QIEEQSG
0901 PYIWVPAKEK L

DLG3, DLG3_RAT (Q62936)

Coverage is 15.0% absolute, 24.9% relative

0001 MHKHQHCCKC PECYEVTRLA ALRRLEPPGY GDWQVPDPYG PSGNGASSG
0051 YGGYSSQTLP SQAGATPTPR TKAKL IPTGR DVGPVPPKPV PGK NTPK LNG
0101 SGPSW WPECT CTNR DWYEQA SPAPLLVNP E ALEPSLSVNG SDGMF K YEEI
0151 VLER GN SGLG FSIAGG IDNP HVPDDPGIFI TKIIPGGAAA MDGR LGVNDC
0201 VLRVNEVDVS EVVHS RAVEA LKEAGPVVRL VVRRF QPPPE TIMEVNLLKG
0251 PKGLGFSIAG GIGNQHIPGD NSIYITKIIE GGAAQKDGR L QIGDR LLAVN
0301 NTN LQDVR HE EA VASL KNTS DMVYLK VAKP GSLH LNDMYA PPDYASTFTA
0351 LADNHISHNS SLGYL GAVES KVTVYP APPQV PPTRYSPIPR HMLAEEDFTR
0401 EPRKII LHKG STGLGF NI VG GEDGE GIFI VS FILAGGPADL SGELRRGDR I
0451 LSVNGVNLRN ATHEQ AAAA AL KRAGQS VTI V AQYRPEEYSR FESKI HDLRE
0501 QMMN SSMSSG SGSLRT SEKR SLYV RALFDY DRTRD SCLPS QGLSF SYGDI
0551 LHVINA SDE WWQARL VTPH GESEQI GVIP SKKR VEKKER ARLKT VKFHA
0601 RTGMIESNRD FPGLSDDYYG AKNLK GVT SN TSDSESSSKG QEDAIL SYEP
0651 VTRQEIH YAR PVII LGPM K RVNDL IS EF PHK FGSCV PH TTRPR RDNEV
0701 DGQDYHFVVS REQMEKDI QD NK FIEAGQ FN DNLYGTSI QS VR AVAERG K H
0751 CILD VSGN AI KRLQQA QL YP IAIFI KPK SI EALMEM NR RQ TYEQANK IFD
0801 KAM K LEQEF G EYFTAIVQGD SLEI YN K IK QI IEDQSGHY IWVPSPEKL

DLG4, DLG4_RAT (P31016)

Coverage is **49.7%** absolute, **80.5%** relative

0001 **MDCLCIVTTK** KYRYQDEDTP PLEHSPAHP NQANSPPVIV NTDTLEAPGY
0051 **ELQVNGTEGE** MEYEEITLER **GNSGLGFSIA** GGTDNPHIGD DPSIFITKII
0101 **PGGAAAQDGR** LRVNDSILEV NEVDVREVTH SAAVEALKEA GSIVRLYVMR
0151 RKPPAEKVME IKLIKGPKG**L** GFSIAGGVGN QHIPGDNSIY VTKIIEGGAA
0201 **HKDGRLQIGD** KILAVNSVGL EDVMHEDAVA ALKNTYDVYY LKVAKPSNAY
0251 LSDSYAPPDI TTSYSQHLDN EISHSSYLGT DYPTAMPTS PRRYSPVAKD
0301 **LLGEEDIPRE** PRRIVIHRGS TGLGFNIVGG EDGEGIFISF ILAGGPADLS
0351 GELRKGDQIL SVNGVDLRNA SHEQAAIALK NAGQTVTIIA QYKPEEYSRF
0401 EAKIHDLRE**Q** LMNSSLGSGT ASLRSNPKR**G** FYIRALFDYD KTKDCGFLSQ
0451 **ALSFRFGDVL** HVIDAGDEEW WQARRVHSDS ETDDIGFIPS KRRVERREWS
0501 RLKAKDWGSS SGSQGR**EDSV** LSYETVTQME VHYARPIIIL GPTKDRANDD
0551 **LLSEFPDKFG** SCVPHTTRPK EYEIDGRDY HFVSSREKME KDIQAHKFIE
0601 AGQYNSHLYG TSVQSVREVA EQGKHCILDV SANAVRRLQA AHLHPIAIFI
0651 RPRSLENVLE INKRITEEQ**A** RKA**FDRATK**L EQEFTECFSA IVEGDSFEEI
0701 YHKVKRVIED LSGPYIWVPA RERL

PRRT1, PRRT1_RAT (Q6MG82)

Coverage is **12.1%** absolute, **100.0%** relative

0001 MSSEKGLPD SVPHTSPPP Y NAPQPPAEPP IPPPQTAPSS HHHHHHHYHQ
0051 SGTATLPR**LG** AGGLASAAAG AQRGPSSSAT LPRPPHHAPP GPAAGAPPPG
0101 CATLPR**MPPD** PYLQETRFEG PLPPPPPAAA APPPPAPAPT AQAPGFVVPT
0151 HAGAVGTLPL GGYVAPGYPL QLQPCTAYVP VYPVGTPTYAS GTPGGPGVTS
0201 TLPPPQQGPG LALLEPRRPP HDYMPIAVLT TICCFWPTGI IAIFKAVQVR
0251 TALAR**GDLVS** AEIASREARN FSFISLAVGI AAMVLCTILT VVIIIAAQHH
0301 ENYWDP

PRRT2, PRRT2_MOUSE (D3Z7L6)

Coverage is **18.9%** absolute, **43.0%** relative

0001 **MAASSSQVSE** MK**GVEDSSKT** QTEGPRHSEE GLGPVQVVAE IPDQPEALQP
0051 GPGITAAPVD SGPKAELAPE TTETPVETPE TVQATDLSN PEEGSKAR**QE**
0101 **PASKPDVNRE** TAAEEGSEPQ STAPPEPTSE PAFOINTQSD PQPTSQPPP
0151 PPLQAEPP**TQ** EDPTTEVLTE STGEK**QENGA** VVPLQAGDGE EGPAPQPHSP
0201 **PSTKTPPANG** APPRVLQ**KLV** EEDRIGRAHG GHPGSPRGSL SRHPSSQLAG
0251 PGVEGGEQTQ KPRDYIILAI LSCFCPMWPV NIVAFAYAVM SRNSLQQGDV
0301 DGAQR**LGRVA** KLLSIVALVG GVLIIIASCV INLGAVYK

Noelin1, NOE1_RAT (Q62609)

Coverage is 46.6% absolute, 70.6% relative

0001 **MSVPLLK** IGV VLSTMAMITN WMSQTLPSLV GLNTTR**LSAA** SGGTLDRSTG
0051 **VLPTNPEESW** QVYSSAQDSE GRCICTVVAP QQTMCSRDA R TKQLRQLLEK
0101 **VQNMSQSIEV** LDRRTQFDLQ YVEK**MENQMK** GLESKFRQVE ESHKQHLARQ
0151 FKAIAK**MDE** LRPLIPVLEE YKADAKLVLQ FKKEEVQNLTS VLNELQEEIG
0201 AYDYDELQSR VSNLEERLRA CMQKLACGK**L** TGISDPVTVK TSGSR**FGSWM**
0251 TDPLAPEGDN RVWYMDGYHN NRFVREYK**SM** VDFMNTDNFT SHRLPHPWSG
0301 TGQVVYNGSI YFNK**FQSHII** IRFDLKETI LKTRSLDYAG YNNMYHYAWG
0351 GHSDIDLMVD ENGLWAVYAT NQNAGNIVIS KLDPVSLQIL QTWNNTSYPKR
0401 SAGEAFIICG TLYVTNGYSG GTK**VHYAYQT** NASTYEYIDI PFQNKYSHIS
0451 MLDYNPKDRA LYAWNNGHQT LYNVTLFHVI RSDEL

Noelin2, NOE2_MOUSE (Q8BM13)

Coverage is 35.0% absolute, 74.4% relative

0001 MRKLRQTGTT IAGGQTLFQS PEEGWQLYTS AQAPDGK**CVC** TAVIPA**QSTC**
0051 ARDGRSRELR QLMEKVQNVS QSMEVLELRT FRDLQYVRSM ETLMRSLDAR
0101 LF**AADGSVSA** KSFQELKDRM TELLPLSSVL EQYKADTRTI VRLREEV**NL**
0151 SGNLAAIQEE MGAYGYEDLQ QRVMALEARL HACAQKLGCG KLTGVSNPIT
0201 IRAMGSRF**FGS** WMTDTMAPSA DSRVWYMDGY YKGRRVLEFR TLGDFIK**GQN**
0251 FIQHLLPQPW AGTGHVYVYNG SLFYNK**YQSN** VVVKYHFRSR SVLVQRSLPG
0301 AGYNNTFPYS WGGFSDMDFM VDESGLWAVY TTQNAGNIV VSP**LDPHTLE**
0351 VVRSWDTGYP KRSAGEAFMI CGVLYVTNSH LAGAKVYFAY FTNTSSYEYT
0401 DVPFNNQYSH ISMLDYNPRE RALYTWNNGH QVLYNVTLFH VISTAGDP

Noelin3, NOE3_RAT (P63057)

Coverage is 32.0% absolute, 52.6% relative

0001 MSAPLLK**LGA** VLSTMAMISN WMSQTLPSLV GLNTTR**LSAP** DTLTQISP**KE**
0051 GWQVYSSAQD PDGRCICTVV APEQNLCSD AKSRQLRQLL EKVQNMSQS**I**
0101 EVLNLR**TQFD** FQYV**VLKMETQ** MKGLKAKFR**Q** IEDDRKTLM**T** KHFQELK**EKM**
0151 DELLPLIPV**L** EQYKTD**AKL** TQFKEEIR**NL** SSVLTGIQEE IGAYDYEELH
0201 QRVLSLET**RL** RDCMKKLT**CG** KLMKITGPIT VKTSGTR**FGA** WMTDPLASEK
0251 NNRVWYMDSY TNNKIVREYK SIADFVSGAE SRTYNLPFKW AGTNHVVYNG
0301 SLYFNK**YQSN** IIIKYSFD**LG** RVLAQRSLEY AGFHNVYP**YT** WGGFSDIDLM
0351 ADEIGLWAVY ATNQNAGNIV ISQLNQDTLE VMK**SWSTGYP** KR**SAGESFMI**
0401 CGTLYVTNSH LTGAK**VYYSY** STK**TSTYEYT** DIPFH**NQYFH** ISMLDYNARD
0451 RALYAWNNGH QVLFNVTLFH II**KTEDDT**

Neuritin, NRN1_RAT (O08957)

Coverage is 41.5% absolute, 76.6% relative

0001 MGLKLN~~GR~~YI SLILAVQIA~~Y~~ LVQAVR~~AAGK~~ CDAVFK~~GFSD~~ CLLKLGD~~SMA~~
0051 NYPQGLDDKT NIKTVCTYWE DFHSCTVTAL TDCQEGAKDM WDKLRKESKN
0101 LNIQGSLFEL CGSGNGAAGS LLPALSVLLV SLSAALATWL SF

GSG1-l protein, GSG1L_RAT (D3ZK93)

Coverage is 32.3% absolute, 100.0% relative

0001 MKTSRRGRAL LAVALNLLAL LFATTAF~~LTT~~ YWCQGTQRVP KPGCGQGGGA
0051 NCPNSGANAT ANSTAAPVAA SPAGAPYSWE AGDERFQLRR FHTGIWYSCE
0101 EELGGPGEKC R~~S~~FIDLAPAS EKGV~~L~~WLSVV SEVLYILLLV VGFSLMC~~EL~~
0151 LHSSSV~~I~~DGL KLNAFAAVFT VLSGLLGMVA HMMYTQVFQV TVSLGPEDWR
0201 PHSWDYGWSF CLAWGSFTCC MAASVTLNS YTK~~T~~VIEFRH KRKVFEQGYR
0251 EEPTFIDPEA IKYFRERIEK GDVSEEE~~D~~FR LACR~~H~~ERYPT RHQPHMGDSW
0301 PRSSAHEAAE LNRQCWVLGH WV

C9orf4, D3ZE85_RAT (D3ZE85)

Coverage is 47.8% absolute, 68.3% relative

0001 MAGQSLRRSA WVPLLRL~~LL~~ AGIAACEASP ADDGAGPGGR GPRGR~~ARGDA~~
0051 GADEAVPRHD SSYGT~~FAGEF~~ YDLRYLSEEG YPFPTAPPVD PFAKIKVEDC
0101 GR~~T~~KGC~~F~~RYG KPGCNAETCD YFLSYRMIGA DVEFELSADT DGWVAVGFSS
0151 DK~~K~~MGGDDVM ACVHDDNGRV RIQHFYNVGQ WAKEVQR~~NPA~~ RDEEGVFENN
0201 RVTCR~~F~~KRPV NVPR~~E~~TIVD LHLSWY~~Y~~LFA WGPAIQGSIT RHDIDSP~~P~~AS
0251 ERVVSIYKYE DIFMP~~S~~AAYQ TFSSPFCL~~LL~~ IVALTFYLLM GTP

Brorin, VWC2_MOUSE (Q8C8N3)

Coverage is 30.6% absolute, 68.3% relative

0001 MPSSSAMAVG ALSSSLLVTC CLMVALCSPS IPLEK~~LAQAP~~ EQPGQE~~K~~REH
0051 ASRDSPGRVS ELGRASRDEG SSARDWKSKG SRALSGREAW SKQK~~Q~~AWAAQ
0101 GGSAKAADWQ VRPR~~GDT~~PQG EPPAAAQ~~EAI~~ SLELVPTPEL PEEYAYPDYR
0151 GK~~G~~CVDES~~G~~F VYAIGEKFAP GPSACPCLCT EEGPLCAQPE CPR~~L~~HPR~~C~~IH
0201 VDNSQCCPQC KEKKNYCEFR GKTYQTLEEF VVSP~~C~~ERC~~R~~C EANGEVLCTV
0251 SACPQTECV~~D~~ PVYEPDQCCP ICK~~N~~GPN~~C~~FA ETAVIPAGRE VKTDECTICH
0301 CTYEEGTWR~~I~~ ERQAMCTRHE CRQM

Brorin-2l, VWC2L_RAT (D4A0X1)

Coverage is **18.9%** absolute, **44.6%** relative

0001 **MALHIHEACI** **LLLVIPGLVT** **PAAISHEDYP** **ADEDGPVCDQ** **PECPKIHPKC**
0051 **TKVEHNGCCP** **ECKEVKNFCE** **YHGKNYKILE** **EFKPSPCEWC** **RCEPSNEVHC**
0101 **VVADCAVPEC** **VNPIYEPEQC** **CPVCKNGPNC** **FAGTTIIPAG** **IEVKVDDCNI**
0151 **CHCHNGDWWK** **PAQCSKRECQ** **GKQTV**

LRRT-4, LRRT4_MOUSE (Q80XG9)

Coverage is **21.0%** absolute, **44.3%** relative

0001 **MGFRLITQLK** **GMSVFLVLFP** **TLLLVMLTGA** **QRACPKNCRC** **DGKIVYCESH**
0051 **AFADIPENIS** **GGSQGLSIRF** **NSIQKLKSNQ** **FAGLNQLIWI** **YLDHNYISSV**
0101 **DEDAFQGIRR** **LKEELILSSNK** **ITYLHNKTFH** **PVPNLRNLDL** **SYNKLQTLQS**
0151 **EQFKGLRKLI** **ILHLRSNSLK** **TVPIRVFQDC** **RNLDFLDLGY** **NRRLRSLSRNA**
0201 **FAGLLKLKEL** **HLEHNQFSKI** **NFAHFPRLFN** **LRSIYLQWNR** **IRSVSQGLTW**
0251 **TWSSLHTLDL** **SGNDIQAIQEP** **GTFKCLPNLQ** **KLNLDNSKLT** **NVSQETVNAW**
0301 **ISLISITLSG** **NMWECRSRIC** **PLFYWLKNFK** **GNKESTMICA** **GPKHIQGEKV**
0351 **SDAVETYNIC** **SDVQVVNTER** **SHLAPQTPQK** **PPFIPKPTIF** **KPDAVPATLE**
0401 **AVSPSPGFQI** **PGTDHEYEHV** **SFHKIIAGSV** **ALFLSVAMIL** **LVIYVSWKRY**
0451 **PASMKQLQQH** **SLMKRRRKKA** **RESERQMNSP** **LQEYYVDYKP** **TNSETMDISV**
0501 **NGSGPCTYTI** **SGSRECEIPH** **HVKPLPYYSY** **DQPVIGYQQA** **HQPLHINKAY**
0551 **EAVSIEQDDS** **PSLELGRDHS** **FIATIARSAA** **PAIYLERITN**

PORCN, PORCN_MOUSE (Q9JJJ7)

Coverage is **8.5%** absolute, **35.8%** relative

0001 **MATFSRQEFFF** **QQLLQGCLLP** **TVQQGLDQIW** **LLLTICFACR** **LLWRLGLPSY**
0051 **LKHASTVAGG** **FFSLYHFFQL** **HMVWVVLSSL** **LCYLVFLCR** **HSSHRGVFLS**
0101 **VTILIYLLMG** **EMHMVDTVTW** **HKMRGAQMIV** **AMKAVSLGFD** **LDRGEVGAVP**
0151 **SPVEFMGYLY** **FVGTIVFGPW** **ISFHSQLQAV** **QGRPLSRRWL** **KKVARSLALA**
0201 **LLCLVLSTCV** **GPYLFYFIP** **LDGDRLLRNK** **KRKARGTMVR** **WLRAYESEAVS**
0251 **FHFNSYFVGF** **LSEATATLAG** **AGFTEEKDHL** **EWDLTVSRPL** **NVELPRSMVE**
0301 **VVTSWNLPMs** **YWLNYYVFKN** **ALRLGTFSAV** **LVTYAASALL** **HGFSFHAAV**
0351 **LLSLAFITYV** **EHVLRKRLAQ** **ILSACILSKR** **CLPDCSHRHR** **LGLGVRALNL**
0401 **LFGALAIFHL** **SYLGSLFDVD** **VDDTTEEQGY** **GMAVTVHKWS** **ELSWASHWVT**
0451 **FGCWIFYRLI** **G**

PIP-PP SAC1, SAC1_RAT (Q9ES21)

Coverage is 44.6% absolute, 62.8% relative

0001 MAATAYEHLK LHITPEKFYV EACDDGADDV LIIDRVSTEV TLAVKDVPP
0051 SAVTRPIYGI MGTIHLVAGN YLVVITKKMK VGEFFNHVIW KATDFDVLSY
0101 KKTMHLTDI QLQDNKTFIA MLNHLSTDG FYFSTTYDLT HTLQLSNTS
0151 PEFQEMSLLE RADQRFWNG HLLRELSAQP EVHRFALPVL HGFITMHSCS
0201 INGKYFDWIL ISRRSCFRAG VRYYVFIDS EGHAANFVET EQIVHYSGNR
0251 ASFVQTRGSI PVFWSQRPNL KYKPDHQINK VANHMDGFQR HFDSQVIIYG
0301 KQVIINLVNH KGSEKPLEQT FAKMVSSLGS GMIRYIAFDF HK ECKNMRWD
0351 RLSILLDQVA EMQDELSYFL VDSAGKVVTN QEGVFRSNCM DCLDRTNVIQ
0401 SILLARRSLQA QLQLRLGVHLV GQKLEEQDEF EKIYKNAWAD NANACAKQYA
0451 GTGALKTDFT RTGKR TQLGL VMDGFNSLLR YYKNNFSDGF RQDSIDLFLG
0501 NYSVDELDSH SPLSVPRDWK FLALPIIMVV AFSMCIIICLL MAGDTWTETL
0551 AYVLFWGVAS IGTFFIILYN GKDFVDAPRL VQKEKID

lipase ABHD6, ABHD6_MOUSE (Q8R2Y0)

Coverage is 62.5% absolute, 88.6% relative

0001 MDLDVVNMFV IAGGTLAIPPI LAFVASFLLW PSALIRIYYW YWRRTLGMQV
0051 RYAHHEDYQF CYSFRGRPGH KPSILMLHGF SAHKDMWLSV VKFLPKNLHL
0101 VCVDMPGHEG TTRSSLDDLS IVGQVKRIHQ FVECLKLNKK PFHLIGTSMG
0151 GHVAGVYAAAY YPSDVCSSLV VCPAGLQYST DNPFVQR LKE LEESAAIQKI
0201 PLIPSTPEEM SEMLQLCSYV RFKVPQQILQ GLVDVRIPHN SFYRKLFLEI
0251 VNEKSRYSLH ENMDKIKVPT QIIWGKQDQV LDVSGADILA KSISNSQVEV
0301 LENCGHSVVVM ERPRKTAKLI VDFLASVHNT DNKKLN

lipase ABD12, ABD12_RAT (Q6AYT7)

Coverage is 53.5% absolute, 74.5% relative

0001 MRKRTEPVTL EHERCAASGS SSSGSAAL DADCSLKQNL RLAGKGTAEP
0051 HSASDAGMKR ALGRRKSLWF RLRKILLCVL GFYIAIPFLV KLCPGIQAKL
0101 IFLNFVRVPY FIDLKKPQDQ GLNHTCNYYL QPEDDVTIGV WHTIPSVWWK
0151 NAQGH DQMWH EDALASNHPY ILYLHGNAGT RGGDHRVELY KVLSLGYHV
0201 VTFDYRGWGD SVGTPSERGM TYDALHVFDW IKARSGDNPV YIWGHSLGTG
0251 VATNLVRRLC ERETPPDALI LESPFTNIRE EAKSHPFSVI YRYFPGFDWF
0301 FLDPITSSGI KFANDENMKH ISCPLLILHA EDDPVVPFHL GRKLYNIAAP
0351 SR SFRDFKVQ FIPFHSDLGY RHKYIYKSPE LPRIILREFLG KSEPERQH

CPT-1, CPT1C_MOUSE (Q8BGD5)

Coverage is 30.1% absolute, 53.6% relative

0001 MAEAHQASSL LSSILSSDGAE VELSSPVWQE IYLCALRSWK RHLWRVWNDF
0051 LAGVVPATPL SWLFLFSTIQ LACLLQLDPS LGLMEKIKEL LPDWGGQHHQ
0101 LQGFLSAAVF ASCLWGAIF TLHVALRLLL SHHGWLLEPH GAMSSPTK**TW**
0151 **LALVRIFSGR** HPR**LFSFQRA** LPR**QPVPSAQ** ETVRKYLESV RPVLGDDAFD
0201 **RATALANDFL** RLHAPR**LQLY** LQLKSWCTSN YVSDWWEFFV YLRSFGSLIN
0251 STYYMMDFLY VTPTPLQAAR AGNAVHTLLL YR**HLLNRQEI** SPTLLMGMRP
0301 LCSAQYERMF NTTRIPGVEK DHLRHLQDSR HVAVFHRGRF FR**VGTHSPNG**
0351 LLSPRALEQQ FQDILDDPSP ACPLEEHLAA LTAAPR**SMWA** QVRESVK**THA**
0401 ATALEAVEGA AFFVSLDSEP AGLTR**EDPAA** SLDAYAHALL AGR**GHDWRFD**
0451 K**SFTLIVFSN** GK**LGLSVEHS** WADCPVSGHL WEFTLATECF QLGYATDGHC
0501 K**GHPDPTLPQ** PQRLQWDLPE QIOPPSISLAI RGAK**TLSGANI** DCHVFPFSHF
0551 G**KSF1KCCHV** SSDSFIQLVL QLAHFR**DRGQ** FCLTYESAMT RLFLEGRTET
0601 VRSC**TREACQ** FVRAMD**NKET** DQHCLALFR**V** AVDKHQALLK AAMSGQQGIDR
0651 HLFALYIMSR LLHMQSPFLT QVQSQQWLLS TSQVPVQQTH LIDVHNYPDY
0701 VSSGGGF GPA HDHGYGISYI FMGENAITFH ISSKK**SSTET** DSHR**LGQHIE**
0751 NALLDVASLF RVGQHFKRQF R**GENSDYRYN** FLSCKTVDPN TPTSSTNL

Rap-2b, RAP2B_RAT (P61227)

Coverage is 62.3% absolute, 71.7% relative

0001 MREYK**VVVLG** SGGVGKSA**L**T VQFVTGSFIE KYDPTIEDFY RKEIEVDSSP
0051 SV**LEILD** TAG TEQFASMR**D**L YIK**NGQGFIL** VYSLVNQQSF QDIKP**MRDQI**
0101 IRVKRYERVP MILVGNKVDL EG**E**REVSYGE GK**ALAEW**SC PFMETSAK**NK**
0151 **ASVDELF** AAEI VR**QMN**YAAQP NGDEGCCSAC VIL

AP at CL-91

Antibody	anti-GluA1-a			anti-GluA1-b			anti-GluA1-c			anti-GluA2-a			anti-GluA2-b			anti-GluA2-c			anti-GluA2/3			anti-GluA3			anti-GluA4-a			
	rb/IgG	mb/IgG	mb/ko	rb/IgG	mb/IgG	mb/ko	rb/IgG	mb/IgG	mb/ko																			
source/control	12	10	12	9	8	5	5	7	7	9	9	8	10	8	9	5	10	5	8	8	5	8	10	8	10	10	8	5
rPV threshold	12	10	12	9	8	5	5	7	7	9	9	8	10	8	9	5	10	5	8	8	5	8	10	8	10	10	8	5
GluA1	9187	7109	7109	8222	9374	4579	802	1504	1016	497	1640	2776	8521	6289	17	490	1516	13	3091	10307	1	428	1480	2	2058	6276	1657	6338
GluA2	3570	7263	6535	14121	7598	2941	1033	1178	1351	2473	4478	5143	40735	15861	18507	2935	4328	3840	16434	23697	27316	7920	16592	20541	1583	2850	2767	3898
GluA3	3448	2399	2399	673	1329	2760	53	171	327	355	1206	3123	5221	4124	12	487	1327	15	2604	7475	2	2118	7876	9	369	828	667	1389
GluA4	3281	1908	1950	4848	3282	2714	367	357	340	175	273	236	4215	1832	8	172	383	9	1503	3030	1	999	1511	2	7287	8823	9689	9647
TARP γ -2	494	401	401	637	1126	1126	19	141	141	93	115	115	1108	626	8	62	70	4	504	693	1	31	804	3	412	719	615	390
TARP γ -3	165	102	102	473	101	101	7	42	25	58	84	84	1026	173	3	60	44	8	423	66	1	105	235	13	48	82	33	26
TARP γ -4	55	124	124	166	20	20	0	13	13	13	0	0	233	169	15	37	0	3	106	141	1	104	212	2	176	126	236	107
TARP γ -7	88	77	77	90	335	335	15	41	41	0	0	0	14	47	18	0	0	0	5	26	0	0	50	0	105	316	107	210
TARP γ -8	33	66	66	62	57	57	0	16	16	0	0	0	15	36	21	0	0	0	0	24	1	0	19	9	0	19	0	14
CNIH2	2372	1005	1005	0	802	802	0	157	157	0	354	354	58	1341	35	85	202	14	453	1052	3	436	2225	14	119	0	226	199
CNIH3	496	358	358	593	388	388	86	76	76	109	141	141	20	19	9	97	0	15	39	633	2	453	988	73	127	159	224	166
CKAMP44	216	43	43	404	191	191	33	13	13	3	0	0	338	119	54	3	0	0	138	20	2	44	66	15	31	0	42	2
CKAMP52																												
MAGUKp55-2																												
DLG1	0	0	0	0	17	0	0	0	0	0	0	0	0	0	0	0	0	0	0	0	0	0	40	0	35	0	0	0
DLG3	0	0	0	0	0	0	0	0	0	0	0	0	0	0	0	0	0	0	0	0	0	0	0	1	22	0	0	0
DLG4	18	159	117	78	27	1	4	5	2	1	0	0	1	0	0	1	0	0	19	28	0	51	124	1	77	55	16	26
PRRT1	540	335	335	650	170	170	32	32	32	14	0	0	435	180	109	17	0	0	156	180	1	44	58	64	59	0	53	0
PRRT2	18	25	25	87	27	10	0	5	3	0	0	0	95	20	11	3	0	0	18	26	1	0	0	0	0	19	0	0
Noelin1	494	280	128	1940	566	566	38	127	127	42	37	37	2029	134	16	44	42	15	1044	448	1	652	913	10	1597	1995	2252	2289
Noelin2	151	89	89	472	191	191	35	27	27	37	61	61	1269	456	68	63	84	70	446	784	3	151	747	11	235	477	405	623
Noelin3	322	120	120	385	274	274	40	29	29	36	20	20	597	239	24	50	40	45	291	360	3	197	329	4	368	465	553	382
Neuritin	18	59	59	65	264	264	0	34	34	5	14	14	26	89	56	5	7	7	14	38	1	64	94	10	132	465	31	88
GSG1-l protein	260	119	119	223	191	191	29	32	32	35	34	36	919	377	35	44	42	43	252	363	4	11	267	151	126	37	36	46
C9orf4	185	55	55	275	89	78	13	11	10	31	17	31	698	82	22	30	22	20	303	188	3	55	65	6	71	49	70	26
Brorin	40	15	15	67	42	42	100	0	0	0	0	0	133	39	3	0	0	0	92	139	2	35	178	178	54	135	148	192
Brorin-2I	30	20	20	56	63	29	0	0	0	0	0	0	88	39	35	15	7	7	65	45	4	0	50	50	26	0	44	24
LRRT4	0	0	0	65	0	0	0	0	0	0	0	0	164	0	0	0	0	0	35	42	35	49	93	75	0	0	10	0
PORCN	0	0	0	0	0	0	0	0	0	0	0	0	0	0	0	0	0	0	0	0	0	0	79	40	0	45	0	0
PIP-PP SAC1																												
lipase ABHD-6	0	0	0	0	25	25	0	11	11	0	0	0	0	19	19	0	0	0	0	16	6	0	0	0	0	0	0	0
lipase ABHD-12	0	18	18	15	12	0	0	0	0	0	0	0	0	0	0	0	0	0	0	0	0	0	43	2	14	39	0	0
CPT-1	32	32	32	33	0	0	0	0	0	0	0	0	80	14	14	0	0	0	51	30	1	0	0	9	0	0	0	0
Rap2B																												

Table S3A, Schwenk et al

AP at CL-47

Antibody source/control rPV treshold	anti-GluA1-a			anti-GluA2-a			anti-GluA2-b			anti-GluA3		anti-GluA4-a	
	rb/IgG 8	mb/IgG 5	mb/ko 5	rb/IgG 5	mb/IgG 5	mb/ko 5	rb/IgG 8	mb/IgG 10	mb/ko 10	rb/IgG 8	mb/IgG 8	rb/IgG 10	mb/IgG 10
GluA1	7527	9213	14214	247	44	103	4022	2982	32	405	291	923	1833
GluA2	22833	6646	1513	1658	314	176	33063	14743	9455	7659	6648	1555	1649
GluA3	4756	5047	5047	1039	205	205	25333	9093	17	12117	8603	1033	984
GluA4	3600	2362	2362	101	20	20	1603	443	11	237	323	4512	3798
TARP γ -2	4392	2168	2168	303	37	37	6319	2917	66	2885	2992	1583	2181
TARP γ -3	4920	2205	2205	211	46	46	8790	1961	51	3686	1059	198	173
TARP γ -4	365	36	5	46	0	0	824	82	45	341	238	224	188
TARP γ -7	425	498	498	16	3	5	374	150	39	249	329	465	480
TARP γ -8	5098	4039	2379	254	36	36	5086	1789	44	1980	1820	431	372
CNIH2	2524	2346	1444	79	29	29	2165	408	52	370	751	76	91
CNIH3	212	307	307	48	0	0	617	190	0	115	395	82	66
CKAMP44	382	301	301	30	7	40	467	118	52	191	57	0	58
CKAMP52	155	146	146	0	0	0	276	81	84	49	110	33	0
MAGUKp55-2	52	55	55	0	0	0	0	0	0	67	29	48	16
DLG1	180	157	157	0	0	0	116	30	30	88	109	98	90
DLG3	40	56	56	0	0	0	19	10	10	24	45	0	0
DLG4	373	106	326	5	0	0	411	23	111	226	64	42	25
PRRT1	1311	905	981	16	0	0	536	189	129	121	0	64	0
PRRT2	56	145	145	0	0	0	50	42	46	0	0	31	0
Noelin1	666	977	178	10	0	0	152	48	45	57	66	525	397
Noelin2	255	144	144	0	0	5	277	51	51	52	0	156	178
Noelin3	317	128	128	11	0	0	259	49	49	110	97	290	218
Neuritin	52	0	0	38	0	0	26	0	0	0	0	67	68
GSG1-I protein	339	309	271	12	4	4	469	182	173	58	116	11	18
C9orf4	220	161	154	36	10	10	328	100	13	55	41	37	24
Brorin	19	29	27	0	0	0	28	14	14	11	14	18	14
Brorin-2I	64	0	0	0	0	0	0	18	18	0	0	0	0
LRRT4	83	54	54	0	0	0	189	32	32	78	110	5	39
PORCN	69	58	58	41	0	0	221	103	103	26	0	35	37
PIP-PP SAC1	74	63	63	6	0	0	147	41	26	56	30	45	43
lipase ABHD-6	324	750	750	224	76	76	1050	1003	230	89	205	110	209
lipase ABHD-12	109	79	79	30	12	12	334	10	36	88	161	35	34
CPT-1	362	302	302	127	18	18	1120	224	28	123	190	89	0
Rap2B	21	16	35	0	0	0	29	12	18	0	0	0	0

Table S3B, Schwenk et al.

Target	Peptide (Sequence)	PV slope factor	SD of fit
ABHD-12	KLYNIAAPSR LIFLNFVR LYNIAAPSR SHPF SVIYR VPYFIDLK VQFIPFHSDLGYR	730400 820580 172220 495980 856590 1073800	3.68e+04 3.91e+04 4.41e+03 2.31e+04 2.35e+04 2.33e+04
ABHD-6	DMWLSVVK IHQFVECLK QDQVL DVSGADILAK SSLDDLSIVGQVK	438120 489610 1168400 1515400	2.91e+04 1.49e+04 5.66e+04 3.73e+04
TARP γ -2 (CCG2)	ATDYLQASAITR DNSFLQVHNCIQK TCCLEGNFK	2668700 535830 606710	6.89e+04 1.02e+05 2.01e+04
TARP γ -3 (CCG3)	DHAFLQFHNSTPK DLSPISK GFHTIPSTDISMFTLSR LTMGTLLNSDR SRDLSPISK TCCLLEGAFR	417450 374340 778890 1066500 53072 487250	4.67e+04 9.66e+03 4.69e+04 2.77e+04 4.35e+03 2.78e+04
TARP γ -4 (CCG4)	EGFHVSMMLNR GDLTHSGLWR ITGAIPMGELSMYTLSR VCCIEGIYK VCCIEGIYR	436070 1237000 471990 470040 121840	1.91e+04 1.17e+05 1.76e+04 3.78e+04 3.30e+03
TARP γ -5 (CCG5)	DAETYFNYK MSLHSGLWR VCFLAGEER	1066100 291550 634210	3.58e+04 3.53e+04 2.72e+04
TARP γ -7 (CCG7)	EGAGVMSVYLFTK MALHAGLWR VCFFAGR YPDHLHISTSPC	1626400 102800 347580 140020	7.00e+04 1.65e+04 1.72e+04 7.54e+03
TARP γ -8 (CCG8)	AGGGAGGGSGGPSAILR DPGGLTHSGLWR GSSAGFLT LHNAPPK ICCLEGLK ICCLEGLKR	1054000 292750 559320 157960 239980	3.78e+04 4.39e+04 8.94e+04 9.44e+03 9.77e+03
C9orf4 (CI004)	DEEGVFENNRR GDAGADEAVPR HDIDSPPASER HDSSYGTFASEFYDLR IQHFYNVGQWAK YGKPGCNAETCDYFLSYR	533790 83364 471710 1027500 811970 508910	1.79e+04 2.55e+03 3.35e+04 8.24e+04 1.07e+05 4.24e+04
CNIH-2	TDFKNPIDQGNPAR NPIDQGNPAR ICCLLR-CM-PA TDFKNPIDQGNPAR-Dea	1052950 542150 22025 35007	3.88e+04 1.63e+04 3.19e+03 1.23e+04
CNIH-3	SPIDQCNPVHAR-CM SPIDQCNPVHAR-PA SPIDQCNPVHAR-CM-Dea SPIDQCNPVHAR ICFLLR-PA TDFKSPIDQCNPVHAR-CM TDFKSPIDQCNPVHAR-PA ICFLLR-CM ICFLLR	822210 80256 9409 937540 11412 187850 33252 336840 298450	3.93e+04 3.21e+03 2.36e+03 4.51e+04 7.77e+03 5.32e+03 9.46e+02 1.34e+04 1.79e+04
CPT-1	AGNAVHTLLLRYR LFSFQR LQLYLQLK SFTLIVFSNGK TWLALVR	790610 355080 294440 951640 625080	2.80e+04 1.12e+04 1.74e+04 3.96e+04 5.31e+04

Target	Peptide (Sequence)	PV slope factor	SD of fit
DLG1	IISVNSVDLR	2254600	1.17e+05
	IITGGAAAQDGR	1035100	4.63e+04
	NAGQAVTIVAQYRPEEYSR	2150500	7.19e+04
	NTSDFVYLK	1207400	2.91e+04
DLG3	DNEVGQDYHFVVSR	2267400	1.36e+05
	ILSVNGVNLR	1340700	7.45e+04
	LLAVNNTNLQDVR	2657600	6.02e+04
	LQQAQLYPIAIFIKPK	1832900	5.84e+04
	VNEVDVSEVVHSR	1905600	1.16e+05
DLG4	EVTHSAAVEALK	498510	1.22e+04
	HCILDVSANAVR	833830	5.29e+04
	IIPGGAAAQDGR	2455500	2.98e+04
	NAGQTVTIIAQYKPEEYSR	1055100	3.16e+04
	NASHEQAAIALK	1132400	8.63e+04
	NTYDVVYLK	1250000	4.49e+04
GluA1 (GRIA1)	FALSQLTEPPK	1049300	2.37e+04
	FEGLTGNVQFNEK	1281600	3.36e+04
	GFCLIPQQSINEAIR	1054400	2.66e+04
	LEIVSDGK	645290	1.24e+04
	LVVVDCESER	331500	9.75e+03
GluA2 (GRIA2)	YTSALTYDGVK	1923100	5.26e+04
	FAYLYDSDR	839830	3.43e+04
	GVYAIFGFYDK	306200	1.01e+04
	IGYWSEVDK	411450	2.02e+04
	LTIVGDGK	287650	8.45e+03
	QVQVEGLSGNIK	1246500	4.34e+04
GluA3 (GRIA3)	VGMVQFSTSEFR	871220	2.44e+04
	ADIAVAPLTITLVR	2506200	1.29e+05
	FVYLYDTER	1228900	6.16e+04
	GAILSLLSYYK	208490	2.00e+04
	INTILEQVVLGK	2047400	7.09e+04
	YLIDCEVER	924080	3.83e+04
GluA4 (GRIA4)	AEIAIAPLTITLVR	827780	3.44e+04
	EYPGSETPPK	80077	5.17e+03
	IAIVPDGK	1009700	1.88e+04
	IQGLTGTVQFDHYGR	941930	2.90e+04
	LQNILEQIVSVGK	1729300	4.51e+04
	LSEAGVLDK	859090	1.43e+04
	LSEAGVLDKLK	515590	5.12e+04
GSG1-I	WWYDKGECKGPK	53940	8.32e+03
	EEPTTFIDPEAIK	183220	1.08e+04
	GDVSEEEDFR	563350	1.27e+04
	SFIDLAPASEK	1978400	6.54e+04
	TVIEFR	601380	1.08e+04
	VFEQGYR	792820	1.82e+04
LRRT4	ELHLEHNQFSK	155660	5.67e+03
	LKELHLEHNQFSK	387060	1.67e+04
	LQTLQSEQFK	1498400	4.78e+04
	NLDLSYNK	815770	3.11e+04
	SAAPAIYLER	1288200	9.12e+04
	SIYLQWNR	897130	4.72e+04
Noelin1	DLQYVEK	634210	2.79e+04
	LSAASGGTLDR	649380	1.19e+04
	LTGISDPVTVK	1913500	3.51e+04
	LVLQFK	565480	1.68e+04
	YSHISMLDYNPK	760260	2.39e+04
Noelin2	DLQYVR	203860	1.49e+04
	LDPHTLEVVR	1445500	3.88e+04
	LTGVSNPITIR	1866500	4.13e+04
	MTELLPLSSVLEQYK	738050	3.01e+04
	VMALEAR	377560	1.97e+04

Target	Peptide (Sequence)	PV slope factor	SD of fit
Noelin3	DFQYVLK	871560	2.96e+04
	SIADFVSGAESR	2043500	9.05e+04
	TYNLPFK	679060	1.90e+04
	VLSLETR	848150	1.32e+04
	YQSNIIIK	1359400	2.09e+04
	YSFDLGR	859220	3.45e+04
Neuritin (NRN1)	GFSDCLLK	388340	1.70e+04
	LGDSMANYPQGLDDK	421810	1.49e+04
	LGDSMANYPQGLDDKTNIK	1883100	5.22e+04
PORCN	AVSLGFDDLDR	978690	2.40e+04
	GAQMIVAMK	412920	1.53e+04
	LAQILSACILSK	1248800	3.27e+04
	LGLPSYLK	675220	2.78e+04
PRRT1	GDLVSAEIASR	1644800	2.77e+04
	LGAGGLASAAAGAQR	2178600	1.84e+05
	LGAGGLASAAASAQR	2159900	3.45e+04
	MPPDPYLQETR	2160400	5.38e+04
PRRT2	EACQEPASRPENVNR	1017900	2.05e+04
	GVEDSSNTHSEGPR	19232	8.07e+02
	NSLQQGDVDGAQR	1474200	3.82e+04
	QEPASKPDVNVR	318860	9.39e+03
RAP2B	ASVDELFAEIVR	1292900	2.61e+05
	SALTQVFVTGSFIEK	161440	2.32e+04
	VDLEGER	20814	1.07e+03
	VDLEGEREVSYGEGK	405470	1.32e+04
	VPMILVGNK	587320	1.82e+04
SAC1	ATDFDVLSYK	475820	1.29e+04
	ELSAQPEVHR	561280	1.59e+04
	LEEQDEFEK	446110	2.74e+04
	NNFSDGFR	500090	3.85e+04
	TNVIQSLRAR	1694900	6.10e+04
CKAMP52 (SHSA6)	ALADILR	748400	2.20e+04
	ETISAIDTSPK	1395600	3.57e+04
	ILSDEQLLSTER	3062200	5.55e+04
	LHSQDPLLSPER	856340	4.57e+04
	QQGPIPIAHCER	897930	5.59e+04
	TAFPEQSLSR	1581100	1.65e+04
CKAMP44 (SHSA9)	AFPSHEGPAQQNGQK	1731700	4.65e+04
	GNLPLHPVR	565530	3.86e+04
	MPPHPPLAYNSTANFK	378790	1.61e+04
	TWDPSDQSLR	1276500	6.90e+04
Brorin (VWC2)	LAQAPEQPGQEK	991430	2.80e+04
	LAQAPEQPGQEKR	194210	1.10e+04
	NGPNCFAETAVIPAGR	753490	5.47e+04
	TDECTICHCTYEEGTWR	613640	5.71e+04
	TYQTLEEFVVSPCR	431970	1.58e+04
Brorin-2I (VWC2L)	GCVDDSGFVYK	845130	2.81e+04
	GKGCVDDSGFVYK	156100	7.20e+03
	ILEEFKPSPCEWCR	389820	2.23e+04
	NGPNCFAGTTIIPAGIEVK	1578700	3.79e+04

Table S4, Schwenk et al.